The influence of maternal HIV and ART exposure on neonate brain white matter integrity and organisation

by

Ndivhuwo Magondo

MGNNDI001

In fulfilment of the requirements for the degree of Master of Science in Biomedical Engineering

Faculty of Health Sciences

UNIVERSITY OF CAPE TOWN

February, 2022

Supervisor: Dr Martha Holmes

Co-supervisor: Dr Marcin Jankiewicz

DECLARATION

I, NDIVHUWO MAGONDO, hereby declare that the work on which this thesis is based is my own original work (except where acknowledgements indicate otherwise) and that neither the whole, nor any part of it, has been, or is to be submitted for any other degree in this or any other University.

I empower the University to reproduce, for the purpose of research, either the whole or part of the contents of this thesis in any manner.

Signed by candidate

Signature

14/02/2022

Date

ACKNOWLEDGEMENTS

I would like to first thank my supervisor, Dr. Martha Holmes, for all her support and guidance throughout this entire process. Your unending patience and constant encouragement truly lifted me up in times when doubt started creeping in, and I can't express my gratitude enough. I would also like to thank my co-supervisor Dr. Marcin Jankiewicz for his endless patience and support as well, and for always helping me find my way through my broken R scripts.

I would also like to thank Prof. Ernesta Meintjes, the National Research Foundation (NRF) and National Institute of Health (NIH) for the financial support they provided that made this project possible.

I would like to thank the entire MRI group for their support and encouragement, with special thanks to Joanah Madzime for spending hours of her time teaching me the steps and processes needed for this work. I greatly appreciate all of your help, and am even more grateful for the wonderful friendship that was formed thereafter.

Last but not least, I would like express my immense gratitude to my family and friends who supported me throughout this journey. Special thanks to my parents for encouraging me to pursue this venture, and to my lovely friends Nicole, Matthew, and Emma for their unwavering belief in my abilities and for always providing stress relief when it was needed. I would not be here without you all.

ABSTRACT

Improved legislation and widespread access to treatment has led to a new cohort of children who have in utero exposure to maternal HIV, but remain HIV negative through the use of antiretroviral therapy (ART), known as HIV exposed-uninfected (HEU) children. While HEU infants and children are healthier than their infected peers, they experience some developmental delays as compared to uninfected unexposed populations. Few brain imaging studies have been done in HEU infants and children, and so the effects of the exposure to in utero HIV and ARVs on their neurodevelopment are not well understood. As this population matures, there is a need for studies to determine how HIV as well as ART exposure in utero and at birth affect white matter (WM) structure and its connectivity.

This study used diffusion tensor imaging (DTI) tractography and graph theory to examine the possible influence of HIV and ART exposure in utero on neonate WM integrity (as measured by DTI parameters) and organisation (evaluated with graph theory measures). We hypothesised that HIV exposure will alter WM integrity, however structural organisation will remain unchanged across groups.

We investigated HIV exposure and ART duration group differences in fractional anisotropy (FA) and mean diffusivity (MD) of the WM connections in the brain, as well as graph measures including strength, local efficiency, nodal efficiency, global efficiency, transitivity, and modularity. To examine these differences, a linear regression analysis was performed between the groups while correcting for maternal weight gained per week of pregnancy and maternal education.

The study found that, regardless of when ART is started by the mothers, certain regions and tracts in the brain are seemingly influenced by HIV exposure. Infants whose mothers have been on ART pre-conception have higher MD values than their unexposed and uninfected peers, while those who have been exposed to ART post-conception were shown to have lower FA values than their unexposed and uninfected counterparts. These results imply that ART duration influences WM integrity and may be neuroprotective for FA, which is more related to WM integrity, but not for MD, which relates to WM organisation.

ARV exposure duration and CD4 count are shown to be positively associated with FA tracts, while CD4 count is negatively associated with MD. This relationship highlights the potential impact of maternal immune health on fetal brain development.

While there are structural differences in certain WM tracts, the overall structural organisation remains unchanged, as no graph theory measures yielded significant results besides nodal efficiency. The brain’s dense connective network may bridge gaps from damage in specific tracts throughout the connectome.

TABLE OF CONTENTS

LIST OF FIGURES

LIST OF TABLES

LIST OF ABBREVIATIONS

AA	absolute alcohol
AD	axial diffusivity
AFNI	analysis of functional neuroimages
AIDS	acquired immunodeficiency syndrome
AP	anterior-posterior
ART	antiretroviral therapy
ARV	antiretrovirals
BL	bundle length
BW	bandwidth
CD4	cluster of differentiation 4
CNS	central nervous system
CSF	corticospinal fluid
CST	corticospinal tract
CT	computed tomography
CUBIC	Cape Universities Body Imaging Centre
DTI	diffusion tensor imaging
DWI	diffusion weighted imaging
EFV	Efavirenz
EPI	echo-planar imaging
FA	fractional anisotropy
FATCAT	functional and tractographic connectivity analysis toolbox
FDR	false discovery rate
fNT	fractional number of tracts
fNV	fractional volume
FOV	field of view
FTC	Emtricitabine
GA	gestational age
GM	grey matter
GRAPPA	generalised auto-calibrating partially parallel acquisitions
HEU	HIV-exposed uninfected

HIV	human immunodeficiency virus
HUU	HIV-unexposed uninfected
IQR	inter-quartile range
IUGR	intrauterine growth restriction
MD	mean diffusivity
MEMPRAGE	multi-echo magnetisation prepared rapid gradient echo
MRI	magnetic resonance imaging
MTCT	mother-to-child transmission
NNRTI	non-nucleoside reverse transcriptase inhibitor
NRTI	nucleoside reverse transcriptase inhibitor
NV	number of voxels
PA	posterior-anterior
PCR	polymerase chain reaction
PI	protease inhibitor
PMTCT	prevention of MTCT
Q_L	lower quartile
Q_U	upper quartile
RBA	region based analysis
RD	radial diffusivity
RF	radiofrequency
ROI	region of interest
SARS	severe acute respiratory syndrome
TB	tuberculosis
TDF	Tenofovir
TE	echo time
TORTOISE	tolerably obsessive registration and tensor optimisation indolent software ensemble
TR	repetition time
VL	viral load
WHO	World Health Organisation
WM	white matter

1. INTRODUCTION

1.1. Background

HIV (human immunodeficiency virus) is a virus that targets and alters the immune system. HIV can lead to increased risk of infection for other diseases such as diabetes, hepatitis, TB, and death if left untreated.

HIV became a global epidemic in the late 20th century and continues to burden humans worldwide. There are approximately 38 million people living with the disease globally as of 2020 (UNAIDS, 2021), with over 79 million infections and 36 million deaths being incurred since the start of the epidemic. Only 70% of people living with HIV are receiving treatment (UNAIDS, 2021).

The impact of the disease changed after the development of antiretrovirals (ARVs), a treatment that helps lower the amount of HIV cells (known as the viral load) in the body. Since the creation of ARVs, UNAIDS and the World Health Organisation (WHO) developed a Global Plan which entails working towards keeping mothers alive and the prevention of mother to child transmissions (PMTCT) by 2015 (World Health Organisation, 2013). Updated guidelines aim to deliver full access to ARV drugs in order to accomplish the goal of ending the HIV epidemic as a major public health threat by 2030 (World Health Organisation, 2016).

The rise of the Global Plan has led to a new cohort of children who have in utero exposure to maternal HIV but remain HIV negative through the use of antiretroviral therapy (ART), known as HIV exposed uninfected (HEU) children. While the children are HIV negative, the effects of exposure to in utero HIV and ARVs on their development is not well known or understood. The rise of this new population creates a need for studies to determine whether HIV and ART exposure in utero and at birth have adverse effects on infants.

The proposed study aims to examine the influence of maternal HIV exposure on white matter organisation in a cohort of neonates. In addition to HIV exposure, the study will also look at the influence of ART exposure duration on in utero infants, as the HEU infants in the study are exposed to ART for either the full gestation term, or from 4-7 months since conception.

1.2. Motivation for study

Sub-Saharan Africa is severely affected by the HIV epidemic, with over 69% of the worldwide population of individuals known to be living with HIV residing in South Africa alone (UNAIDS, 2021). In 2019, over 7.5 million people in the country were living with the disease. UNAIDS estimates that 24% of the 15 million HEU children worldwide live in South Africa (Slogrove et al., 2020; UNAIDS, 2021). Even though new infections in South Africa have decreased by approximately 16% since 2010 (UNAIDS, 2021), HIV and its many consequences are still a major issue in South Africa due to its high prevalence.

South Africa has the world's largest ART programme (UNAIDS, 2021). In the Western Cape province of South Africa, where the current study is taking place, the number of pregnant women given ART has increased due to the government's implementation of WHO's PMTCT Option B+ treatment plan. The Option B+ treatment plan ensures that all pregnant women living with HIV receive a triple-drug ARV regimen regardless of their CD4 count or clinical stage; treatment boosts the women's immune system and prevents vertical HIV transmission (World Health Organisation, 2013; National Department of Health, 2019; Mudaly & Voget, 2020). This has subsequently contributed to an increased number of uninfected newborns born to mothers living with HIV. While the number of perinatal HIV infections has decreased to 0.74% as of 2019 (compared to 3.6% in 2011) as a result of the implemented treatment plan (National Department of Health, 2019), the long-term effects of the treatment are not well understood. While ART taken during pregnancy reduces the risk of transmission, there is some evidence suggesting that children born under the ART scheme experience a greater risk of neurodevelopmental delay compared to HIV-unexposed-uninfected (HUU) children (McHenry et al., 2018).

Previous studies established that the basic structural wiring of the brain is already in place at birth (Girault et al., 2019). White matter (WM) connections play an integral role in cognition because they facilitate rapid transmission of information between different brain areas (Girault et al., 2019). WM connections can be studied using diffusion weighted imaging (DWI), a form of imaging that uses the random movement of water molecules in the brain to generate contrast (Pannek et al., 2013). Diffusion tensor imaging (DTI) is a specific type of modelling of DWI data that yields measures reflecting WM properties.

One way to use DTI outputs is by characterising the anatomical WM connections as networks. Graph theory is a mathematical framework used in imaging studies to describe aspects of brain organisation. The WM connectome (a network of WM connections) may be represented as a graph, i.e., a set of WM connections characterised by DTI measures (graph's edges) (Song et al., 2017) between a set of grey matter (GM) regions of interest (ROIs) (graph's nodes) (He et al., 2018). WM connectomes may be used to quantify the structural integrity and organisation of the brain (Song et al., 2017).

Few brain imaging studies have been done in HEU infants and children, making the proposed work unique. Identifying WM abnormalities within this population will provide insight into the early effects of HIV and ART exposure in infants. In a broader context, these results will be useful in better understanding the influence of maternal health in pregnancy on fetal and infant brain growth.

Economic and environmental exposure factors that may cofound the results of the study are minimised in a newborn cohort. This study has access to a large, homogeneous population of women that have a low prevalence of substance abuse. The presence of a government regulated and standardised treatment programme further reduces variation within the study group, making this an ideal study cohort.

The proposed study aims to quantify the influence of maternal HIV exposure on WM development in neonates by examining differences in WM connectomes between HUU and HEU children. In addition, the study will assess whether duration of in utero exposure to ART influences WM connectomes.

2. LITERATURE REVIEW

2.1. HIV development

Since HIV is a viral infection, it primarily assaults the body's immune system by attacking T cells (lymphocytes) called CD4 cells. HIV invades them and uses the cells as a mechanism to multiply and spread throughout the body. This mechanism weakens a person's immune system, which gives the virus access to the central nervous system (CNS), releases neurotoxic factors and causes neurological damage (Wachsler-Felder & Golden, 2002).

HIV has been known to affect the brain in various ways since the beginning of the epidemic (Robinson-Papp & Saylor, 2021). While the associated damage from HIV infection has been mitigated through the adoption of ART, even individuals who receive ART treatment can still develop less severe neurological and cognitive difficulties and suffer damage to specific brain structures (Robinson-Papp & Saylor, 2021). The basal ganglia, a subset of subcortical structures in the brain, has been particularly affected by HIV in numerous studies (Berger & Nath, 1997; Cohen et al., 2010; Vera et al., 2016; Wedderburn et al., 2022).

HIV enters the brain by migrating across the blood-brain barrier (BBB) through infected monocytes or lymphocytes (Ene, 2018). HIV does not directly infect neurons. Increased levels of macrophages (differentiated monocytes) and increased extracellular neurotoxic protein levels from glial cell (astrocyte) activation results in neuronal disturbances and subsequent neuronal injury (Ene, 2018). The presence of these neurotoxins results in white matter damage like diminished myelin and axon integrity throughout the brain (Ellis, Langford & Masliah, 2007). The injuries may also result in cognitive impairment (Everall et al., 1999; Baker et al., 2017). Local production of chemokines and cytokines – proteins that coordinate the immune response within the body (Ramesh, Maclean & Philipp, 2013) – together with systemic inflammation may also contribute to neuronal injury (Vera et al., 2016; Ene, 2018). Deviations in immune response protein production are a main proponent of neurodegeneration, demyelination and neuroinflammation in the CNS (Ramesh, Maclean & Philipp, 2013).

HIV is transmitted in three ways: by unprotected sexual intercourse or donated semen; through blood or blood products or organs; or from a mother living with HIV to her child via vertical or mother-to-child transmission (MTCT) (World Health Organisation and UNAIDS, 1998). Through the implementation of ART the rates of MTCT have greatly decreased, but the influence of maternal HIV exposure on the HEU infants and their brains is still not well understood.

2.2. ART regimen protocol

The provision of ARVs for PMTCT has notably risen in low and middle-income countries through the Global Plan, with the number of pregnant women receiving ART in Eastern and Southern Africa rising from 10% in 2004 to 49% in 2010 (WHO, UNAIDS & Unicef, 2010), and to 93% in 2020 (UNAIDS, 2021). With the new Global Plan, the rate of MTCT has dropped to less than 1% in the Western Cape province in

South Africa, where our study is conducted. As such, there is a burgeoning population of HEU children in the area.

Early research into the effects of ART exposure in utero suggest that there is a small increased risk of congenital anomalies in HEU children (Williams et al., 2015). Certain individual ARV drugs have been flagged for having particular risks (Heidari et al., 2011).

There are several ways to administer ARVs to patients. Examples of ARV administration include monotherapy, where only one ARV drug is used, or triple therapy, as stipulated in the treatment B+ plan, where three different ARV drugs are given for the patient's entire lifetime (Heidari et al., 2011). Option B+ is an expansion on the previously available treatment options A and B, where pregnant mothers are given triple therapy for their entire lifetime regardless of their CD4 count (World Health Organisation, 2013). Option B+ drastically improved the distribution of ART, and current guidelines have since shifted to ensure all people living with HIV at any CD4 count have access to ART (World Health Organisation, 2016).

The use of triple therapy stipulates mothers utilise the treatment from as early as 14 weeks of gestation through to the end of breastfeeding (approximately 12 months postpartum) (Heidari et al., 2011). Some patients may already be on triple therapy prior to or at the very beginning of conception. Varying lengths of ART exposure during pregnancy may affect uninfected infants differently. The newborn is also given a dosage of a single ARV daily for the first 4-6 weeks (Heidari et al., 2011).

Certain studies have reported that triple therapy regimes run an increased risk of infants being born with birth defects like low birth weight (Heidari et al., 2011). Triple therapy has also been shown to suppress the viral load within pregnant mothers more effectively (Mathis et al., 2011), which in turn decreases the likelihood of the child contracting HIV. More research is needed to establish the safest treatment approach for both pregnant women living with HIV and their infant.

There are a host of factors that may influence the effectiveness of the chosen ART programme such as modes of ART service delivery, ART regimen choice, patient adherence, cost and availability of human resources, cost effectiveness of the programme, and family planning (Unicef, 2012). The use of the Western Cape province in South Africa as the study environment mitigates many of these factors as all the participants follow the same plan and receive the medication in a central location.

2.3. Fetal brain development

Brain development commences within a few weeks of conception, continuing throughout childhood and into early adulthood (Dreier, 2017). The brain is particularly vulnerable while the child is still in the womb, as fundamental structures are developing.

The fetal brain develops from the third week of gestation. At this time, neural cells start dividing and differentiating into neurons and glia (the two main cells that form the basis of the nervous system) (Konkel, 2018). Neuronal proliferation (rapid cell production) then occurs during months three to four, neuronal migration during months three to five, and finally myelination (the increased formation of fatty myelin sheaths around fibers that allows for more rapid transmission of neural information) begins during the second trimester of pregnancy and continues into adulthood (Poduri & Volpe, 2018).

2.3.1. Brain divisions

The brain can be subdivided in various ways, but it is typically broken down into three main divisions that comprise of the initial structures created by the neural tube in the embryo – the forebrain, midbrain and hindbrain (Ackerman, 1992). Another way the brain may be subdivided is through the main structures within it: the cerebrum, cerebellum and brain stem. The cerebrum is primarily involved with thinking, remembering and feeling. The cerebellum is responsible for motor control. And, lastly, the brain stem manages reflexes and automatic processes like breathing (Ackerman, 1992; Rita Carter, 2019).

2.3.1.1. Forebrain

The forebrain is the largest part of the brain, which is comprised of the cerebrum. The cerebral cortex is the outer layer and contains of over two thirds of the brains total mass (Eid, 2021). The cerebrum is further divided into four lobes in both hemispheres of the brain, according to their relative position (frontal, parietal, temporal and occipital). The cerebral cortex contains the structures that are mainly responsible for higher cognitive function such as decision making, motivation, attentiveness, learning, memory, problem-solving, the ability to produce and understand language, and conceptual thinking (Rita Carter, 2019; Kenhub, 2021). The cerebral cortex also has a wide range of functions such as maintaining awareness of sensory information, initiation of motor activity, and carrying out actions from inputs from different brain regions (Rita Carter, 2019; Eid, 2021).

Beneath the cerebral cortex lie several other specialised structures that are essential for movement, consciousness, emotion, pleasure and more, which are known as subcortical (“beneath the cortex”) structures (Ackerman, 1992). Subcortical regions are CNS information centres because they regulate and relay information across different regions of the brain (Kenhub, 2021). Subcortical structures include the thalamus, diencephalon, limbic structures and the basal ganglia.

The thalamus – the largest subcortical structure – is a relay centre between the cerebrum and the brainstem. The thalamus sorts information from the four senses – sight, taste, touch and hearing – and relays it to the cerebral cortex. The nerve impulses that initiate voluntary movement as well as pain, temperature and pressure are also transmitted through the thalamus (Ackerman, 1992; Rita Carter, 2019; Eid, 2021)

The limbic system is a group of linked structures that play a role in emotional regulation. The limbic system is comprised of both cortical (coming from the cortex) and subcortical structures. The main limbic structures in the subcortical region consist of the amygdala – a set of structures responsible for the processing of fear – and the hippocampus, which is responsible for long term memory and special navigation (Ackerman, 1992; Rita Carter, 2019; Eid, 2021).

The basal ganglia are another set of subcortical structures in the forebrain that assist in fine tuning motor function (Kenhub, 2021). The basal ganglia are comprised of the caudate, putamen, pallidum, nucleus accumbens, substantia nigra, and subthalamic nucleus. The basal ganglia fine tunes voluntary movements. The cerebral cortex sends impulses for movement to the basal ganglia, which conveys this information to the thalamus which then relays it back to the cortex. Additional higher cortical functions, such as reward processing, memory, motivation, planning and modulation of movement, and eye movements, are also mediated by the basal ganglia (Ackerman, 1992; Rita Carter, 2019; Grohs et al., 2021; Kenhub, 2021). These structures have been linked with HIV neuronal damage and neurological disorders in numerous studies (Everall et al., 1999; Berger & Arendt, 2000; Vera et al., 2016; Robinson-Papp & Saylor, 2021).

2.3.1.2. Midbrain

The midbrain is the second area of the brain, and lies between the forebrain and hindbrain. It is involved in visual and auditory processing and lies at the top of the brainstem (Eid, 2021). The midbrain is further divided into three main parts – the colliculi, the tegmentum, and the cerebral peduncles.

2.3.1.3. Hindbrain

The hindbrain, at the back of the brain, is an extension of the spinal cord. The hindbrain contains the medulla oblongata, the pons and the cerebellum. The midbrain and hindbrain combined make up the brain stem, excluding the cerebellum. The brainstem controls breathing, heart rate and blood vessel diameter (Ackerman, 1992; Eid, 2021).

The medulla oblongata, commonly referred to as the medulla, is the lowest part of the brain stem and the main connection to the nervous system. The medulla is primarily involved in heart rate regulation, digestion, breathing and sneezing, which are all autonomic actions (Eid, 2021). The nerves that pass between the spinal cord and brain traverse the medulla and cross over from one side of the body to another. This crossover results in the right brain controlling movement for the left side of the body, and the left brain controlling the right (Ackerman, 1992; Rita Carter, 2019).

The pons, which means “bridge” in Latin, is responsible for sleep, motor control, arousal and muscle tone and acts as the bridge between the lower brainstem and the midbrain (Ackerman, 1992; Eid, 2021)

The cerebellum, at the back of the head, is the second largest region of the brain. It is responsible for co-ordinating the brain's instructions for maintaining balance and for

skilled repetitive movements (Ackerman, 1992). The cerebellum is also thought to be a critical area for processing procedural memory. Many disorders of the cerebellum are associated with motor impairment (Eid, 2021).

The structures that were outlined above are already present in neonates at birth. Understanding the structure and function of the different brain regions may help us interpret any differences within structures and hypothesise on their effects on the infant cohorts being studied.

2.4. Effect of viruses on maternal and fetal health

Fetuses depend entirely on their mothers during conception to provide nutrients and a suitable environment for their development to occur. Brain development commences within a few weeks of conception, continuing throughout childhood and into early adulthood (Dreier, 2017). The brain is particularly vulnerable while the child is still in the womb, as fundamental structures are still developing. The maternal response to adverse situations, such as viral infection, during this sensitive period may influence the development of the fetus's brain, leading to short or long-term consequences.

Since different stages of pregnancy control brain development, the timing of maternal illness may impact the fetus differentially. Early exposure to harm is related to structural defects such as neural tube defects, while later damage is associated with abnormal cortical development. Damage incurred during late gestation was associated with cognitive, behavioural and psychiatric disorders (Ginsberg et al., 2017).

Various research studies have established a relationship between an unhealthy intrauterine environment and abnormal fetal brain development (Dreier, 2017; Ginsberg et al., 2017; Racicot & Mor, 2017). Maternal infection can potentially alter the fetal environment, and therefore impact the developing brain. While viral infections in pregnancy are related to adverse pregnancy outcomes and birth defects in offspring, there are not many therapeutic or preventative tools that can be used to protect the mother and fetus during viral outbreaks or pandemics (Racicot & Mor, 2017). However, in the case of HIV infection, ART may be a potential preventative measure through its ability to prevent HIV proliferation.

Viruses are tiny infectious agents that reproduce inside living hosts. They result in various diseases such as the common cold, influenza, and herpes. Many serious diseases such as rabies, Ebola virus disease, Zika virus disease, AIDS (HIV), and Severe acute respiratory syndrome (SARS) are also caused by viruses. Viral infections in humans result in the body provoking an immune response that typically eradicates the infection (Racicot & Mor, 2017). However, in pregnant women the resulting immune response may result in adverse effects in the fetus through actions such as inflammation and fever. The findings from studies about the immune response generated from different viruses can potentially help us better understand the impact of HIV on fetal development.

The biological mechanisms through which prenatal infection can cause neurodevelopmental impairment are not clearly understood (Dreier, 2017). While some infections may be directly transmitted from the mother to the fetus during pregnancy, this phenomenon is typically quite rare. Despite viral infections rarely crossing over into the placenta, their presence on the maternal side may still affect fetal development. Neuronal development is vulnerable to infections through maternal immune system activation, although the specific mechanisms are not clear (Racicot & Mor, 2017)

Studies have established that even indirect contact with a viral infection can lead to adverse effects in fetuses, and that specific neurodevelopmental outcomes have been linked to several types of infection. This suggests that the factors common in infection, such as the immune response and symptoms of infections, rather than the infection itself, may be the underlying factor for adverse prenatal development (Dreier, 2017).

Viral infection of cells at the maternal-fetal interface can disturb placental function, as it can result in the production of soluble immune factors that may potentially affect fetal development (Racicot & Mor, 2017). The interaction may also lead to adverse pregnancy complications such as preterm birth, intrauterine growth restriction (IUGR), or miscarriage (Racicot & Mor, 2017).

Since we are unable to directly study the biological mechanisms that affect fetal development in humans, animal models are a helpful tool for understanding the complex mechanisms that are taking place. Research using animal models has found possible maternal immune pathways and cytokines that may be responsible for behavioural changes in offspring (Racicot & Mor, 2017).

When viral infection occurs during pregnancy, the maternal immune response may lead to fever. It has been hypothesised that the cellular processes during fetal brain development, such as proliferation, migration, differentiation, myelination and apoptosis, may be disrupted as a result of the elevated maternal body temperature (Dreier, 2017). This disruption may then cause neurodevelopmental impairment in the child, which in turn which may become more evident as the child grows.

Animal studies have implicated elevated body temperature in a range of adverse effects such as IUGR, malformations, fetal death, behavioural alterations and impaired cognitive function (Dreier, 2017). The results from various animal studies also indicate that severe maternal inflammation can disturb the pro-inflammatory status of the amniotic fluid, fetal serum, and the chorio-amnion membranes, which are all associated with fetal brain injury (Dreier, 2017). These studies have also established that the time of infection may also be a factor. In early gestation, the fetal immune system is still being developed and the fetal anti-inflammatory response at this time is less effective. As a result, the earlier maternal inflammation occurs, the more harmful the impact on the fetus (Ginsberg et al., 2017). This finding will be contrasted against our cohort as ART duration will hopefully displace or decrease the impact of maternal infection and inflammation proportionally.

Infections such as influenza, urinary tract infections, vaginal infections, upper respiratory tract infections, and diarrhoea are examples of common infections (Dreier, 2017). It has been estimated that around 60% of all pregnant women experience at least one infection while pregnant (Dreier, 2017). This highlights the need to further clarify and investigate the impact that exposure to various viral infections may have on fetal development.

2.5. HIV and pregnancy

HIV has been shown to have some adverse effects on maternal health, fetal development and later development of the child. In this section we investigate how HIV may affect pregnancy and vice versa to determine how the body may change when women living with HIV become pregnant and whether there are any associated adverse effects.

2.5.1. Effect of pregnancy on the natural history of HIV infection

During pregnancy, the body's immune function decreases in women living with and without HIV. This is shown through a decrease in antibodies and reduced complement levels (levels of immune-supporting proteins in the blood) in early pregnancy (Abu-Raya et al., 2020). These common changes during pregnancy led to initial concern that pregnancy and its effects could accelerate the progression of HIV infection (World Health Organisation & UNAIDS, 1998). While early studies showed support for this idea, more recent global cohort studies found no significant difference in the rate of disease progression between pregnant and non-pregnant women living with HIV (Gray & McIntyre, 2007). During the postpartum period, the decline in the CD4 cell count experienced during pregnancy typically resolves, and is generally attributed to haemodilution. However, some studies have shown an increase in the viral load postpartum despite HIV RNA levels seemingly remaining stable during pregnancy (González et al., 2017).

2.5.2. Effect of HIV infection on pregnancy

Earlier studies conducted in the developed world reported that HIV infection has a negligible effect on pregnancy outcome or complications (World Health Organisation & UNAIDS, 1998). However, these earlier studies were conducted primarily in affluent countries, where both health systems and disease burden are significantly different when compared to developing countries (González et al., 2017). Adverse pregnancy outcomes, including early and late pregnancy complications, have been reported more commonly in studies done on the African continent. However, it is hard to determine the contribution of HIV in these studies, as other factors like drug use, inadequate antenatal care due to overburdened health systems and the prevalence of concurrent infections may also influence pregnancy health and pregnancy outcomes. HIV may be the direct cause of adverse pregnancy effects or, more likely, it indicates a complicated relationship between medical and social conditions that influence pregnancy. Thus far, studies have not demonstrated any significant association between HIV and

pregnancy outcomes (World Health Organisation & UNAIDS, 1998; González et al., 2017). Pregnancy complication rates differ across studies and may show the scope of the HIV epidemic as well as the varied nature of HIV-related disease across the globe (World Health Organisation & UNAIDS, 1998).

In terms of physical health, HIV infection during pregnancy can result in health risks becoming more common than in cases where pregnancy occurs in women who are not living with HIV. HIV infection during pregnancy increases the likelihood of certain infections and early and late complications occurring during conception.

The following pregnancy complications have been found to occur more often in women living with HIV: infections such as pulmonary and extra-pulmonary tuberculosis, pneumonia, urinary tract infections, sexually transmitted diseases, opportunistic infections, severe chicken pox or shingles; early complications such as miscarriage and ectopic pregnancies; and late complications such as chorioamnionitis, doubled risk of stillbirth, IUGR, (especially if the mother is underweight), anaemia, preterm labour, abruptio placentae, and prelabour rupture of the membranes, especially if chorioamnionitis is present (González et al., 2017). One study performed in Mozambique found that incidences of hospitalisation amongst women living with HIV during pregnancy were increased when compared to those of the controls (González et al., 2017).

A study conducted by Zaba et al. (2013) found that HIV infection posed an increased risk in maternal deaths either during pregnancy or post-partum in Sub-Saharan Africa. In developed countries, HIV infection is a rare cause of maternal mortality due to better access to specialist care. In contrast, HIV infection has been found to be a significant contributing cause of maternal mortality in Africa, especially in areas of high HIV prevalence (Gray & McIntyre, 2007). Pregnant or post-partum women living with HIV had eight times higher mortality than their counterparts living without HIV (Zaba et al., 2013), though the study was completed during a time when ART was only just beginning to become widely available. This highlights the importance of programmes like the WHO Option B+ programme that provides participants access to appropriate healthcare services and medication.

2.5.3. Effect of HIV infection on neonatal birth outcomes

In the era before widespread ART was administered worldwide, maternal HIV infection was related to increased prematurity, neurological impairments, and low birth weights (<2500g) (Heidari et al., 2011). These birth defects have also been identified amongst HEU children. Other birth defects that have been associated with HEU children include mitochondrial toxicity, structural and functional changes in the CNS, and hematological abnormalities (Heidari et al., 2011; Sirois et al., 2013). Several studies have also gone on to state that children born to mothers living with HIV have a higher risk of mortality regardless of their HIV infection status (Newell et al., 2004). While the impacts of HIV on general and neurological development are better understood, the

potential consequences of HIV and ART exposure on uninfected infants is not yet well understood.

Thus, HIV infection has been shown to have long-term effects on maternal morbidity and future neonatal health outcomes, especially within Sub-Saharan Africa.

2.6. Overall impact of in utero ART exposure

The rates of birth defect prevalence in HEU children globally have typically been close to the general expected rate amongst all births, with some studies finding a slight increase in percentage being observed (Heidari et al., 2011). These numbers often do not account for the presence of HIV status or overall ARV exposure.

Studies from the era before ARVs have the advantage of being able to explore the effects of HIV exposure without the potential confounding effects of ART (Wedderburn et al., 2019). However, these studies may not be relevant in the modern era where almost all HEU children have also experienced in utero ART exposure.

The impact of in utero exposure to HIV and ART (as all HEU children are given ART for the first month) on neurological development are difficult to study in isolation as external factors such as economic, environmental and psychological impacts may also be an influence. Infant cohorts from similar environments are advantageous as they minimise socioeconomic and parental confounders.

Different classes of ARV drugs attack different key components of HIV molecules to render them ineffective, the most notable being protease inhibitors (PIs), nucleoside reverse transcriptase inhibitors (NRTIs) and non-nucleoside reverse transcriptase inhibitors (NNRTIs) (Sirois et al., 2013). According to Heidari et al. (2011), the presence of efavirenz, a NNRTI drug, was thought to cause neural tube defects. However, data from a US study shows a birth defect rate of 2.8% versus the overall birth defect rate of 2.7% among uninfected women (Heidari et al., 2011), so this again suggests that the risks associated with this specific ARV are mild.

Studies on the prevalence of prematurity in HEU infants yield mixed results, with triple drug ART therapy being associated with premature births in European and English cohorts but not in US cohorts (Heidari et al., 2011). The studies considered made use of different screening systems for isolating variables such as ART exposure period and drug use, making consequent results difficult to compare.

While there is controversy around the safety of these ARVs during pregnancy (Slogrove, Cotton & Esser, 2010), they are currently the best methods for ensuring MTCT does not occur. While the benefits of ARVs on preventing MTCT ensure ART's continuous use, there is still potential for ART to have negative effects on the neonate body and brain, and fetus brain development (Wedderburn et al., 2019). The impact of in utero exposure of ARVs on overall development should be further explored where possible.

2.7. Neurological impact of HIV and ART exposure

Most studies on HEU children primarily focus on their neuropsychological outcomes as opposed to the physical structure of the brain. Studies on the neurodevelopment of HEU and HUU cohorts are already limited as different studies have diverse study environments and no standardised definitions of certain outcomes (Wedderburn, et al., 2019). Furthermore, these studies conclude with varying and inconsistent results.

The suggested impacts on HEU children include increased risk of neurological symptoms such as hindered social and motor developments, slow early growth and subtle speech and language delay (Slogrove, Cotton & Esser, 2010; Heidari et al., 2011; le Doaré, Bland & Newell, 2012), though some studies suggest there are no differences between HEU and HUU children at all. Neurodevelopment studies using neuropsychological tests show conflicting stories regarding HEU children. Some studies report exposure differences, while some do not. The lack of consensus makes the proposed research project especially relevant.

The impact of HIV and ARV exposure in utero on neurodevelopment were investigated as separate variables in the review article by McHenry et al. (2018). The study finds children with ARV exposure have lower cognitive and motor scores than those without ARV exposure. The authors advise caution interpreting these results as ARV exposure is difficult to measure in isolation (McHenry et al., 2018).

Although there is a growing number of neonatal imaging studies, little is known about the features of the neonatal brain that support the consequent development of neurocognitive abilities in early childhood (McHenry et al., 2018). Within HIV and ART exposure, there has only been one neonatal imaging study. The few brain imaging studies in infants/children find either no differences or small exposure differences, and the impact of the identified small changes are unknown.

2.8. Magnetic Resonance Imaging

Magnetic resonance imaging (MRI) is used in clinical and research applications to study the body in vivo non-invasively. MRI produces 3-dimensional detailed anatomical images (NIH & NIBIB, 2021). MRI has been greatly applied in neuroimaging in particular as it enables the different tissue types present in the brain, GM, WM, and cerebrospinal fluid (CSF), to be visualised and investigated in great detail (le Bihan, 2020). MRI enables soft tissues to be visualised in good contrast, unlike other imaging modalities, e.g., X-ray or CT scans.

MRI works by studying the interaction of high static magnetic fields with the magnetic moments of atoms inside of specific tissues (Berger, 2002). Only atoms with nuclei consisting of an odd number of protons or neutrons can be used for MRI.

Over 60% of the entire body is composed of water, with the brain itself containing 73%. Water has two hydrogen atoms; whose nuclei are comprised of a single proton. Because of this fact, hydrogen is regularly used as an imaging source in MRI (Vassiliou et al., 2018).

The main components of an MRI machine include a large magnet, magnetic field gradients and radiofrequency (RF) coils (Moser et al., 2009). The large magnet creates a strong static magnetic field of 1.5 or 3 Tesla (T) in the direction of the z axis, which is also referred to as the longitudinal direction (Grover et al., 2015). This strong magnetic field, referred to as $\mathbf{B_0}$, makes the hydrogen protons align in the direction of the field, producing a net magnetisation vector **M**.

As the magnetic field $\mathbf{B_0}$ is applied to the body, the hydrogen proton's angular momentum from its spin makes it rotate, or precess, around the $\mathbf{B_0}$ field at a specific frequency that is proportional to the field strength (Grover et al., 2015). This frequency is called the Larmor frequency, described by the equation below:

$$\omega_0 = \gamma B_0 \tag{1}$$

Where ω_0 is the angular precession frequency of the protons, and γ is the gyromagnetic ratio that is constant for each atom (for hydrogen, it is 42.6 MHz/T).

When energy, in the form of radio waves, is added to the magnetic field, the magnetisation vector can be deflected away from its original axis. In MRI machines, a RF pulse is tuned in to the Larmor frequency (creating an oscillating magnetic field denoted as $\mathbf{B_1}$) and is applied (typically perpendicularly) to $\mathbf{B_0}$ and results in the hydrogen protons precessing along the xy axis in the transverse plane for as long as the RF pulse is on (Berger, 2002). This process of supplying energy at the Larmor frequency is known as nuclear magnetic resonance (Pooley, 2005). The amount that the magnetisation vector deviates from $\mathbf{B_0}$ is given by the flip angle, which is characterised by the amplitude and duration of the RF pulse.

After $\mathbf{B_1}$ has been terminated, the magnetisation vector returns to its original state, i.e., realigns with the axis of $\mathbf{B_0}$, the main magnetic field (Berger, 2002; Grover et al., 2015). The gradual return to $\mathbf{B_0}$ is marked by two independent time constants: T_1 "spin-lattice" relaxation time and T_2 "spin-spin" relaxation time (Vassiliou et al., 2018). T_1 is defined as the time it takes for the longitudinal component of the magnetisation vector to return to at least 63% of its net magnetisation M_0, while T_2 is defined as the time it takes for the transverse component of the magnetisation vector to decay to 37% of net magnetisation M_0 (Grover et al., 2015). Both of these time constants are represented by the following equations and corresponding figure below:

$$M_z(t) = M_0\left(1 - e^{-\frac{t}{T_1}}\right) \tag{2}$$

$$M_{xy}(t) = M_0 e^{-\frac{t}{T_2}} \tag{3}$$

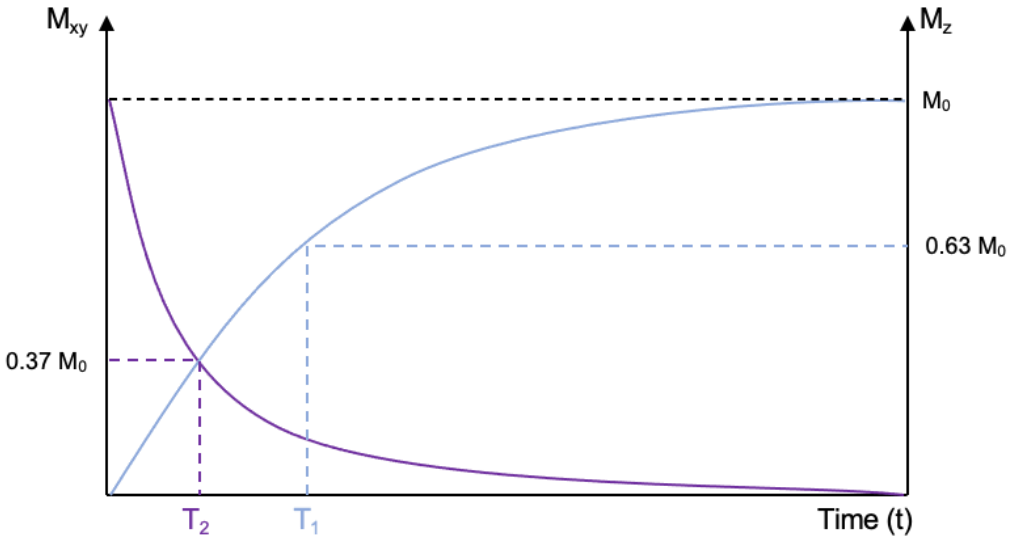

Figure 1: T_1 and T_2 relaxation times shown across the M_z and M_{xy} magnetisation planes. Adapted from (Ohene, 2020).

What is important in the context of this study is that different tissue types in the brain (grey and white matter and even different brain structures) have different values of T_1 and T_2, due to different signal contrasts. Furthermore, in order to study WM, the MRI sequence that excites the protons additionally utilises gradient field pulses to capture the signal of the water molecules moving across the brain through an imaging technique called diffusion tensor imaging (DTI) (Mori & Zhang, 2006) (further detailed in section 2.9 below).

The proposed study intends to utilise DTI to identify structural differences in WM within the neonate brains. Previous DTI studies including HEU children are summarised in Table 1 below.

There are GM regions connected by WM tracts that are found to have common (HEU/HUU) group differences between DTI properties in the studies highlighted below. Common GM regions include the inferior occipital gyrus, middle frontal gyrus, the cuneus, superior frontal gyrus, right supramarginal gyrus and the right superior frontal gyrus. Common WM tracts that were identified in the studies include the right posterior corona radiata, the cortical spinal tract, middle cerebellar peduncles and the left superior and inferior fronto-occipital fasciculus (Tran et al., 2016; Jankiewicz et al., 2017; Yadav et al., 2020).

Table 1: Summary of studies completed on HEU and HUU subjects using DTI and cognitive tests.

Study Author	**Study Aim**	**Sample size, age range and ART exposure**	**Study Results**
(Jahanshad et al., 2015)	Using DTI and volumetrics to compare brain anatomy between HEU and age-matched HIV-unexposed and uninfected (HUU) children from Thailand	30 HEU children and 33 age-matched HUU children Age range: 5-15 years Mean age: 10.3 ±2.8 58% of cohort was male ART-exposed	Brain volume maps and microstructural anatomy were compared across groups; and neuropsychological test performance and neuroimaging measures were tested for any associations between them. No group differences in DTI metrics or brain volume was found between HEU and HUU after controlling for age, sex, maternal education level and income. The mean fractional anisotropy in the corpus callosum was 0.375 in HEU verses 0.370 in HUU. Higher IQ scores were associated with higher FA and lower mean diffusivity (MD) in both group analyses.
(Tran et al., 2016)	Using DTI to explore the integrity of regional white matter	15 HEU neonates and 24 age-matched controls	The middle cerebellar peduncles of HEU infants had higher FA

	microstructure in HEU infants shortly after birth.	Age range: 2-4 weeks old Mean age: 38.4 weeks (HUU) 37.8 weeks (HEU) 54% of cohort was male ART-exposed	compared to HUU infants after controlling for age and gender. In HEU infants, FA in the left uncinate fasciculus (UF) was positively associated with scores on the Dubowitz abnormal neurological signs subscale
(Jankiewicz et al., 2017)	Using DTI to examine WM in HIV+, HEU and HUU 7-year-old children. The study conducted was a follow up of the same cohort that was studied at 5 years old.	65 HIV+ children, and 46 age-matched controls, further broken down as 19 HEU and 27 HUU children Age range: 7 years Mean age: 7.3 ± 0.2 (HUU) 7.2 ± 0.1 (HEU) 54% of cohort was male ART-exposed (HEU control group)	At 7+ years, the study found two clusters in WM tracts with lower FA in HIV+ children compared to HUU controls in the left inferior fronto-occipital fasciculus (IFOF), and left inferior longitudinal fasciculus (ILF). In a cluster in the IFOF, higher MD was observed in both the left and right hemispheres (bilaterally), as well as in multiple clusters bilaterally in the superior corona radiata (SCR), the anterior thalamic radiation (ATR) and the right forceps minor.

			Unlike HIV+ children at 5 years, they found ART initiation had no impact on WM. In HEU children, the study found a cluster in the right posterior corona radiata with higher FA compared to HUU children, while lower MD was found in bilateral regions in the corticospinal tract (CST).
(Yadav et al., 2020)*****	To investigate the effect of in-utero exposure of ART on cerebral gray and white matter. This was done by evaluating the brain's microstructural integrity (using DTI) and cognitive function in HIV uninfected children born to HIV infected mothers (HUC) compared to healthy children born to normal mothers (CHNM) and HIV infected children born to HIV infected mothers (HIC). Using DTI data for neuropsychological (NP) assessment.	22 HIC, 8 HUC and 18 age matched controls (CHNM) Age range: 10-13 years Mean age: 12 ± 2.8 (CHNM) 10 ± 1.8 (HUC) 10 ± 2.3 (HIC) 54% of cohort was male ART exposed	In the study, NP test scores in several sections were found to be significantly decreased in HIC and HUC groups compared to CHNM. HIC had lower NP test scores than those seen in HUC. In multiple brain regions, HIC had decreased FA and increased MD values compared to both CHNM and HUC. HUC had lower FA as well as both increased and decreased MD in different brain regions compared to CHNM.

			Altered FA and MD values from different brain regions in HIC and HUC had both positive and negative associations with NP test scores.
(Madzime et al., 2021)	Mapping DTI white matter connections linking gray matter regions that form resting-state (RS) functional networks to demonstrate whether structural and functional connectivity alterations in HIV infection and exposure may be related in HIV+ and HEU children (CHEU)	61 HIV+ children, and 46 age-matched controls, further broken down as 19 HEU and 27 HUU children Age range: 7 years Mean age: 7.2 ± 0.1 (HIV+) 7.3 ± 0.2 (HUU) 7.2 ± 0.1 (HEU) 50% of cohort was male ART-exposed (HEU control group)	Study found altered white matter integrity in the somatosensory, salience, default mode, and motor networks of CPHIV compared with CHU. The superior temporal cortex, superior frontal cortex, and putamen were affected in all four networks and have also been reported to demonstrate morphological alterations in the same cohort. In CHEU, white matter integrity was higher in the visual network, pDMN, and motor network compared with CHUU.

*Study uses different naming convention to classify HIV+, HEU and HUU children. HIC is HIV+, HUC is HEU and CHNM is HUU. The naming convention is specified in the table.

2.9. Diffusion Tensor Imaging and its applications in neonates

DTI is a technique to describe the properties of WM microstructure using the random movement of water molecules in the brain (Pannek et al., 2013). DTI's basic principle asserts that water molecule diffusion depends on tissue type, integrity, architecture and presence of barriers, which then can be mapped quantitatively. The nature of diffusion in the brain allows different structures to be identified relative to the direction of their water movement, such as axonal organisation and hence neural (WM) tracts (Mori & Zhang, 2006).

Diffusion in WM is anisotropic, i.e. dependent on tissue orientation and direction, in contrast to isotropic diffusion of water observed in GM tissue (Soares et al., 2013). Diffusion of water molecules can be modelled geometrically as an ellipsoid. This ellipsoid is a 3-dimensional representation of the diffusion distance of water molecules in the X, Y, and Z planes in a set diffusion time (Curran, Emsell & Leemans, 2016) as calculated in an imaging voxel (a small 3-dimensional volume). The ellipsoid's radii in each of its principal directions define a diffusion vector (Soares et al., 2013).

One can extract different diffusion metrics from the diffusion vector. The metrics can be further assessed to give information on the properties of WM tracts. Metrics that are typically assessed include the overall molecular diffusion rate, often done using mean diffusivity (MD); the directional preference of diffusion, known as fractional anisotropy (FA); the diffusion rate along the main axis of diffusion, axial diffusion (AD); or the rate of diffusion along the transverse direction of diffusion, radial diffusion (RD) (Soares et al., 2013). Each of the standard measures and their significance within WM is further detailed below.

2.9.1. Mean Diffusivity

Mean diffusivity (MD) reflects the average amount of water diffusion within a voxel (Curran, Emsell & Leemans, 2016), where a voxel is a unit of volume of the 3-dimensional image (voxel can be defined by resolution of the image: 2x2x2 mm^3). Mathematically, MD is given as a mean of components of the diffusion vector and therefore one can say that MD gives an overall diffusivity independent of direction. MD is high in regions where water diffuses more freely, and lower in regions of high tissue complexity as this creates diffusion obstacles (Curran, Emsell & Leemans, 2016). This property means that MD is typically low within WM due to the large number of axonal connections present (Curran, Emsell & Leemans, 2016).

In infant brains, MD is often significantly higher than in mature adult brains because brain water content decreases during maturation (Curran, Emsell & Leemans, 2016). In infant brains, the majority of axons are unmyelinated and structures such as cell and axonal membranes are less densely packed, so water is more readily able to diffuse perpendicularly. It is important to note behavioural brain differences within different age groups so that results may be interpreted appropriately.

2.9.2. Fractional Anisotropy

Fractional anisotropy (FA) is used as an index of the amount of anisotropy within a specified region (Soares et al., 2013). FA is generally used to quantify the ratio between the magnitude of the anisotropic component of the diffusion vector, and the magnitude of that vector. FA values lie in the range of 0-1 – where 0 means diffusion is isotropic (no preferred direction) and 1 means the diffusion is only occurring along one direction – and is typically lower within infants (Curran, Emsell & Leemans, 2016). In tissue, FA describes the directional coherence of diffusivity and for this reason is used as a quantitative marker of WM integrity (Curran, Emsell & Leemans, 2016). This stance developed from pathological studies showing that reduced FA is associated with neurodegenerative processes (Assaf & Pasternak, 2008) and developmental studies showing that an increase in FA occurs through infancy to adolescence. In addition, improved performance in cognitive areas is often associated with increased FA (Curran, Emsell & Leemans, 2016).

The degree of anisotropy is associated with axon density and axon count, and while the degree of myelination relates to FA as well, it does not define tissue anisotropy. Since axon count and myelination are strongly related, it is very difficult to distinguish between changes in their structure when looking at FA differences (Assaf & Pasternak, 2008); hence FA should not be equated as being a direct indicator of myelination or myelin damage (Curran, Emsell & Leemans, 2016). FA changes need to be assessed in combination with changes in the other principal directions of diffusion to give a more holistic interpretation.

2.9.3. Axial and Radial Diffusivities

Axial diffusivity (AD), also known as longitudinal or parallel diffusion, refers to diffusivity on the principal axis of the diffusion ellipsoid. Radial diffusivity (RD), also known as transverse or perpendicular diffusion, refers to diffusivity perpendicular to the principal direction of the diffusion ellipsoid, i.e., RD is an average of diffusion along the ellipsoid's two minor axes (Curran, Emsell & Leemans, 2016).

Studies have found associations between AD and RD and specific microstructural features (Curran, Emsell & Leemans, 2016). AD is typically associated with axonal damage and fragmentation, while RD has been related to fiber coherence, myelin integrity, axonal diameter, and axonal density (Curran, Emsell & Leemans, 2016). While this a general application of these two parameters, it is important to note that the directional diffusivity is not always aligned with the underlying tissue structure and is not consistently preserved in pathological tissue (Curran, Emsell & Leemans, 2016). Changes in AD and RD typically drive changes in FA due to their manipulation of the diffusion tensor in the longitudinal and transverse planes (Lebel et al., 2012; Tian & Ma, 2017).

The specified measures will be related to the study dataset to determine whether there are any structural differences in the WM connections of HEU compared to HUU neonates.

2.10. WM organisation and connectomes in neonates

The brain's WM tissue is composed of various cell types and fibers that interact with one another and connect different anatomical regions (made of GM tissue) (Dubois et al., 2014). The human brain has a vast network of WM connections that mature throughout the human lifespan, but most especially at the early stages of life (Girault et al., 2019).

As stated above, brain development may be broken down into two main stages. The first stage, during the last trimester of pregnancy, is the formation of short and long connections between areas of the brain (Dubois et al., 2014), which has been shown to be an early adult-like organisation of neural networks. The final stage, which continues to progress well into adulthood, involves the maturation and myelination of these fibers to allow for efficient information transfer between the regions (Dubois et al., 2014). Thus, at birth, a large network of WM connections has already been developed, which may be referred to as a connectome (Ball et al., 2014).

Previous tractography studies support the idea that most of the functional wiring within the brain is established in utero (Girault et al., 2019), and may be studied by looking at the properties of WM connectomes of early brain scans of neonates. This study aims to identify whether there are any differences in the structure and development of the existing WM networks present at birth between the HEU and HUU groups. The more expansive nature of connectomes should allow for increased insight into the structure of neonate brains and the differences between the two groups should there be any.

2.10.1. Graph theory

Graph theory, in the context of the WM connectome, requires discretisation of the brain into distinct nodes (GM regions) and interconnecting edges (WM tracts, each characterised by a set of DTI measures) (Fornito, Zalesky & Breakspear, 2013). Graph theory metrics give a quantitative measure of how WM within the brain is organised. Analysis of the WM connectome utilises certain metrics from graph theory to quantify and distinguish the nature of the WM connections within the brain. For completeness, it is important to state that the graph may be created from functional data (e.g. functional connectome using resting-state fMRI) or DTI data; the proposed project aims to study the latter.

A useful property of the graph is that it can be represented as a matrix (adjacency matrix), with each row representing a node and each column represents the relationship between that node and every other node in the network (Vecchio, et al., 2017). The edges between the nodes may be weighted or unweighted. In the context of WM connectomes, weighted links typically represent the size, density or coherence

of structural tracts in structural networks (Vecchio, Miraglia & Maria Rossini, 2017). Unweighted, or binary, networks are used by applying a threshold to a weighted network, where edges indicate the presence or absence of a connection (Vecchio, Miraglia & Maria Rossini, 2017). Typically, unweighted networks are utilised, but weighted networks are gaining interest due to the more detailed information they can provide (Rubinov & Sporns, 2010; Vecchio, Miraglia & Maria Rossini, 2017).

Connections between brain regions are weighted according to the strength of their interaction, as given by the fractional number of tracts (fNT) in the case of this study.

2.10.1.1. Clinical interpretation

The different graph theory measures may be subdivided according to how they contribute towards the brain's functioning. There are three general subdivisions: brain network, segregation, and integration.

An individual network measure characterises features of global and local brain connectivity. This relates to how the different nodes connect to one another, and is measured by degree and strength (Caiazzo et al., 2003; Griffa et al., 2013).

Structural segregation is the capacity for specialised processing to occur within densely interconnected regional brain groups (Griffa et al., 2013). Measures of segregation mainly quantify the occurrence interconnected groups, known as modules, clusters or communities, within the network. The presence of densely connected groups in structural networks highlights the potential for segregation within these networks (Rubinov & Sporns, 2010). Examples of segregation measures include clustering coefficient, transitivity, local efficiency and modularity (Griffa et al., 2013).

Structural integration represents the capacity to combine specific information from dispersed brain regions rapidly (Rubinov & Sporns, 2010). Measures of integration characterise this principle by estimating how easily different brain regions communicate with one another, and are commonly based on path metrics. Paths are defined as sequences of distinct nodes and edges in the network. In anatomical graphs, paths represent possible routes of information flow between different areas of the brain (Griffa et al., 2013). Lengths of paths assess the possibility of structural integration between parts of the brain. Shorter paths typically imply a higher potential for integration. Examples of integration measures include characteristic path length and global efficiency (Griffa et al., 2013).

In some studies, structural brain networks have been shown to be highly integrated (i.e., consisting of several short path lengths amongst different modules) and highly segregated (as a result of several clusters of interconnected brain regions) (Caiazzo et al., 2003; Rubinov & Sporns, 2010; Griffa et al., 2013).

Disruptions to integration measures have been linked to associative fiber damage, while a simultaneous disruption of integration and segregation properties has been related to both short and long connection damages in localised intracortical regions (Griffa et al., 2013). Weak structural segregation is shown by low clustering coefficient

and transitivity, while weak structural integration is shown by high characteristic path length and low global efficiency (Baker et al., 2017).

2.10.1.2. Graph theory measure definitions

A summary of the measures and their definitions is given in the table and figure below.

Table 2: Overview of graph measure definitions and their clinical interpretations

Graph measure	Definition	Clinical application
Network measures		
Degree	Node degree is the number of edges connected to a node. Connection weights are ignored in calculations. The higher its value, the more a node is important in a graph as many edges connect to it (Rodrigue, 2020)	Node degree is a simple, but effective measure of nodal importance. Nodes with higher degree act as hubs of communication between more specialised and spatially constraint brain areas (Griffa et al., 2013). A network measure.
Strength	Node strength is the sum of weights of edges connected to the node. Strength is also a measure of how many connections a node has.	Similar to degree. Diminished nodal strength has be linked to axonal damage and traumatic brain injury in young children (Caeyenberghs et al., 2012; Watson, DeMaster & Ewing-Cobbs, 2019).
Segregation measures		
Modularity	Modularity in the brain quantifies the degree to which the network may be subdivided into delineated groups/clusters/modules (Rodrigue, 2020). Modularity is thus a measure of the community structure of a network. The optimal community structure subdivides the network into nonoverlapping groups of nodes while maximising the number of within-group edges, and minimising the number of between-group edges (Rubinov & Sporns, 2010)	Modular networks are best adapted to tasks performed in a changing environment. They guarantee optimal component positioning and network robustness (Rodrigue, 2020). A measure of segregation.

Clustering coefficient	The fraction of triangles around an individual node, equivalent to the fraction of the node's neighbours that are also neighbours of each other (Rodrigue, 2020).	High levels of clustering are commonly interpreted as high levels of local organisation of network modules (Bell et al., 2018). A high clustering coefficient highlights the presence of densely interconnected groups of regions within each module CC is associated with the efficient transfer of information in a local cluster of nodes (Rubinov & Sporns, 2010; Vecchio, Miraglia & Maria Rossini, 2017). A measure of segregation.
Transitivity	An alternative to the clustering coefficient, transitivity is the overall probability for the network to have adjacent nodes interconnected. Transitivity is given by the ratio between the observed number of closed triplets and the maximum possible number of closed triplets in the graph (Rodrigue, 2020). It is a normalised version of the clustering coefficient.	Similar to that of clustering coefficient. Complex and small-world networks often have high transitivity (Rubinov & Sporns, 2010). A measure of segregation.
Local efficiency	The local efficiency is the global efficiency calculated for the neighbourhood of the node, and is related to the clustering coefficient (Brain Connectivity Toolbox, 2021)	A measure of segregation. Decreased local efficiency has been linked to traumatic brain injury in children (Caeyenberghs et al., 2012)
Nodal efficiency	The nodal efficiency characterises how well a node exchanges information with its neighbours when it is removed.	A measure of segregation.
Integration measures		
Global efficiency	The average inverse shortest path length in the network. Inversely related to the characteristic path length	A measure of integration.

	(Brain Connectivity Toolbox, 2021)	
Characteristic path length	The average shortest path length between all pairs of nodes in the network. Gives the average number of stops needed to reach two distant nodes in the graph (Rubinov & Sporns, 2010)	It may be used as a measure of efficiency. The lower the result, the more efficient the network is in providing ease of circulation (Rodrigue, 2020) A measure of integration.

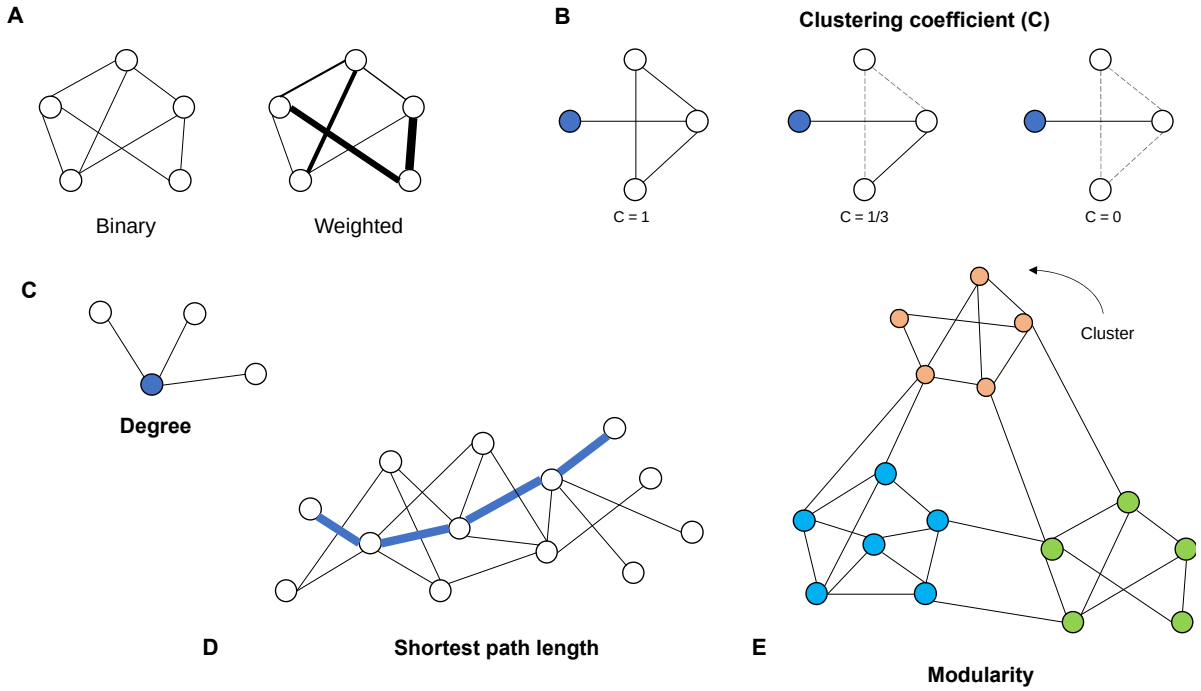

Figure 2: A visual summary of various graph measures. Nodes in the diagram are represented by circles, while edges are represented as the interconnecting lines between nodes. ***A*** *depicts how graphs can be binary, which represents edges as values of 1s and 0s, or weighted, which assigns a numerical value to each edge that is present according to the size, density, or coherence of structural tracts in structural networks.* ***B*** *depicts the clustering coefficient, which shows fraction of triangles around an individual node of interest (in this diagram the node of interest has been coloured in blue). For the first of the 3 scenarios, the clustering coefficient (depicted as C) is 1, as all the edges are present in a triangle around the node of interest. In the second scenario, C is 1/3 as only one edge is present in the triangle, while in the third scenario C is equal to 0.* ***C*** *depicts the degree, which is a measure of how many connections a node has. In this diagram, the node of interest (shown in blue) has 3 interconnecting edges, so the degree for that node is 3.* ***D*** *depicts the shortest path length, which is the average shortest path length between all pairs of nodes in the network. The shortest path is shown as the edges highlighted in blue.* ***E*** *shows the modularity of the graph, which quantifies the degree to which the network may be subdivided into clearly delineated clusters. An example of a cluster is shown in the highlighted blue pentagon. The different colour dots represent different clusters within the same graph.*

For the proposed project, a WM connectome will be created for each child. The graph's nodes will be identified through GM automatic parcellation using the Infant Freesurfer tool (Zöllei et al., 2020) and the edges will be defined using DTI probabilistic tractography using AFNI's FATCAT tool (Taylor & Saad, 2013). Finally, graph theoretical measures will be extracted, followed by statistical group analyses.

3. METHODOLOGY

3.1. Study Cohort

The healthy baby study (HBS) study includes pregnant women living with and without HIV. As part of standard care, the HIV status of all pregnant women was determined. If positive, pregnant women living with HIV started first line therapy (Tenofovir (TDF), Emtricitabine (FTC) and Efavirenz (EFV) in a daily fixed dose combination.

The study recruited women with low-risk pregnancies in Cape Town, South Africa before 20 weeks' gestation, half of whom initiated ART for PMTCT prior to conception and half of whom initiated PMTCT care after 12 weeks gestational age (GA). The mothers were then screened according to the criteria specified below. Detailed health information including haemoglobin, HIV viral load (VL), CD4 count and ART records was obtained throughout pregnancy at the time of their monthly antenatal visits. They were also interviewed at each clinic visit regarding their alcohol and drug use habits. After delivery, mothers and their infants were followed for 19 months with clinical evaluations, laboratory tests, neurodevelopmental testing and neuroimaging.

The overall project pipeline is given in Figure 3.

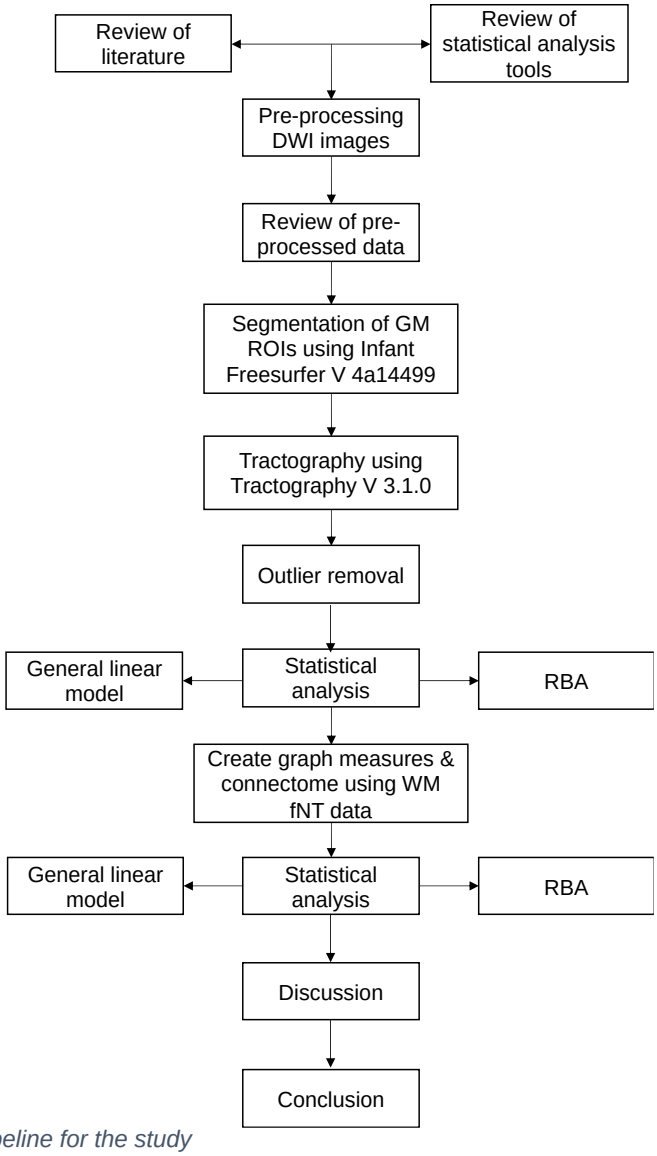

Figure 3: Overall project pipeline for the study

3.2. Exclusion criteria

The following parameters resulted in exclusion from the study: preterm delivery <36 weeks GA, birth weight <2500 g or positive on HIV-1 PCR. Neonates that tested positive for HIV were referred for immediate ART commencement. Thereafter, some infants were excluded because of poor image quality in their DWI data.

Maternal study exclusion criteria included underlying chronic disorders (e.g., diabetes, epilepsy, tuberculosis, hypertension), a history of recurrent premature deliveries, known tuberculosis contact, or use of medication other than essential pregnancy supplements or ART, poor adherence to ART, non-standard ART regimens, and nondisclosure of HIV status to family members; binge drinking (4 or more drinks per occasion) and illicit drug use.

3.3. MRI acquisition

The study performed brain scans on a birth cohort of HEU and HUU neonates using a 3T Siemens Skyra MRI scanner (Siemens, Erlangen, Germany) at the Cape Universities Body Imaging Centre (CUBIC) located at Groote Schuur Hospital. The infants were scanned according to protocols that were approved by the Human Research Ethics Committee of the University of Cape Town.

Prior to scanning, a paediatrician blinded to HIV and ART exposure status weighed, examined and administered the Dubowitz Infant Neurological Examination (Dubowitz, Ricci & Mercuri, 2005) roughly one hour before the scheduled scan. Infants were then fed, had their diaper changed, had sponge earplugs inserted in their ears which were then covered with mini-muffs and a beanie, and a pulse oximeter attached to one of their feet to monitor oxygen saturation. They were tightly swaddled, put to sleep supine on a special pillow containing styrofoam beads (Vac Fix pillow) in the Siemens 16-channel paediatric head coil, and imaged without sedation.

The protocol included a high-resolution T1-weighted 3D echo-planar imaging (EPI) navigated multi echo magnetisation prepared rapid gradient echo (MEMPRAGE) acquisition (FOV 192x192 mm^2, TR 2540 ms, TI 1450 ms, TE's = 1.69/3.55/5.41/7.27 ms, bandwidth 650 Hz/px, 144 sagittal slices, voxel size 1.0x1.0x1.0 mm^3). Two diffusion-weighted imaging (DWI) sets with opposite (Anterior-Posterior, Posterior-Anterior; AP/PA) phase encoding directions were acquired with a multi-band (Setsompop et al., 2012) twice refocused spin-echo EPI sequence: TR 4800 ms, TE 84 ms, matrix 62 axial slices of 96x96 voxels (each voxel 2x2x2 mm^3), 6/8 partial Fourier encoding, BW 1628 Hz/px, with slice-acceleration factor 2 and GRAPPA factor 2. Each acquisition contained six b = 0 s mm^{-2} (b0) reference scans and 30 DW gradient directions with b = 1000 s mm^{-2}.

3.4. Image processing

All analyses were carried out using a combination of predeveloped in-house scripts and tools available in standard software packages such as the Analysis of Functional Neuroimages (AFNI) toolbox (Cox, 1996), the Tolerably Obsessive Registration and

Tensor Optimisation Indolent Software Ensemble (TORTOISE) version 3.1.0 (Pierpaoli et al., 2010), Infant Freesurfer (Zöllei et al., 2020), and the Functional And Tractographic Connectivity Analysis Toolbox (FATCAT) (Taylor & Saad, 2013) within AFNI.

3.4.1. Preprocessing

Prior to tractography, graph theory and statistical analyses, the DWI data needed to be preprocessed to sort the data into a format that was appropriate for analysis. An overview of the preprocessing steps is outlined below in Figure 4.

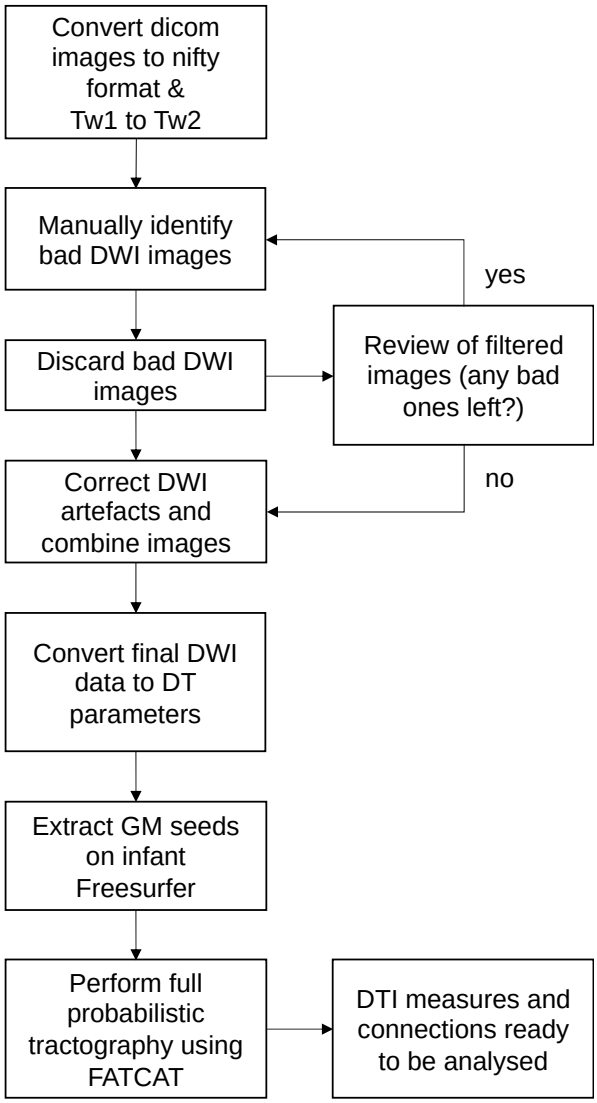

Figure 4: Pre-processing pipeline

A set of in-house scripts were used to convert each subject's DW images from DICOM to NIfTI format using the dcm2niix AFNI tool. Once converted, the images were readable in TORTOISE and T1-weighted images were used to create T2-weighted images. Next, each subject's DWI images was quality checked across both AP and PA directions. Any distorted volumes in the image directions were placed on a filter list and subsequently removed. Subjects with less than 15 viable diffusion directions

and/or no viable b0 images were excluded. After exclusions the DIFF_PREP function in TORTOISE was used to correct for DWI artefacts such as motion and eddy current and EPI distortions. The DRBUDDI function combined the AP and PA directions to create a new subset of images for each subject. After DRBUDDI, the images were converted into usable NIfTIs and exported to AFNI. AFNI's *fat_proc_dwi_to_dt* function was used to estimate diffusion tensors and DTI parameters.

In order to perform tractography, structural GM ROIs needed to be extracted. We used Infant Freesurfer tool V 4a14499 (which can be requested at http://surfer.nmr.mgh.harvard.edu/fswiki/infantFS), which uses an automated algorithm to segment the infant brain (de Macedo Rodrigues et al., 2015; Zöllei et al., 2020) into a total of 28 cortical and subcortical ROIs. The list of structures being used for the study is as follows:

- Left Cerebral Cortex
- Left Lateral Ventricle
- Left Cerebellum Cortex
- Left Thalamus
- Left Caudate
- Left Putamen
- Left Pallidum
- 3rd Ventricle
- 4th Ventricle
- Left Hippocampus
- Left Amygdala
- Left Accumbens area
- Left VentralDC
- Right Cerebral Cortex
- Right Lateral Ventricle
- Right Cerebellum Cortex
- Right Thalamus
- Right Caudate
- Right Putamen
- Right Pallidum
- Right Hippocampus
- Right Amygdala
- Right Accumbens area
- Right VentralDC
- Vermis
- Midbrain
- Pons
- Medulla

The ventricles of the brain were kept as seeds in our analysis because of their location relative to other subcortical structures that were identified for analysis in this study. The third ventricle is between the right and the left thalamus, while the fourth ventricle sits within the brainstem, at the intersection between the pons and medulla oblongata. All the regions surrounding the ventricles, most notably the basal ganglia, are included as regions of interest in this study. Any potential adverse effects that may be occurring to these regions as a result of fetal or maternal mechanisms like inflammation or exposure to harmful substances may also potentially be affecting the ventricles surrounding these areas as well.

A visual representation of the GM structures being included in the analyses is given in Figure 5 below.

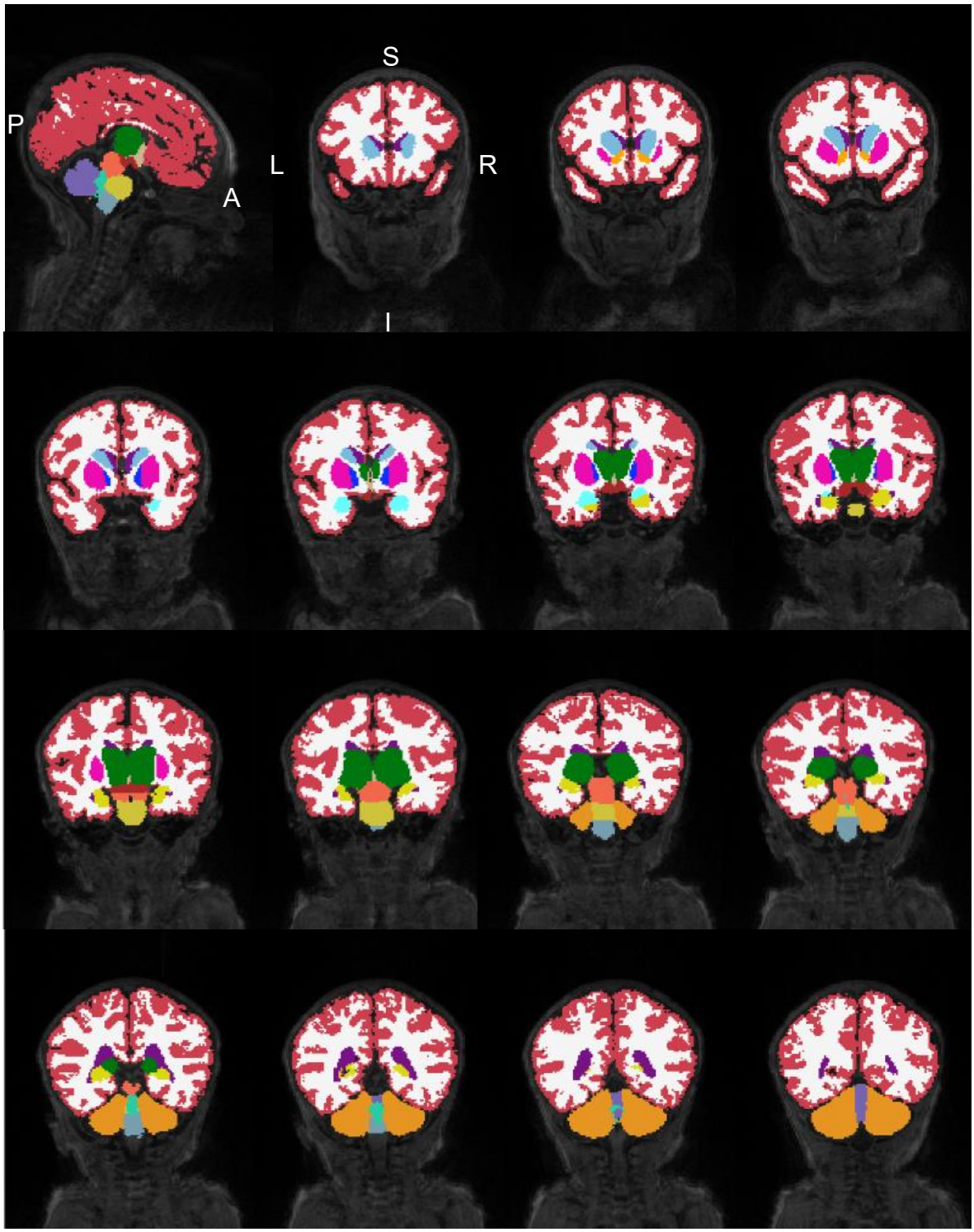

KEY

Cerebral Cortex	A – Anterior
Lateral Ventricle	P – Posterior
Cerebellum Cortex	L – Left hemisphere
Thalamus	R – Right hemisphere
Caudate	S – Superior
Putamen	I – Inferior
Pallidum	
3rd Ventricle	
4th Ventricle	
Hippocampus	
Amygdala	
Accumbens area	
Ventral diencephalon	
Vermis	
Midbrain	
Pons	
Medulla	

Figure 5: Sagittal and coronal view of neonatal brain showing the GM structures and their corresponding labels. Coronal slices move from the anterior to posterior direction to visualise different structures. The slices in this diagram are taken from a random HUU infant's images in Infant Freesurfer.

The following brain regions have been abbreviated in the summary tables and diagrams as follows:

Table 3: List of abbreviated grey matter seeds along with their full names, with the abbreviations corresponding to the table and figures presented below.

Abbreviation	**Name**
CC	Cerebral cortex
Cb	Cerebellar cortex
Thal	Thalamus
Caud	Caudate
Put	Putamen
Pal	Pallidum
VDC	Ventral diencephalon
Lat	Lateral
Vent	Ventricle
Hipp	Hippocampus
AA	Accumbens area

3.4.2. Tractography

Tractography utilises DT eigenvectors and eigenvalues to estimate the properties and locations of WM tracts between pairs of target ROIs through propagation.

DTI tractography is performed by first specifying the number of seed points in a voxel. Tracts are then propagated parallel to the major eigenvector within a voxel until they meet grey matter or any of the stopping criteria are reached. The stopping criteria dictate the conditions in which tracking may be terminated. The stopping criteria for this study included the following: angle threshold (turning angle > 60°), FA threshold (FA < 0.1) and tract length (<20 mm). The turning angle should not exceed 60° to prevent doubling back on the propagation of a tract that has already been specified. The FA threshold is defined by subject age, as neonatal WM structure differs from WM in children and adults. WM in infants have FA values of 0.1 or less since their brains are only partially developed and myelinated (Vassar, Barnea-Goraly & Rose, 2014). This also ensures that regions that are not WM will not be included during tracking. Tract length defines the minimum length that a WM bundle must reach to be considered a tract.

3dTrackID, a function in AFNI, has three modes that can be used to conduct tractography: deterministic tractography, mini-probabilistic, and full probabilistic tractography. The outputs of the 3dTrackID are a set of the following measures – FA, MD, AD, RD, bundle length (BL), number of voxels in a bundle (NV), fractional volume of the bundle (fNV) and fractional number of tracts (fNT) – for each tract connecting the GM ROIs and subject. For further analysis an intersect of all individual sets of tracts was taken, thus ensuring we ended up with a subset of all of the tracts and their

DTI measures that are common for the entire population in the study. We utilised these outputs from the full probabilistic tractography for our DTI and graph theory analyses.

3.5. Graph theory

After the WM tractography parameters were collected, these were used as inputs for the graph theory analysis. We defined a graph as set of nodes (GM ROIs) and weighted edges (connections/ WM tracts). The weight of each tract was defined by a tract parameter fNT, the fractional number of streamlines in a given tract.

The graph theory analysis was computed using R statistical software (R Core Team, 2020) and the igraph package for brain network analysis. Graph theoretical measures were extracted and utilised to create connectomes for the study groups. After the measures were extracted, we conducted statistical group analyses in R (described below). An overview of the graph theory analysis pipeline is shown below in Figure 6.

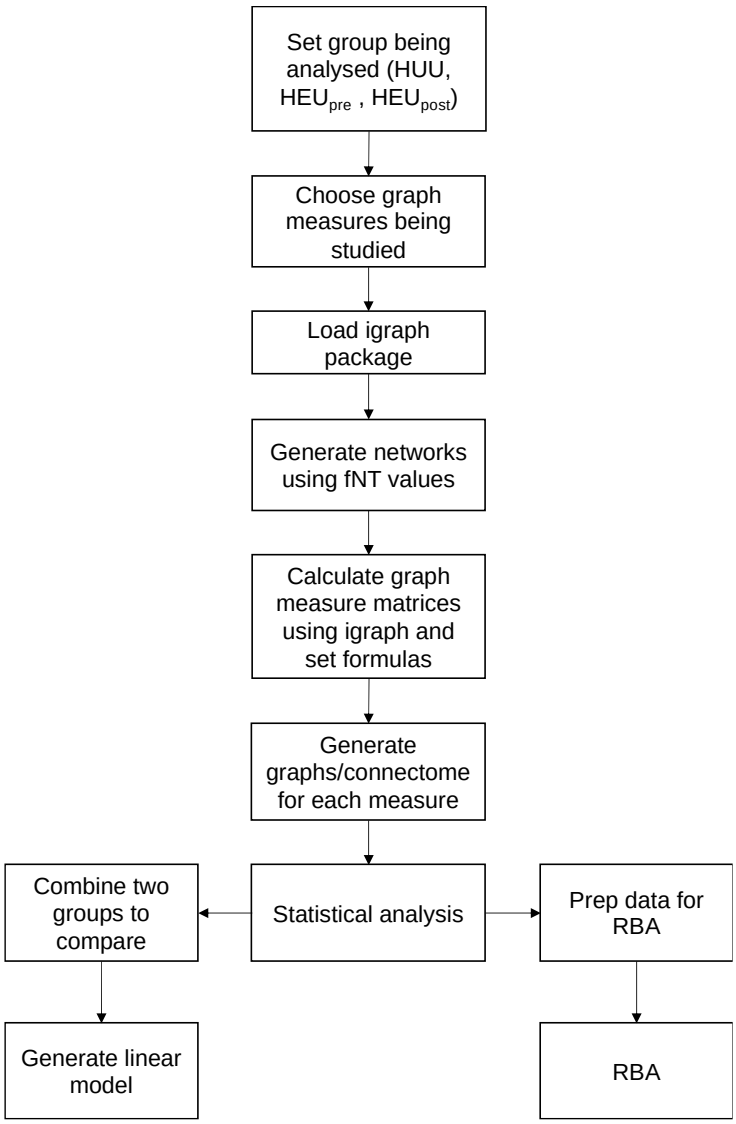

Figure 6: Graph theory pipeline

To calculate the various graph measures, an adjacency matrix of all the GM nodes and their connections needed to be completed. Entries of the n-by-n adjacency matrix (n being number of nodes) are 1s and 0s, with 1s corresponding to an existing connection between two nodes and 0 to a lack of such connection. This gave us a matrix of connectivity between nodes – known as the adjacency matrix – that could be used in subsequent calculations.

After the adjacency matrix was created, it was used to calculate the graph theory measures of interest. In this study, the graph measures being considered include modularity, strength, characteristic path length, transitivity, local efficiency, nodal efficiency and global efficiency.

A connectome graph was then created for each exposure group (HUU, HEU, HEU_{pre} and HEU_{post}) using the weighted adjacency matrix. Groups of nodes were placed into clusters (also referred to as communities) using the membership and cluster_louvain functions in igraph. These are community structure detection algorithms that attempt to find dense subgraphs in directed or undirected graphs.

Thereafter, statistical analysis of the graph theory measures was performed as described in the following section. To compute the statistics for the graph theory measures, various matrices were prepped and transformed into the format required for linear regression analysis.

3.6. Statistical analysis

Statistical analyses were performed using R statistical software (R Core Team, 2019). We utilised general linear modelling to compare the differences in HIV exposure (HUU vs HEU) and ART duration (HUU vs HEU_{pre} and HEU_{post}) in both WM and graph theory measures.

DTI measures of interest such as FA, MD, AD and RD were extracted and outliers were removed from every common pairwise WM connection between target ROIs. Outliers were identified as any values less than Q_L - 1.5(IQR) and over Q_U + 1.5(IQR). The DTI measures that did not include outliers were then inputted into linear regression models, with weight gained per week of pregnancy (WGpw) and maternal education as confounding variables. The confounders were chosen after charting causal diagrams that summarised the likely associations between confounders (such as MRI gestational age, sex, and maternal birth age), exposure variables (HIV exposure) and outcome variables (DTI measures).

For the graph measures, after fNT values were extracted and used to calculate the graph theory measures, these measures had any outliers removed and were inputted into the linear regression models.

For the general linear models, we chose an alpha significance level of p=0.05. Subsequently, we corrected the calculated alpha values for multiple comparisons using the false discovery rate (FDR) method. This helps minimise the discovery of false positives. This can occur when the results from two similar distributions

incorrectly indicate that there is at least one significant p value, even if all of the tests are actually not significant (Muller, Parmigiani & Rice, 2006).

A visual representation of the corrected p values (q values) was plotted in Figure 7 and 8 as heat maps. Heat maps are graphical representations of data that utilise colour-coded systems (Zenko, 2020). The main purpose of a heatmap is to better visualise the volume of events in the dataset (in this case the number of significant results, shown by $q<0.05$), how they're interconnected, and which visualisations are most significant. The heat map plots in this study make use of an adjacency matrix to show the GM seeds, which WM tracts are present between them, and which of these tracts include significant group differences between the HEU groups and HUU. This allows us to better visualise the GM seed locations and how they are connected, as well as draw a more direct visual comparison of the trends within distinct DTI measures. The heat maps also allows us to highlight significant entries clearly.

Lastly, an exploratory correlation analysis was conducted for FA and MD for both HEU groups to identify whether these DTI measures were associated with maternal clinical and treatment variables like ART exposure duration and maternal CD4 count. All of the tracts (173) were tested for significant correlations ($p<0.05$) with these maternal clinical and treatment variables. An exploratory correlation analysis was also performed on all the local graph theory measures.

3.7. Limitations and assumptions

3.7.1. Diffusion tensor imaging

While diffusion tensor imaging is an incredibly powerful tool that enables tissue microstructure to be studied in vivo – a feat that enables much more detailed study of the brain than previously accessible – the results that are derived from its analysis are based on several initial assumptions and are highly sensitive to methodological procedure (Campbell & Pike, 2014). Acquisition parameters, pre-processing steps, reconstruction/propagation models, and statistical analysis all affect the final sensitivity, specificity, and accuracy of a study (Jones & Cercignani, 2010; Campbell & Pike, 2014). In the case of tractography, false positive and false negative results (incorrect estimates of streamlines due to modelling errors) may occur, and any interpretations of the results must take into consideration the potential shortcomings of the techniques used. Below is a summary of the limitations of DTI and tractography, which may be looked at in conjunction with the analysis presented in this study to ensure that plausible conclusions are being drawn.

An initial limitation to the study of diffusion MRI data is the limited spatial resolution at scanning and spatial distortions in the data. DTI acquisitions conducted on 3 Tesla MRI scanners (including this one) use voxel sizes of 2x2x2 mm^3. This is due to limitations related to signal strength. The voxels are then super-sampled to match a resolution of a structural image (1 mm^3). As a result, a single voxel will contain thousands of fiber pathways within it (Campbell & Pike, 2014). On top of that, there is a high likelihood of a voxel to contain not only WM, but also GM and CSF (le Bihan &

Johansen-Berg, 2012; Campbell & Pike, 2014). These two intrinsic limitations (collectively called partial volume averaging) reduce predictive power and increase uncertainty in the calculated diffusion parameters (Maier-Hein et al., 2017). With limited spatial resolution, WM tracts can only be modelled as 3D 'streamlines'. It is important to note that the individual streamlines do not represent actual axons, but rather they depict estimations of the average trajectories of axon bundles, given the assumption that diffusion is least hindered along the length of the axons (Craddock et al., 2013). The partial volume effects have a number of consequences on the resulting tract propagation, as it becomes hard to distinguish streamlines that cross each other through kissing (i.e., temporarily running adjacent to one another), merging, splaying or branching (Jbabdi & Johansen-Berg, 2011). More elaborate models of axon diffusion mapping (e.g., q-balls, HARDI) allow for several diffusion orientations to be mapped within the same voxel.

Tractography algorithms are highly sensitive to user-defined or algorithm-specific parameters (so called tracking stopping criteria) (Jones, Knösche & Turner, 2013), and thus requires active engagement. Another limitation of tractography is its lack of standardised procedure and a gold standard to compare results with (Maier-Hein et al., 2017). Therefore, where possible, tractography should be used in conjunction with reliable anatomy datasets from ex-vivo histology or complementary imaging modalities (e.g., myelin-water imaging) for optimal guidance (Maier-Hein et al., 2017).

3.7.2. Graph Theory

Since the graph theory analysis is based on DTI tractography, the study of the structural connectome is thus also impacted and affected by the same methodological issues that impact tractography's analysis and interpretation of results.

The use of DTI parameters to quantify graph theoretical measures must be carefully considered as the uncertainties from the DTI methodological procedure may be carried forward into graph theory calculations.

The location of tract origin and termination sites is still not fully known or reflected in tractography studies, and traditional metrics that require streamlines to end in head or tail regions of a bundle are too restrictive for a bundle connectivity assessment. Unknown and restrictive bundle termination sites create decreased reliability and increased uncertainty both in tractography but more especially within graph theory which relies on the detailed definition of GM nodes and WM edges (Maier-Hein et al., 2017). Future studies should include ground truth parcellations of the WM/GM cortical band to have better defined graph theory metrics (Maier-Hein et al., 2017).

Moreover, it's not clear which choice of weighting/edges of the graph in the analysis is best at describing structural connectivity, with some authors (Yuan et al., 2019) suggesting that for example FA is more robust as a measure of pairwise connectivity, than a streamline-count or fractional number of streamlines in a connection.

4. RESULTS

4.1. Sample demographics

212 pregnant women were recruited for the study. Infants born to 186 of the enrolled mothers met inclusion criteria. 26 infants were excluded - 13 due to low birthweight; 3 due to birth defects; 2 withdrew consent, and 8 were lost to follow up. Out of the 160 remaining neonate infants, 106 had complete sets of relevant imaging datasets. Therefore, the infant cohort consisted of 35 HUU and 71 HEU infants. The HEU group is further subdivided by ART duration exposure, with 36 infants having been exposed to ART for the full gestation term (HEU_{pre}) and 35 being exposed 3-6 months post conception (HEU_{post}).

The sample demographics are presented in Table 4 below.

Table 4: Demographic data of HUU controls and HEU groups at birth and at time of MRI scanning

Demographics	HUU	HEU	
		HEU_{pre}	HEU_{post}
Number of subjects (n)	35	36	35
Sex (Male: Female)	18:17	18:18	20:15
Birth measures			
Weight (g)	3285 ± 407	3215 ± 333	3250 ± 403
Length (cm)	50 ± 4	50 ± 2	50 ± 3
MRI measures			
Gestational age (weeks)	42 ± 1	41 ± 1	42 ± 1
Weight (g)	3561 ± 439	3143 ± 411	3509 ± 379
Length (cm)	52 ± 2	51 ± 2	52 ± 2
Head circumference (cm)	35 ± 1	36 ± 1	35 ± 1
Maternal measures			
Birth age (years)	28 ± 6	31 ± 6	28 ± 5
CD4	N/A	568 ± 169	424 ± 196
ARV exposure length (weeks)	N/A	40 ± 1	25 ± 6
Weight gain per week (g)	0.41 ± 0.16	0.35 ± 0.28	0.27 ± 0.24
Absolute alcohol per day*	0.02 ± 0.02	0.01 ± 0.02	0.02 ± 0.03
Maternal trauma score**	40 ± 10	43 ± 15	42 ± 13

*Ounces of absolute alcohol (AA, 1 ounce ~ 2 standard drinks) per drinking day across pregnancy.
**Based on the Harvard Trauma questionnaire, a self-report questionnaire assessing traumatic experiences and PTSD symptom severity.

4.2. DTI Tractography analysis

The following results are the outputs of the linear models comparing the HEU groups to the HUU control group for various DTI measures calculated using the DTI tractography processing pipeline described in sub-section 3.4.2 of the Methods section. Associations between various DTI measures and maternal clinical and

treatment variables were also tested and are presented below per the processing pipeline described in sub-section 3.6 of the Methods section.

A total of 173 tracts were found through full-probabilistic DTI tractography to be common to all the subjects. These tracts were analysed for group differences (HUU vs HEU_{pre} and HUU vs HEU_{post}). We see group differences in 22 tracts in the HUU vs HEU_{pre} group comparison after FDR correction; and 28 tracts in the HUU vs HEU_{post} group comparison after FDR correction. From the heat maps in Figure 7 – 8 we can see that there are more significant tracts in FA in HEU_{post} while there are more significant tracts in MD, AD and RD in HEU_{pre}.

Group analysis of other DTI measures such as bundle length, total number of tracts, number of voxels in a bundle and fractional volume of the bundle yielded no statistically significant group difference results.

4.2.1. FA related differences

Several tracts coming from the left and right cerebral cortex (CC) showed differences in FA, as well as to and from the ventricles and the putamen. We report the following summary of our HIV and ART exposure group analysis:

- Mean FA values for certain tracts across both groups (HEU_{pre} and HEU_{post}) are significantly less than those of the HUU groups.
- HEU_{post} have more implicated tracts than HEU_{pre}, with 28 tracts for HEU_{post} and 5 tracts for HEU_{pre}.
- Four out of the five implicated FA tracts in the HEU_{pre} group (80%) are also present in the HEU_{post} group (shown in Table 8). All of the implicated tracts in the HEU_{pre} group originate from the left cerebral cortex, with three out of the five also occurring only on the left hemisphere of the brain. The tracts with significant group differences all involve structures associated with the basal ganglia.
- Most of the significant tracts in the HEU_{post} group also originate from the left hemisphere, either from the left cerebral cortex or the left cerebellar cortex. The main anatomical structures connecting to it include: the caudate, putamen, thalamus, medulla, midbrain, ventral diencephalon, and the 4^{th} ventricle.
- RD values for the same significant FA tracts are higher in the HEU groups than HUU controls. In the HEU_{pre} group, RD tracts have higher values that are trending towards significant for 40% of the FA implicated tracts (L CC – L Thal and L CC – Midbrain). In the HEU_{post} group, none of the same FA implicated tracts have any significant RD values after correction, but, before correction, approximately 14 tracts (50%) have significantly higher values.
- For the same tracts that display statistically significant lower FA values, AD values are not significantly different in both group comparisons (HUU vs HEU_{pre} and HUU vs HEU_{post}).

4.2.2. MD related differences

For MD, different tracts than those found in the FA tract analysis are significantly higher than HUU controls in the HEU_{pre} group. There are no significant differences in MD, AD and RD in the HEU_{post} group in any of the 173 tracts that were analysed after correction. We report the following summary of our HIV exposure/ART group analysis in MD:

- HEU_{pre} has 17 tracts with significantly higher MD than the HUU group while HEU_{post} has no tracts with significant differences in MD, AD or RD as compared to the HUU group.
- Of the 17 tracts with significant differences in MD, 13 had significant differences in AD while 12 had significant differences in RD.
- Only one tract originating from the L CC is higher in MD for HEU_{pre} as compared to HUU, unlike the majority being implicated in FA.
- For RD, all the remaining tracts in the group trended towards significance, with there being no q value higher than 0.08. For AD, two tracts out of the remaining four (50%) trended towards significance with q = 0.055 and q = 0.057.
- L thal – L put and L put – L hipp were both not significant in AD or RD but significant in MD.
- The most commonly implicated regions included connections from the left and right thalamus, left hippocampus and left ventral diencephalon. Most implicated tracts are located within the left hemisphere of the brain.

4.2.3. Associations with maternal clinical and treatment variables

In Figure 9 – 13 we present an exploratory analysis of significant associations ($p<0.05$) between maternal clinical and treatment variables and FA and MD values among HEU infants.

For 83 of the tracts (approximately 50% of all connections) in HEU_{pre}, there is a positive association of duration of ART exposure with FA. Similarly, for 22 tracts (13%) in HEU (HEU_{pre} and HEU_{post} combined), there is a positive association of duration of ART exposure with FA. Of the 22 tracts found to have positive associations with ARV duration, six were also found to have significantly lower FA values in the regression analysis of HEU_{post} vs HUU infants as shown Table 9. ARV exposure duration was found to have no associations with the overall HEU group in MD, but 60 tracts (35%) were identified as being positively associated with it in HEU_{pre}.

For maternal CD4 count, FA values were positively associated with increased counts in both HEU_{pre} and HEU_{post} groups. In MD, increased CD4 count was associated with decreased MD values in both HEU_{pre} and HEU_{post} groups in 3 tracts.

Table 5: Tracts showing significant differences in Fractional anisotropy (FA), Axial diffusivity (AD), and Radial diffusivity (RD) in HUU vs. HEU_{pre} infants before and after FDR correction SD – standard deviation. L/R – Left/right hemisphere

	FA						AD						RD					
connections	mean HUU (SD)	mean early (SD)	p	q	std beta	std error	mean HUU (SD)	mean early (SD)	p	q	std beta	std error	mean HUU (SD)	mean early (SD)	p	q	std beta	std error
L CC - L Caud	0.221(0.007)	0.214(0.009)	0.0006	0.036	-0.479	0.002	1.633(0.069)	1.630(0.044)	0.990	0.990	-0.002	0.016	1.172(0.057)	1.181(0.031)	0.379	0.456	0.126	0.013
L CC - L Put	0.208(0.008)	0.200(0.008)	0.0012	0.046	-0.451	0.002	1.605(0.063)	1.618(0.051)	0.372	0.473	0.125	0.016	1.172(0.060)	1.194(0.047)	0.141	0.231	0.203	0.015
L CC - L VDC	0.224(0.009)	0.216(0.008)	0.0002	0.028	-0.499	0.002	1.648(0.061)	1.653(0.061)	0.611	0.674	0.071	0.018	1.173(0.058)	1.191(0.051)	0.197	0.292	0.178	0.015
L CC - R Thal	0.235(0.009)	0.228(0.011)	0.0013	0.046	-0.402	0.002	1.676(0.078)	1.705(0.058)	0.052	0.138	0.270	0.019	1.169(0.054)	1.197(0.046)	0.043	0.113	0.277	0.014
L CC - Midbrain	0.225(0.007)	0.219(0.007)	0.0005	0.036	-0.499	0.002	1.632(0.062)	1.647(0.061)	0.367	0.473	0.127	0.017	1.156(0.050)	1.182(0.046)	0.049	0.117	0.274	0.013

Table 6: Tracts showing differences Mean diffusivity (MD), Axial diffusivity (AD), and Radial diffusivity (RD) in HUU vs. HEU_{pre} infants before and after FDR correction SD – standard deviation. L/R – Left/right hemisphere

	MD						AD						RD					
connections	mean HUU (SD)	mean early (SD)	p	q	std beta	std error	mean HUU (SD)	mean early (SD)	p	q	std beta	std error	mean HUU (SD)	mean early (SD)	p	q	std beta	std error
L CC - R Caud	1.306(0.048)	1.345(0.057)	0.0011	0.026	0.432	0.014	1.660(0.041)	1.703(0.057)	0.0004	0.017	0.475	0.014	1.134(0.055)	1.166(0.060)	0.0095	0.057	0.344	0.015
L Thal - L Caud	1.219(0.043)	1.247(0.048)	0.0019	0.032	0.414	0.012	1.519(0.063)	1.537(0.059)	0.0526	0.138	0.260	0.016	1.076(0.044)	1.099(0.043)	0.0107	0.057	0.342	0.012
L Thal - L Put	1.211(0.048)	1.242(0.043)	0.0043	0.046	0.381	0.012	1.524(0.062)	1.557(0.054)	0.0103	0.057	0.345	0.016	1.055(0.043)	1.081(0.035)	0.0072	0.050	0.364	0.011
L Thal - L Amyg	1.293(0.044)	1.345(0.043)	0.0000	0.001	0.616	0.012	1.602(0.053)	1.658(0.058)	0.0001	0.012	0.549	0.016	1.145(0.045)	1.189(0.053)	0.0006	0.027	0.473	0.014
L Thal - L VDC	1.248(0.046)	1.283(0.041)	0.0004	0.016	0.487	0.012	1.572(0.057)	1.607(0.055)	0.0022	0.023	0.427	0.016	1.087(0.035)	1.121(0.041)	0.0002	0.012	0.496	0.010
L Thal - R VDC	1.277(0.050)	1.303(0.053)	0.0033	0.046	0.388	0.013	1.632(0.086)	1.663(0.063)	0.0041	0.032	0.383	0.019	1.100(0.045)	1.126(0.052)	0.0047	0.047	0.376	0.013
L Put - L Hipp	1.297(0.078)	1.344(0.046)	0.0042	0.046	0.390	0.018	1.650(0.095)	1.694(0.058)	0.0095	0.055	0.353	0.021	1.120(0.072)	1.163(0.052)	0.0182	0.070	0.318	0.017
L Hipp - L Amyg	1.319(0.060)	1.389(0.052)	0.0001	0.004	0.519	0.016	1.617(0.093)	1.705(0.077)	0.0005	0.017	0.456	0.024	1.175(0.057)	1.230(0.055)	0.0012	0.035	0.414	0.015
L Hipp - L VDC	1.377(0.076)	1.429(0.071)	0.0043	0.046	0.396	0.020	1.719(0.102)	1.785(0.068)	0.0016	0.020	0.443	0.024	1.195(0.081)	1.250(0.072)	0.0027	0.043	0.409	0.021
L Hipp -Midbrain	1.363(0.073)	1.416(0.076)	0.0013	0.026	0.429	0.020	1.713(0.101)	1.788(0.105)	0.0020	0.023	0.413	0.028	1.187(0.067)	1.231(0.070)	0.0030	0.044	0.394	0.018
L VDC - R Thal	1.267(0.043)	1.304(0.043)	0.0007	0.025	0.444	0.012	1.629(0.063)	1.668(0.045)	0.0040	0.032	0.401	0.015	1.087(0.034)	1.127(0.041)	0.0000	0.003	0.524	0.010
L VDC - R VDC	1.278(0.043)	1.319(0.072)	0.0010	0.026	0.434	0.016	1.637(0.068)	1.682(0.073)	0.0014	0.020	0.427	0.019	1.105(0.052(	1.130(0.065)	0.0236	0.081	0.299	0.015
R CC - Midbrain	1.306 0.046)	1.341(0.054)	0.0047	0.047	0.384	0.014	1.620(0.062)	1.645(0.059)	0.0681	0.169	0.250	0.016	1.153(0.045)	1.190(0.053)	0.0041	0.047	0.385	0.014
R Lat Vent -Mid	1.321(0.057)	1.364(0.055)	0.0040	0.046	0.385	0.015	1.673(0.073)	1.731(0.064)	0.0005	0.017	0.451	0.018	1.145(0.056)	1.184(0.054)	0.0070	0.050	0.361	0.015
R Thal - R Caud	1.216(0.042)	1.256(0.046)	0.0001	0.004	0.521	0.012	1.510(0.055)	1.549(0.055)	0.0006	0.017	0.451	0.014	1.070(0.029)	1.106(0.040)	0.0000	0.001	0.584	0.009
R Thal - R Hipp	1.372(0.056)	1.406(0.042)	0.0035	0.046	0.424	0.014	1.695(0.063)	1.737(0.051)	0.0006	0.017	0.490	0.016	1.211(0.056)	1.240(0.043)	0.0163	0.069	0.353	0.015
R Amyg -R VDC	1.321(0.059)	1.359(0.042)	0.0014	0.026	0.426	0.014	1.654(0.067)	1.698(0.055)	0.0030	0.028	0.398	0.017	1.155(0.056)	1.190(0.044)	0.0021	0.041	0.404	0.013

Table 7: Tracts showing significant differences in Fractional anisotropy (FA), Axial diffusivity (AD), and Radial diffusivity (RD) in HUU vs. HEU_{post} infants before and after FDR correction SD – standard deviation. L/R – Left/right hemisphere

	FA						AD						RD					
connections	mean HUU (SD)	mean late (SD)	p	q	std beta	std error	mean HUU (SD)	mean late (SD)	p	q	std beta	std error	mean HUU (SD)	mean late (SD)	p	q	std beta	std error
L CC - L Thal	0.209(0.011)	0.200(0.010)	0.0015	0.024	-0.413	0.003	1.635(0.067)	1.652(0.071)	0.530	0.993	0.083	0.018	1.190(0.061)	1.218(0.048)	0.143	0.348	0.192	0.014
L CC - L Caud	0.221(0.007)	0.213(0.011)	0.0013	0.024	-0.436	0.003	1.633(0.069)	1.646(0.067)	0.583	0.993	0.074	0.018	1.172(0.057)	1.188(0.050)	0.261	0.439	0.150	0.014
L CC - L Put	0.208(0.008)	0.198(0.008)	0.0001	0.010	-0.542	0.002	1.605(0.063)	1.625(0.065)	0.392	0.993	0.114	0.017	1.172(0.060)	1.194(0.056)	0.174	0.365	0.177	0.015
L CC - L Pall	0.224(0.009)	0.217(0.010)	0.0066	0.048	-0.372	0.003	1.620(0.067)	1.630(0.063)	0.638	0.993	0.063	0.017	1.152(0.056)	1.176(0.059)	0.123	0.328	0.201	0.015
L CC - L Amyg	0.220(0.013)	0.210(0.013)	0.0018	0.026	-0.432	0.004	1.693(0.058)	1.709(0.093)	0.824	0.993	0.030	0.020	1.205(0.054)	1.236(0.056)	0.087	0.287	0.216	0.014
L CC - L VDC	0.224(0.009)	0.215(0.006)	0.0000	0.000	-0.642	0.002	1.648(0.069)	1.658(0.075)	0.778	0.993	0.038	0.019	1.173(0.058)	1.192(0.056)	0.295	0.469	0.139	0.015
L CC - R CC	0.195(0.008)	0.189(0.005)	0.0075	0.048	-0.372	0.002	1.620(0.072)	1.641(0.054)	0.286	0.993	0.140	0.017	1.208(0.063)	1.235(0.047)	0.038	0.265	0.272	0.014
LCC - R Lat Vent	0.227(0.009)	0.221(0.010)	0.0057	0.048	-0.376	0.002	1.742(0.097)	1.756(0.090)	0.809	0.993	0.032	0.025	1.227(0.074)	1.251(0.064)	0.306	0.477	0.139	0.019
L CC - Midbrain	0.225(0.007)	0.215(0.010)	0.0007	0.023	-0.474	0.003	1.632(0.062)	1.637(0.070)	0.918	0.993	-0.014	0.018	1.156(0.050)	1.184(0.045)	0.061	0.274	0.246	0.013
L CC - Pons	0.224(0.009)	0.216(0.010)	0.0063	0.048	-0.387	0.003	1.641(0.067)	1.652(0.058)	0.769	0.993	0.040	0.017	1.170(0.055)	1.199(0.042)	0.052	0.274	0.262	0.013
L Cb - R CC	0.179(0.015)	0.168(0.010)	0.0015	0.024	-0.409	0.003	1.474(0.079)	1.476(0.082)	0.818	0.993	0.031	0.021	1.119(0.066)	1.152(0.086)	0.092	0.287	0.226	0.020
L Cb - 4th Vent	0.234(0.011)	0.223(0.011)	0.0011	0.023	-0.457	0.003	1.596(0.052)	1.611(0.065)	0.662	0.993	0.058	0.015	1.106(0.049)	1.144(0.052)	0.008	0.250	0.339	0.013
L Cb - R Cb	0.174(0.016)	0.162(0.009)	0.0004	0.023	-0.471	0.004	1.427(0.050)	1.424(0.043)	0.826	0.993	-0.032	0.013	1.085(0.058)	1.111(0.035)	0.040	0.265	0.285	0.013
L Cb - Pons	0.185(0.017)	0.172(0.015)	0.0008	0.023	-0.437	0.004	1.497(0.073)	1.522(0.089)	0.277	0.993	0.146	0.022	1.130(0.068)	1.174(0.084)	0.022	0.250	0.300	0.020
L Cb - Medulla	0.189(0.019)	0.176(0.021)	0.0021	0.028	-0.401	0.005	1.501(0.095)	1.534(0.105)	0.201	0.979	0.170	0.026	1.125(0.092)	1.169(0.092)	0.058	0.274	0.251	0.024
4th Vent - R CC	0.243(0.020)	0.231(0.012)	0.0078	0.048	-0.355	0.005	1.595(0.069)	1.604(0.047)	0.542	0.993	0.081	0.015	1.100(0.062)	1.126(0.040)	0.062	0.274	0.244	0.014
4th Vent - Pons	0.210(0.024)	0.198(0.017)	0.0078	0.048	-0.357	0.006	1.570(0.094)	1.571(0.097)	0.973	0.993	-0.004	0.025	1.139(0.073)	1.175(0.084)	0.080	0.287	0.228	0.020
4th Vent- Medulla	0.193(0.026)	0.173(0.019)	0.0031	0.034	-0.382	0.006	1.55(0.110)	1.583(0.112)	0.449	0.993	0.100	0.029	1.157(0.094)	1.220(0.102)	0.025	0.250	0.290	0.026
R CC - R Cb	0.201(0.010)	0.193(0.011)	0.0038	0.038	-0.401	0.003	1.577(0.053)	1.577(0.051)	0.789	0.993	-0.037	0.014	1.150(0.049)	1.176(0.043)	0.055	0.274	0.241	0.012
R CC - R Thal	0.207(0.009)	0.200(0.009)	0.0056	0.048	-0.372	0.002	1.624(0.063)	1.634(0.065)	0.930	0.993	0.011	0.016	1.187(0.058)	1.203(0.057)	0.447	0.581	0.096	0.014
R CC - R Put	0.205(0.011)	0.198(0.007)	0.0067	0.048	-0.355	0.002	1.589(0.057)	1.599(0.056)	0.723	0.993	0.047	0.015	1.161(0.058)	1.174(0.055)	0.433	0.571	0.101	0.014
R CC - R VDC	0.218(0.013)	0.210(0.007)	0.0074	0.048	-0.356	0.003	1.640(0.062)	1.652(0.055)	0.615	0.993	0.069	0.016	1.169(0.055)	1.196(0.058)	0.153	0.361	0.189	0.015
R Cb - Vermis	0.168(0.015)	0.160(0.008)	0.0067	0.048	-0.372	0.004	1.403(0.067)	1.398(0.067)	0.535	0.993	-0.084	0.018	1.083(0.052)	1.090(0.043)	0.670	0.776	0.057	0.013
R Cb - Midbrain	0.193(0.017)	0.185(0.015)	0.0073	0.048	-0.357	0.004	1.475(0.047)	1.472(0.071)	0.408	0.993	-0.111	0.016	1.097(0.053)	1.106(0.044)	0.669	0.776	0.057	0.013
R Cb - Medulla	0.188(0.021)	0.173(0.013)	0.0010	0.023	-0.435	0.005	1.478(0.077)	1.501(0.086)	0.350	0.993	0.124	0.021	1.120(0.084)	1.149(0.060)	0.080	0.287	0.236	0.020
R Put - Pons	0.251(0.012)	0.240(0.015)	0.0026	0.032	-0.422	0.004	1.574(0.055)	1.559(0.058)	0.251	0.993	-0.162	0.016	1.076(0.046)	1.077(0.040)	0.937	0.959	-0.011	0.012
Vermis - Pons	0.187(0.016)	0.177(0.013)	0.0029	0.033	-0.392	0.004	1.484(0.056)	1.496(0.090)	0.952	0.993	-0.008	0.020	1.108(0.050)	1.139(0.066)	0.070	0.274	0.232	0.015
Vermis -Medulla	0.186(0.025)	0.172(0.013)	0.0010	0.023	-0.434	0.005	1.472(0.103)	1.483(0.099)	0.985	0.997	-0.003	0.027	1.102(0.086)	1.134(0.080)	0.122	0.328	0.212	0.022

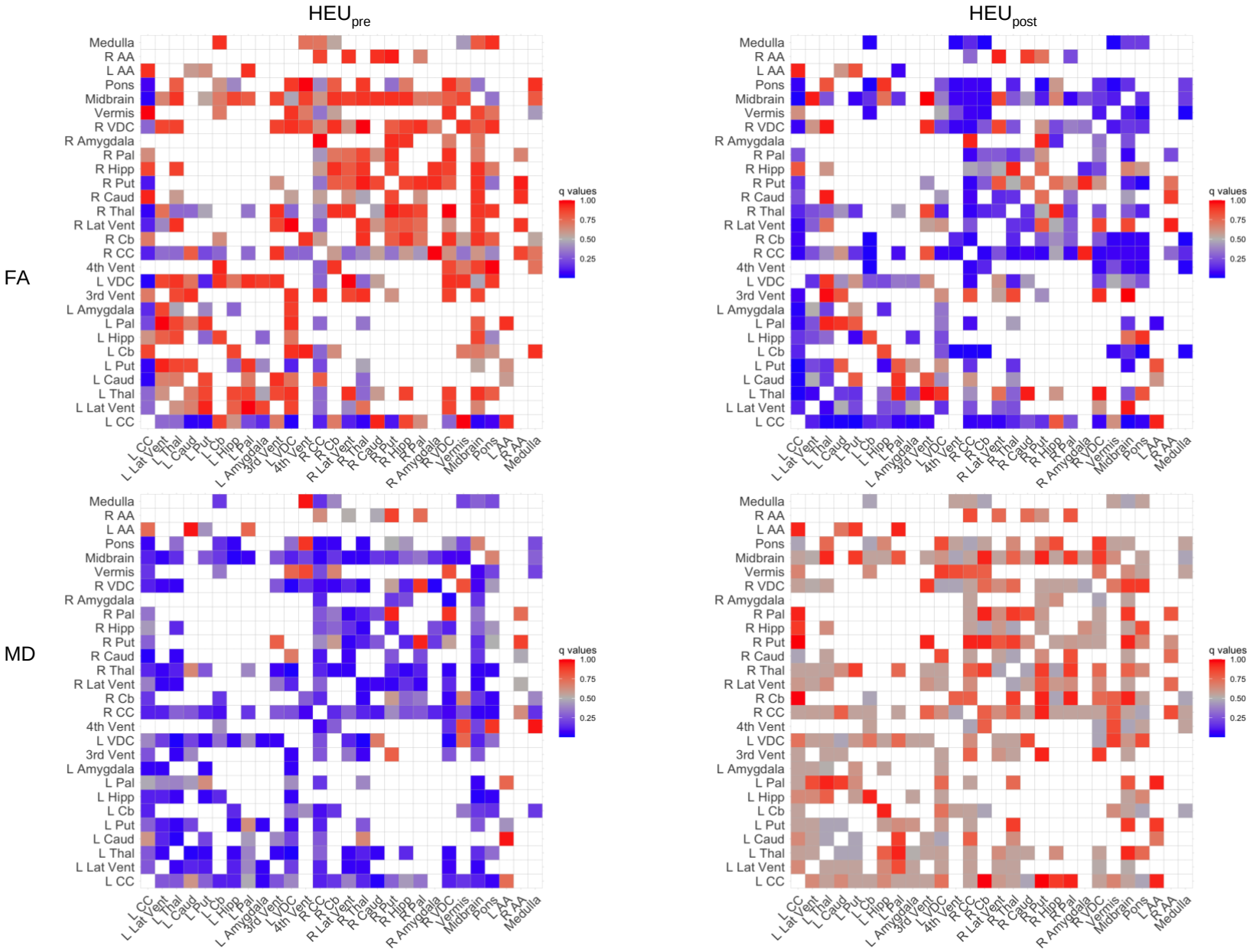

Figure 7: Plots showing heat maps of significance in WM connections for HEU$_{pre}$ and HEU$_{post}$ infants after FDR correction. Red values signify high q values, grey shows mid-range values while blue highlights low and significant values. L/R – Left/right hemisphere.

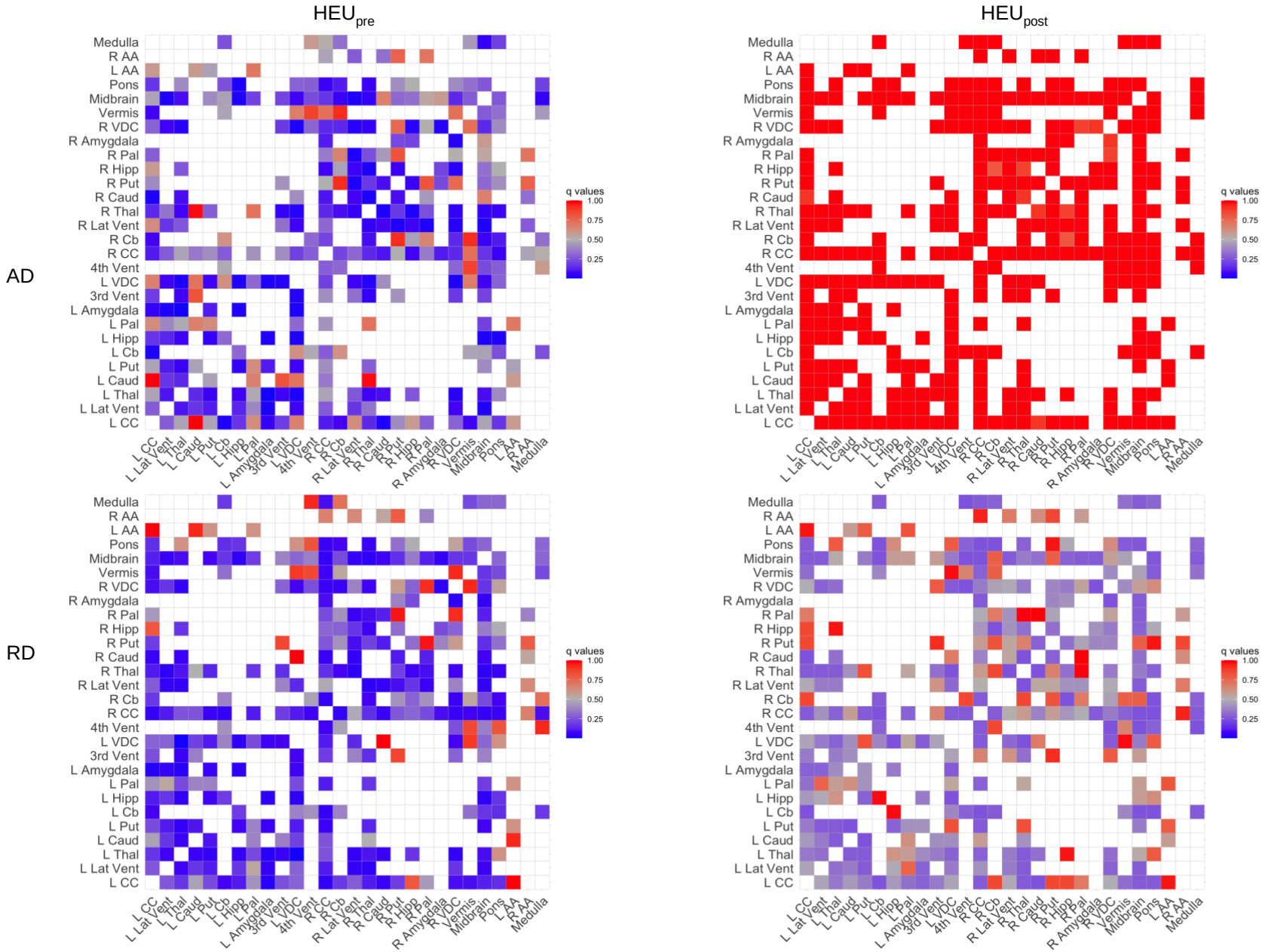

Figure 8: Plots showing heat maps of significance in WM connections for HEU_{pre} and HEU_{post} infants after FDR correction. Red values signify high q values, grey shows mid-range values while blue highlights low and significant values. L/R – Left/right hemisphere.

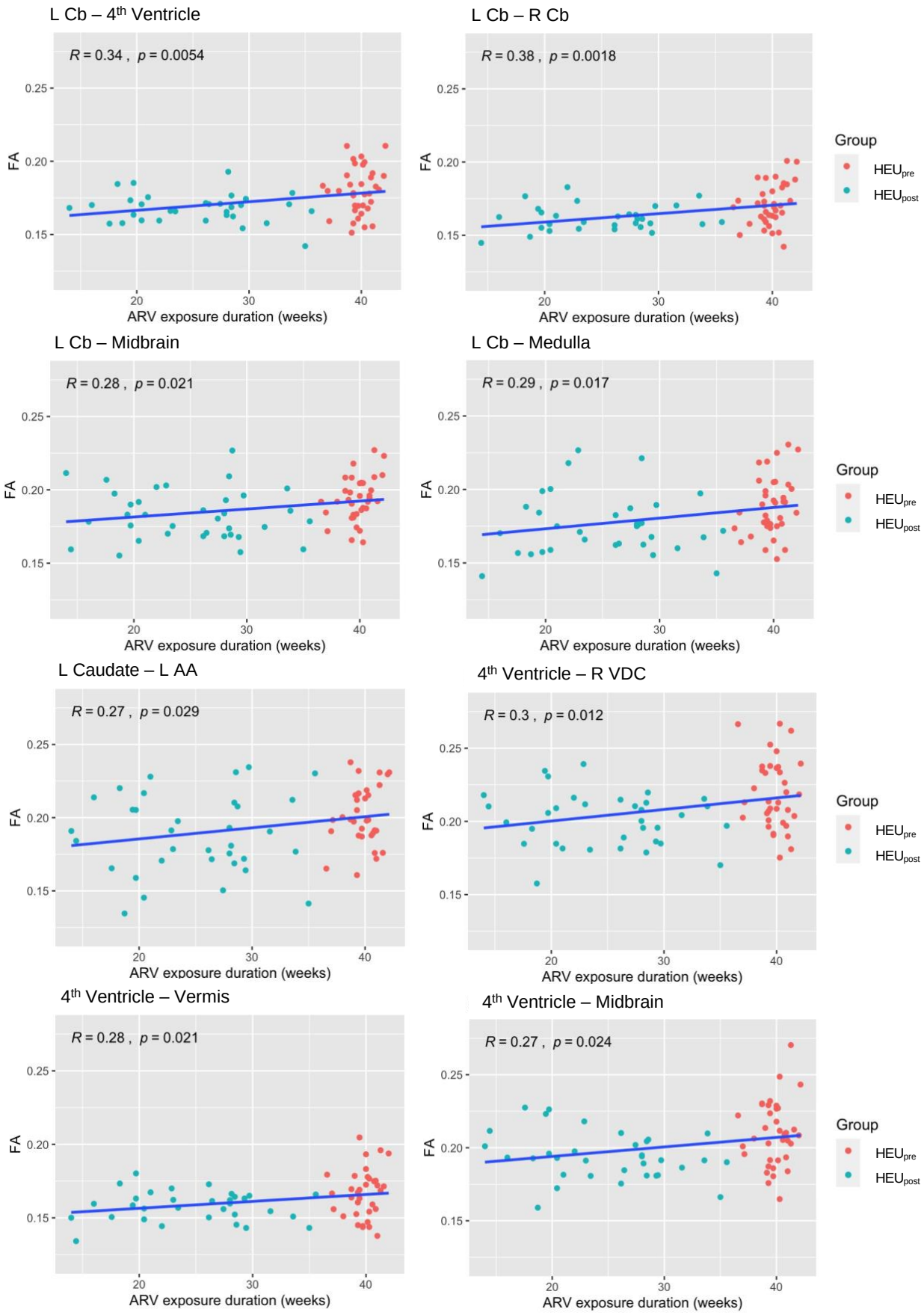

Figure 9: Plots showing associations of FA values in significant tracts (p<0.05) among HEU infants with maternal ARV exposure duration. L/R – Left/right hemisphere.

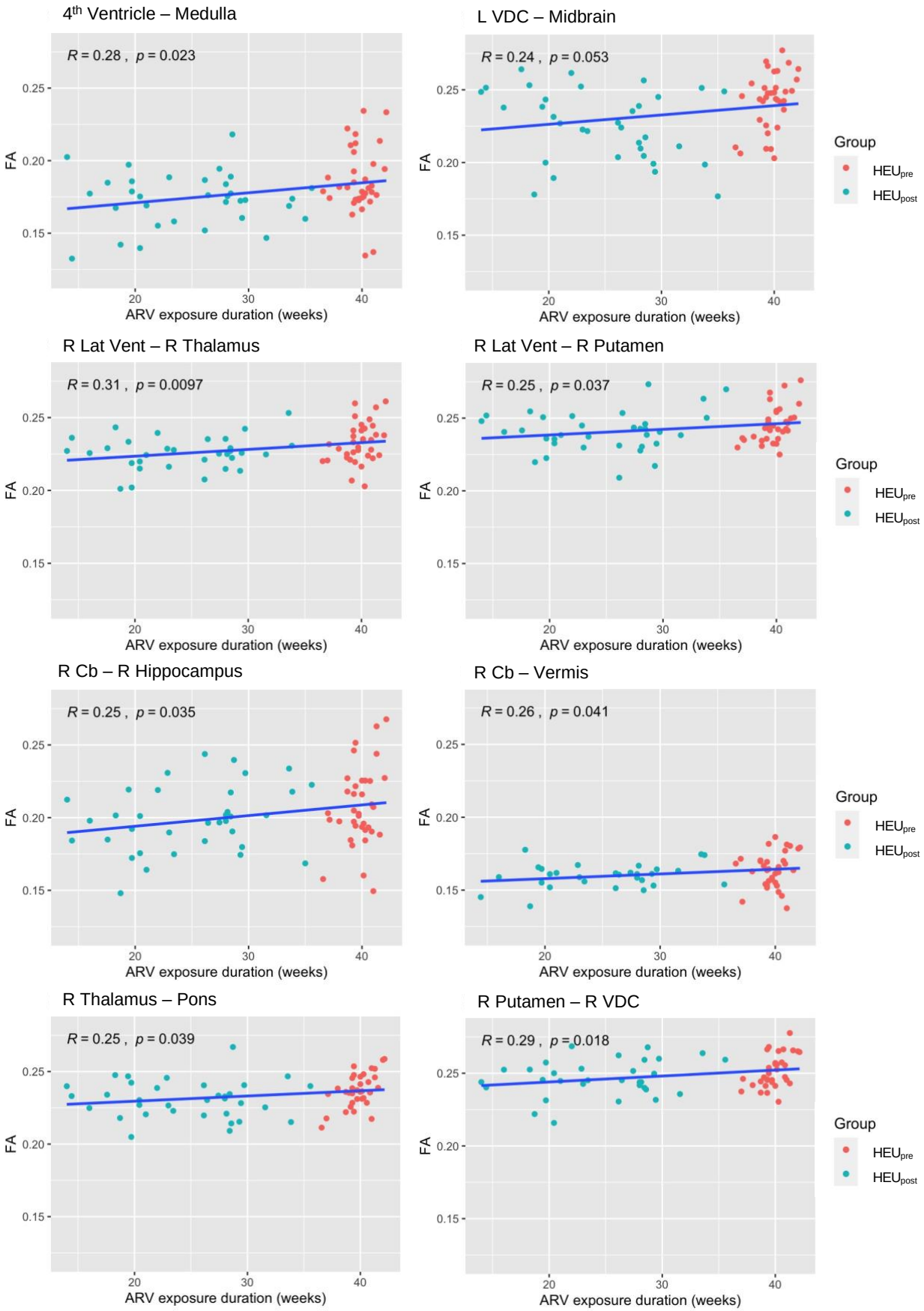

Figure 10: Plots showing associations of FA values in significant tracts (p<0.05) among HEU infants with maternal ARV exposure duration. L/R – Left/right hemisphere.

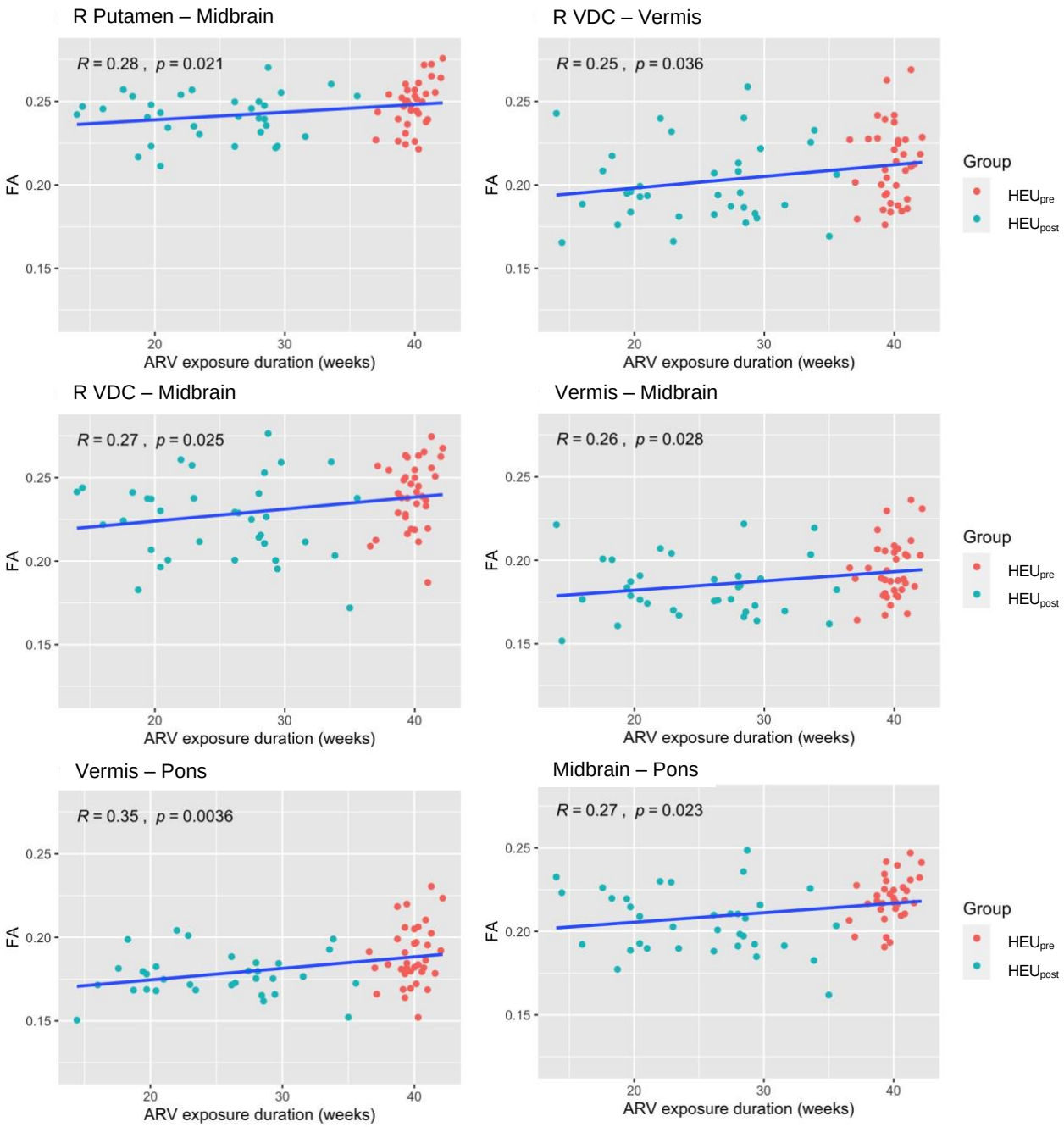

Figure 11: Plots showing associations of FA values in significant tracts (p<0.05) among HEU infants with maternal ARV exposure duration. L/R – Left/right hemisphere.

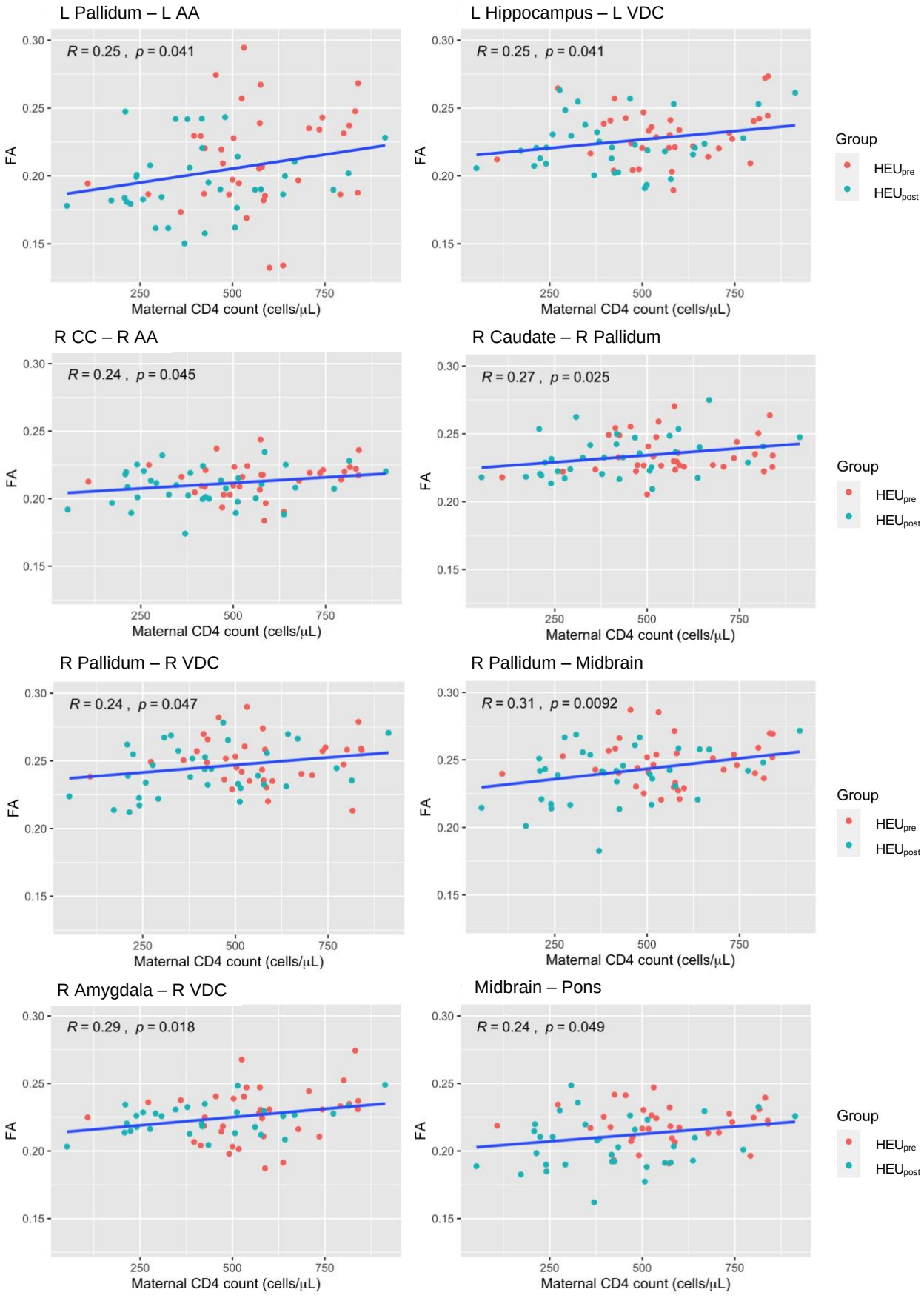

Figure 12: Plots showing associations of FA values in significant tracts (p<0.05) among HEU infants with maternal CD4 count. L/R – Left/right hemisphere.

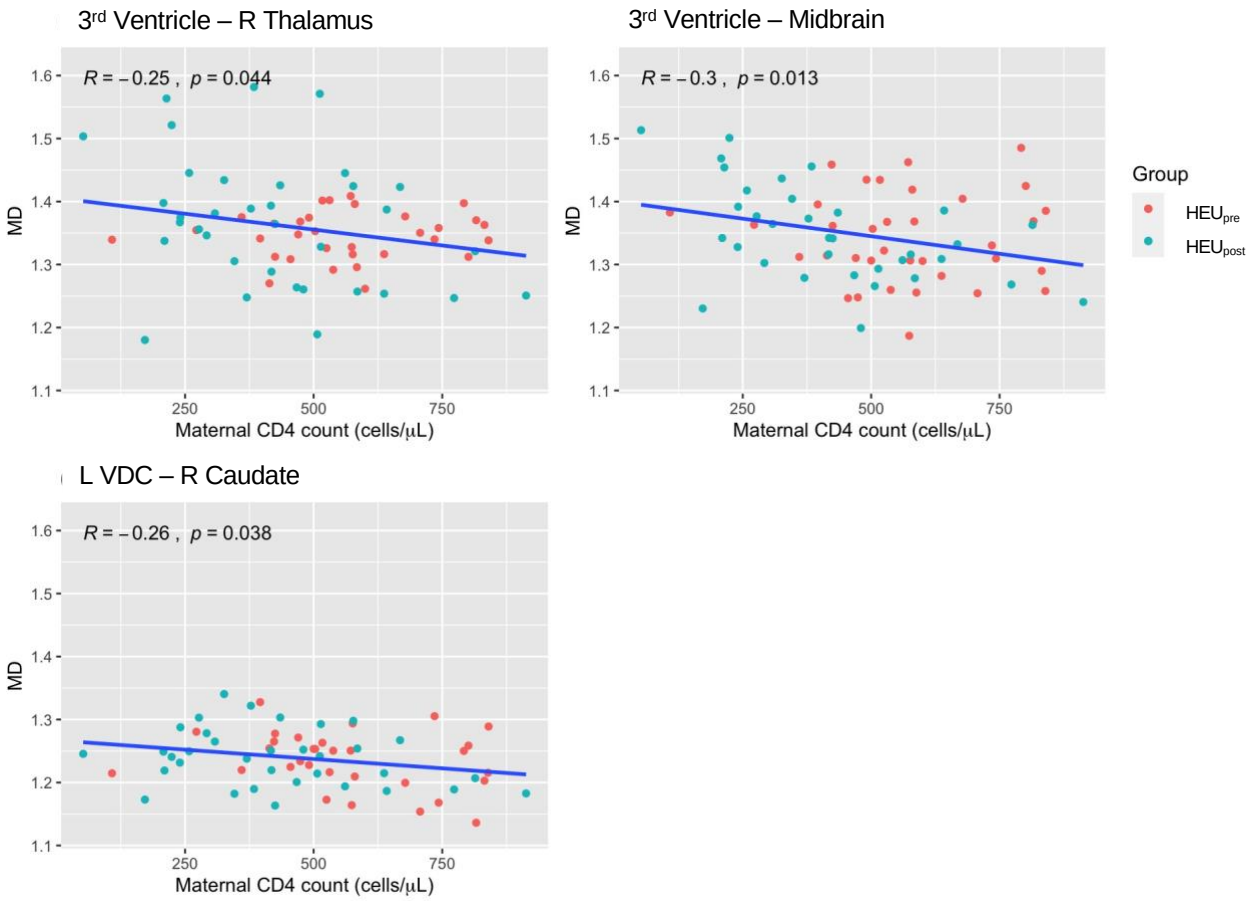

Figure 13: Plots showing associations of MD values in significant tracts (p<0.05) among HEU infants with maternal CD4 count. L/R – Left/right hemisphere.

Table 8: Summary of tracts that have significantly lower FA values compared to HUU infants in both HEU_{pre} and HEU_{post} groups.

connections	HEU_{pre} q value	HEU_{post} q value
L CC - L Caudate	0.036	0.024
L CC - L Putamen	0.046	0.010
L CC - L VDC	0.028	0.001
L CC - Midbrain	0.036	0.023

Table 9: Summary of tracts that have significantly lower FA values compared to HUU infants and are also significantly associated with ART exposure duration.

connections	HEU_{post} q value	correlation q value
L Cb - 4th Ventricle	0.023	0.005
L Cb - R Cb	0.023	0.002
L Cb - Pons	0.023	0.052
L Cb - Medulla	0.028	0.017
4th Ventricle - Medulla	0.034	0.023
R Cb - Vermis	0.048	0.041
Vermis - Pons	0.033	0.004

4.3. Graph Theory Analysis

The following results are the outputs from the linear models comparing the HEU groups to HUU controls for various graph measures, and their associations with maternal clinical and treatment variables.

4.3.1. Linear model analysis

There were no significant differences in the q values in any of the measures in both groups aside from nodal efficiency, which had 2 regions in HEU_{pre} with significantly reduced efficiency (the left putamen and the right accumbens area) after multiple comparison correction.

Considering the p values before multiple comparison correction, we see that strength and transitivity both have significantly lower values in HEU_{pre} when compared to HUU in the left and right basal ganglia communities (specifically for the right caudate and left and right putamen, with the left and right ventral diencephalons trending towards significance at $p<0.05$). The pons in the hindbrain also has a significantly lower strength than HUU before correction. The local and nodal efficiencies in HEU_{pre} are nearly all significantly lower than HUU for all communities, but most especially in the hindbrain. In HEU_{post} vs HUU, strength and transitivity are significantly lower in the left and right basal ganglia communities and the hindbrain once again, but for fewer nodes. The local and nodal efficiency are most significantly impacted in the left basal ganglia community and the hindbrain as well.

For the graph modularity, there were 4 communities that were formed in all groups, comprising of the left subcortical structures from the basal ganglia (shown in green in Table 10 – 15 and Figure 14 below), right subcortical structures from the basal ganglia (shown in purple), the brain stem and cortical structures from the hindbrain (shown in pink) and a remainder group containing a mixture of cortical and subcortical structures (the cerebral cortex, left and right hippocampi, amygdala and lateral ventricles) from the forebrain (shown in blue). The 3rd ventricle changes a membership status from the right subcortical structure group in HEU_{pre} and HUU to the left subcortical structure group in HEU_{post}. This does not significantly impact the overall modularity of the different groups.

4.3.2. Associations with maternal clinical and treatment variables

In Figure 15 – 19 we present an exploratory analysis of significant associations ($p<0.05$) between maternal clinical and treatment variables and graph measures (strength, local and nodal efficiency) among HEU infants.

The results are varied across the different measures and are inconsistent, with regions showing positive and negative correlations with ARV exposure duration and CD4 count.

A summary of the graph theory results and the connectome graphs is presented below.

Table 10: Summary of linear regression outputs for strength and transitivity graph measures in HUU vs. HEU_{pre} infants before and after FDR correction for all nodes

		Strength						Transitivity					
	region name	mean HUU (SD)	mean HEU_{pre} (SD)	p	q	std beta	std error	mean HUU (SD)	mean HEU_{pre} (SD)	p	q	std beta	std error
Forebrain	L CC	0.337 (0.063)	0.339 (0.057)	0.760	0.863	0.042	0.016	0.629 (0.031)	0.632 (0.025)	0.429	0.969	0.105	0.007
	L Lat Vent	0.144 (0.042)	0.138 (0.032)	0.802	0.863	-0.034	0.010	0.834 (0.015)	0.832 (0.014)	0.831	0.969	-0.029	0.004
	L Hipp	0.060 (0.020)	0.055 (0.014)	0.303	0.741	-0.135	0.004	0.860 (0.012)	0.860 (0.010)	0.678	0.969	0.030	0.002
	L Amygdala	0.018 (0.011)	0.019 (0.009)	0.878	0.911	0.020	0.003	1.000 (0.000)	1.000 (0.000)	-	-	-	-
	R CC	0.336 (0.065)	0.340 (0.053)	0.583	0.863	0.076	0.016	0.629 (0.024)	0.630 (0.019)	0.598	0.969	0.070	0.006
	R Lat Vent	0.147 (0.043)	0.147 (0.044)	0.501	0.863	0.090	0.011	0.837 (0.015)	0.840 (0.013)	0.720	0.969	0.046	0.004
	R Hipp	0.058 (0.019)	0.059 (0.022)	0.478	0.863	0.081	0.005	0.856 (0.016)	0.852 (0.017)	0.100	0.546	-0.124	0.002
	R Amygdala	0.010 (0.004)	0.011 (0.005)	0.781	0.863	0.036	0.001	1.000 (0.000)	1.000 (0.000)	-	-	-	-
L Basal Ganglia	L Thal	0.202 (0.049)	0.206 (0.047)	0.595	0.863	0.063	0.011	0.726 (0.016)	0.724 (0.015)	0.533	0.969	-0.084	0.004
	L Caud	0.050 (0.022)	0.045 (0.011)	0.198	0.615	-0.176	0.005	0.876 (0.011)	0.874 (0.010)	0.945	0.969	-0.009	0.003
	L Put	0.119 (0.033)	0.138 (0.026)	0.060	0.389	0.241	0.008	0.876 (0.011)	0.871 (0.011)	0.009	0.203	-0.327	0.002
	L Pal	0.063 (0.015)	0.063 (0.014)	0.557	0.863	-0.076	0.004	0.923 (0.014)	0.918 (0.012)	0.119	0.546	-0.210	0.003
	L AA	0.003 (0.002)	0.003 (0.002)	0.770	0.863	0.039	0.000	1.000 (0.000)	1.000 (0.000)	-	-	-	-
	L VDC	0.098 (0.027)	0.113 (0.025)	0.083	0.389	0.229	0.007	0.705 (0.030)	0.707 (0.043)	0.626	0.969	0.066	0.010
R Basal Ganglia + 3rd Vent	3rd Vent	0.023 (0.010)	0.020 (0.008)	0.195	0.615	-0.165	0.002	0.937 (0.010)	0.937 (0.013)	0.888	0.969	0.019	0.003
	R Thal	0.197 (0.048)	0.206 (0.053)	0.423	0.863	0.091	0.011	0.723 (0.017)	0.721 (0.013)	0.800	0.969	0.033	0.004
	R Caud	0.063 (0.025)	0.056 (0.016)	0.029	0.269	-0.285	0.005	0.878 (0.025)	0.867 (0.013)	0.064	0.546	-0.253	0.005
	R Put	0.127 (0.035)	0.152 (0.033)	0.018	0.269	0.309	0.009	0.804 (0.016)	0.808 (0.011)	0.212	0.754	0.169	0.004
	R Pal	0.065 (0.016)	0.073 (0.016)	0.311	0.741	0.132	0.004	0.891 (0.016)	0.892 (0.012)	0.802	0.969	0.034	0.004
	R AA	0.004 (0.003)	0.004 (0.002)	0.914	0.914	-0.015	0.001	1.000 (0.000)	1.000 (0.000)	-	-	-	-
	R VDC	0.105 (0.030)	0.116 (0.030)	0.081	0.389	0.224	0.007	0.753 (0.025)	0.752 (0.026)	0.651	0.969	-0.059	0.006
Hindbrain	L Cb	0.064 (0.017)	0.065 (0.015)	0.774	0.863	0.039	0.004	0.885 (0.019)	0.884 (0.018)	0.969	0.969	-0.005	0.005
	4th Vent	0.028 (0.013)	0.029 (0.010)	0.668	0.863	0.058	0.003	0.948 (0.012)	0.945 (0.014)	0.388	0.969	-0.114	0.003
	R Cb	0.075 (0.023)	0.077 (0.021)	0.797	0.863	0.035	0.006	0.828 (0.020)	0.824 (0.017)	0.229	0.754	-0.153	0.005
	Vermis	0.028 (0.012)	0.029 (0.011)	0.616	0.863	0.067	0.003	0.903 (0.008)	0.903 (0.010)	0.958	0.969	-0.007	0.002
	Midbrain	0.217 (0.071)	0.237 (0.059)	0.168	0.615	0.196	0.011	0.585 (0.022)	0.588 (0.023)	0.733	0.969	0.046	0.006
	Pons	0.179 (0.059)	0.197 (0.055)	0.029	0.269	0.310	0.010	0.739 (0.013)	0.738 (0.011)	0.114	0.546	-0.138	0.002
	Medulla	0.039 (0.017)	0.041 (0.016)	0.318	0.741	0.134	0.004	1.000 (0.000)	1.000 (0.000)	-	-	-	-

**The colours in the node column correspond to the colours of the communities that are present in the modularity graph for the group. The communities in the graph are comprised of the left and right basal ganglia (in green and purple respectively), the forebrain (in blue) and the hindbrain (in pink).*

**For transitivity, some nodes had the same values for both groups, hence a group comparison was not possible. These entries are shown by the dash (-) in the table above.*

Table 11: Summary of linear regression outputs for local and nodal efficiency graph measures in HUU vs. HEU_{pre} infants before and after FDR correction for all nodes

		Local efficiency						Nodal efficiency					
	region name	mean HUU (SD)	mean HEU_{pre} (SD)	p	q	std beta	std error	mean HUU (SD)	mean HEU_{pre} (SD)	p	q	std beta	std error
Forebrain	L CC	15246 (32732)	10791 (19609)	0.391	0.522	-0.117	7193	21498 (73617)	12794 (59021)	0.371	0.452	-0.119	17471
	L Lat Vent	12077 (26203)	7281 (23012)	0.553	0.667	-0.082	6733	12188 (39148)	6524 (18038)	0.528	0.536	-0.085	8026
	L Hipp	925 (866)	466 (191)	0.014	0.145	-0.374	190	2704 (2353)	5259 (5059)	0.133	0.280	0.201	1102
	L Amygdala	389 (225)	292 (147)	0.161	0.281	-0.194	53	1923 (1221)	1186 (475)	0.019	0.179	-0.335	272
	R CC	19853 (47880)	12082 (22000)	0.245	0.404	-0.158	9871	6328 (10079)	3100 (2564)	0.095	0.265	-0.229	1994
	R Lat Vent	3894 (3762)	2013 (1157)	0.004	0.109	-0.403	782	9952 (26603)	18041 (83512)	0.323	0.430	0.136	16829
	R Hipp	21562 (65165)	6078 (12241)	0.087	0.186	-0.230	12293	6838 (9285)	14603 (52942)	0.414	0.483	0.112	10350
	R Amygdala	1034 (712)	729 (374)	0.043	0.165	-0.278	155	27646 (65659)	8232 (12594)	0.035	0.196	-0.282	12383
L Basal Ganglia	L Thal	11939 (20721)	12736 (29807)	0.691	0.774	0.055	6922	8274 (19383)	5179 (9513)	0.208	0.311	-0.166	3931
	L Caud	5577 (12585)	3345 (7445)	0.572	0.667	-0.078	2790	32432 (107783)	15958 (21138)	0.219	0.311	-0.167	20647
	L Put	12790 (30380)	4748 (5905)	0.087	0.186	-0.233	5837	2590 (2393)	1322 (768)	0.002	0.034	-0.454	509
	L Pal	13119 (41501)	2874 (3467)	0.089	0.186	-0.231	7846	11540 (24077)	6716 (13418)	0.459	0.514	-0.101	5230
	L AA	137 (43)	164 (49)	0.048	0.165	0.293	14	5704 (11193)	3649 (7360)	0.365	0.452	-0.119	2443
	L VDC	8489 (10547)	6631 (5917)	0.466	0.593	-0.100	2309	44369 (131919)	26087 (101323)	0.511	0.536	-0.090	31666
R Basal Ganglia + 3rd Vent	3rd Vent	15070 (42538)	10238 (39743)	0.734	0.791	-0.047	11228	15781 (35976)	29593 (55353)	0.536	0.536	0.077	11540
	R Thal	15666 (43946)	15870 (34436)	0.893	0.926	-0.018	10537	6812 (9353)	3820 (2938)	0.108	0.275	-0.237	2010
	R Caud	11035 (32073)	12945 (38986)	0.926	0.926	0.013	9665	7930 (14775)	21000 (74068)	0.154	0.287	0.188	13942
	R Put	16827 (34923)	9227 (20773)	0.093	0.186	-0.223	7438	5940 (7366)	2803 (1957)	0.066	0.229	-0.266	1572
	R Pal	1295 (779)	914 (448)	0.021	0.145	-0.344	187	24816 (69913)	12440 (37876)	0.089	0.265	-0.225	14439
	R AA	529 (717)	1397 (5715)	0.285	0.444	0.146	1099	2697 (1903)	1535 (575)	0.002	0.034	-0.441	418
	R VDC	4578 (3866)	2763 (1424)	0.070	0.186	-0.277	906	32789 (93579)	11557 (32274)	0.190	0.311	-0.179	18772
Hindbrain	L Cb	12919 (35043)	3562 (3401)	0.053	0.165	-0.257	6478	2642 (2211)	4340 (3810)	0.222	0.311	0.164	860
	4th Vent	2176 (2253)	1249 (892)	0.036	0.165	-0.316	513	2471 (2552)	1242 (607)	0.042	0.197	-0.300	555
	R Cb	1940 (1361)	1170 (753)	0.041	0.165	-0.309	336	5019 (4788)	2996 (2071)	0.189	0.311	-0.199	1134
	Vermis	1396 (1470)	536 (225)	0.016	0.145	-0.354	320	25392 (77136)	4836 (5658)	0.058	0.229	-0.253	14273
	Midbrain	15440 (34599)	10357 (21821)	0.367	0.514	-0.122	7662	21034 (43148)	11289 (16159)	0.140	0.280	-0.198	8573
	Pons	17300 (45964)	6877 (16331)	0.103	0.192	-0.217	8967	11236 (29952)	4585 (6890)	0.126	0.280	-0.204	5665
	Medulla	3377 (7646)	1297 (1747)	0.314	0.463	-0.136	1478	6264 (14337)	2916 (4761)	0.034	0.196	-0.208	2029

**The colours in the node column correspond to the colours of the communities that are present in the modularity graph for the group. The communities in the graph are comprised of the left and right basal ganglia (in green and purple respectively), the forebrain (in blue) and the hindbrain (in pink). Significant q values are shown in orange.*

Table 12: Summary of linear regression outputs for strength and transitivity graph measures in HUU vs. HEU_{post} infants before and after FDR correction for all nodes

		Strength						Transitivity					
	region name	mean HUU (SD)	mean HEU_{post} (SD)	p	q	std beta	std error	mean HUU (SD)	mean HEU_{post} (SD)	p	q	std beta	std error
Forebrain	L CC	0.337 (0.063)	0.335 (0.043)	0.989	0.991	0.002	0.013	0.629 (0.031)	0.630 (0.021)	0.865	0.880	0.023	0.007
	L Lat Vent	0.144 (0.042)	0.130 (0.029)	0.294	0.667	-0.131	0.009	0.834 (0.015)	0.838 (0.019)	0.404	0.876	0.112	0.005
	L Hipp	0.060 (0.020)	0.060 (0.018)	0.895	0.991	0.016	0.005	0.860 (0.012)	0.864 (0.011)	0.022	0.205	0.168	0.002
	L Amygdala	0.018 (0.011)	0.020 (0.016)	0.704	0.922	0.052	0.004	1.000 (0.000)	1.000 (0.000)	-	-	-	-
	R CC	0.336 (0.065)	0.338 (0.035)	0.863	0.991	0.023	0.014	0.629 (0.024)	0.632 (0.018)	0.670	0.880	0.058	0.006
	R Lat Vent	0.147 (0.043)	0.132 (0.033)	0.332	0.667	-0.125	0.010	0.837 (0.015)	0.844 (0.016)	0.419	0.876	0.098	0.004
	R Hipp	0.058 (0.019)	0.059 (0.018)	0.502	0.703	0.087	0.005	0.856 (0.016)	0.854 (0.017)	0.067	0.388	-0.134	0.002
	R Amygdala	0.010 (0.004)	0.011 (0.004)	0.139	0.628	0.188	0.001	1.000 (0.000)	1.000 (0.000)	-	-	-	-
L Basal Ganglia + 3rd Vent	L Thal	0.202 (0.049)	0.208 (0.045)	0.337	0.667	0.112	0.011	0.726 (0.016)	0.731 (0.019)	0.387	0.876	0.117	0.005
	L Caud	0.050 (0.022)	0.047 (0.018)	0.455	0.703	-0.100	0.004	0.876 (0.011)	0.876 (0.010)	0.724	0.880	0.047	0.003
	L Put	0.119 (0.033)	0.114 (0.033)	0.338	0.667	-0.122	0.008	0.876 (0.011)	0.874 (0.015)	0.704	0.880	-0.049	0.003
	L Pal	0.063 (0.015)	0.057 (0.015)	0.108	0.628	-0.208	0.004	0.923 (0.014)	0.920 (0.009)	0.288	0.876	-0.140	0.003
	3rd Vent	0.023 (0.010)	0.022 (0.008)	0.958	0.991	0.007	0.002	0.937 (0.010)	0.937 (0.011)	0.823	0.880	-0.027	0.003
	L AA	0.003 (0.002)	0.003 (0.002)	0.991	0.991	-0.002	0.001	1.000 (0.000)	1.000 (0.000)	-	-	-	-
	L VDC	0.098 (0.027)	0.108 (0.026)	0.038	0.499	0.276	0.007	0.705 (0.030)	0.713 (0.035)	0.373	0.876	0.121	0.009
R Basal Ganglia	R Thal	0.197 (0.048)	0.196 (0.046)	0.725	0.922	0.045	0.012	0.723 (0.017)	0.729 (0.016)	0.027	0.205	0.292	0.004
	R Caud	0.063 (0.025)	0.052 (0.022)	0.157	0.628	-0.177	0.006	0.878 (0.025)	0.878 (0.020)	0.815	0.880	0.031	0.006
	R Put	0.127 (0.035)	0.139 (0.035)	0.357	0.667	0.117	0.009	0.804 (0.016)	0.811 (0.013)	0.119	0.549	0.196	0.004
	R Pal	0.065 (0.016)	0.067 (0.017)	0.842	0.991	0.027	0.004	0.891 (0.016)	0.895 (0.015)	0.669	0.880	0.057	0.004
	R AA	0.004 (0.003)	0.003 (0.002)	0.384	0.672	-0.117	0.001	1.000 (0.000)	1.000 (0.000)	-	-	-	-
	R VDC	0.105 (0.030)	0.111 (0.030)	0.492	0.703	0.091	0.008	0.753 (0.025)	0.752 (0.018)	0.533	0.876	-0.082	0.006
Hindbrain	L Cb	0.064 (0.017)	0.071 (0.014)	0.053	0.499	0.254	0.004	0.885 (0.019)	0.880 (0.019)	0.267	0.876	-0.151	0.005
	4th Vent	0.028 (0.013)	0.029 (0.011)	0.298	0.667	0.137	0.003	0.948 (0.012)	0.940 (0.010)	0.013	0.205	-0.325	0.003
	R Cb	0.075 (0.023)	0.084 (0.022)	0.019	0.499	0.307	0.005	0.828 (0.020)	0.828 (0.021)	0.868	0.880	-0.022	0.005
	Vermis	0.028 (0.012)	0.033 (0.017)	0.232	0.667	0.159	0.004	0.903 (0.008)	0.902 (0.012)	0.880	0.880	-0.020	0.003
	Midbrain	0.217 (0.071)	0.225 (0.061)	0.473	0.703	0.093	0.017	0.585 (0.022)	0.590 (0.016)	0.503	0.876	0.090	0.005
	Pons	0.179 (0.059)	0.192 (0.056)	0.265	0.667	0.143	0.015	0.739 (0.013)	0.738 (0.016)	0.505	0.876	-0.062	0.003
	Medulla	0.039 (0.017)	0.045 (0.017)	0.115	0.628	0.209	0.004	1.000 (0.000)	1.000 (0.000)	-	-	-	-

**The colours in the node column correspond to the colours of the communities that are present in the modularity graph for the group. The communities in the graph are comprised of the left and right basal ganglia (in green and purple respectively), the forebrain (in blue) and the hindbrain (in pink).*

**For transitivity, some nodes had the same values for both groups, hence a group comparison was not possible. These entries are shown by the dash (-) in the table above.*

Table 13: Summary of linear regression outputs for strength and transitivity graph measures in HUU vs. HEU_{post} infants before and after FDR correction for all nodes

		Local efficiency						Nodal efficiency					
	region name	mean HUU (SD)	mean HEU_{post} (SD)	p	q	std beta	std error	mean HUU (SD)	mean HEU_{post} (SD)	p	q	std beta	std error
Forebrain	L CC	15246 (32732)	13098 (22500)	0.456	0.608	-0.097	7173	21498 (73617)	7271 (17759)	0.165	0.517	-0.186	14095
	L Lat Vent	12077 (26203)	2067 (1221)	0.008	0.125	-0.386	921	12188 (39148)	10544 (30836)	0.703	0.820	-0.052	9456
	L Hipp	925 (866)	18599 (63797)	0.908	0.960	0.015	13931	2704 (2353)	15491 (52113)	0.411	0.606	0.111	10189
	L Amygdala	389 (225)	382 (260)	0.712	0.831	-0.050	73	1923 (1221)	12042 (51327)	0.442	0.618	0.104	9752
	R CC	19853 (47880)	12136 (21776)	0.260	0.513	-0.149	9644	6328 (10079)	4144 (6075)	0.305	0.538	-0.140	2236
	R Lat Vent	3894 (3762)	9586 (23414)	0.960	0.960	0.007	5863	9952 (26603)	6771 (11204)	0.670	0.816	-0.058	5510
	R Hipp	21562 (65165)	1626 (1071)	0.030	0.138	-0.325	822	6838 (9285)	9221 (14845)	0.548	0.698	0.081	3305
	R Amygdala	1034 (712)	1577 (1887)	0.622	0.757	-0.067	607	27646 (65659)	3979 (2470)	0.033	0.306	-0.311	1585
L Basal Ganglia + 3rd Vent	L Thal	11939 (20721)	12023 (21296)	0.863	0.960	-0.023	5576	8274 (19383)	3986 (3576)	0.082	0.393	0.250	844
	L Caud	5577 (12585)	7332 (18173)	0.544	0.692	0.083	4195	32432 (107783)	4325 (3567)	0.023	0.306	-0.340	2272
	L Put	12790 (30380)	8870 (20750)	0.321	0.513	-0.131	6739	2590 (2393)	16335 (53698)	0.222	0.517	0.165	10205
	L Pal	13119 (41501)	7856 (17888)	0.392	0.549	-0.116	8491	11540 (24077)	15261 (34591)	0.775	0.835	0.038	7813
	3rd Vent	15070 (42538)	5802 (14502)	0.156	0.438	-0.190	8397	15781 (35976)	17951 (48895)	0.734	0.822	0.047	11541
	L AA	137 (43)	178 (70)	0.035	0.138	0.285	16	5704 (11193)	2530 (1677)	0.099	0.396	0.229	389
	L VDC	8489 (10547)	12590 (20438)	0.329	0.513	0.131	4315	44369 (131919)	22695 (91135)	0.178	0.517	-0.174	28708
R Basal Ganglia	R Thal	15666 (43946)	9525 (16771)	0.288	0.513	-0.142	8746	6812 (9353)	15874 (41357)	0.493	0.657	-0.091	10659
	R Caud	11035 (32073)	8318 (27573)	0.936	0.960	-0.011	8061	7930 (14775)	8482 (21750)	0.808	0.838	0.033	5012
	R Put	16827 (34923)	9555 (20286)	0.331	0.513	-0.130	7554	5940 (7366)	8739 (12687)	0.204	0.517	-0.171	13571
	R Pal	1295 (779)	3631 (9536)	0.347	0.513	-0.128	8807	24816 (69913)	12062 (43534)	0.345	0.568	-0.128	15580
	R AA	529 (717)	442 (260)	0.023	0.128	0.334	65	2697 (1903)	11200 (45045)	0.293	0.538	0.142	8985
	R VDC	4578 (3866)	6998 (8410)	0.090	0.316	-0.222	7754	32789 (93579)	17296 (40991)	0.244	0.526	-0.156	19010
Hindbrain	L Cb	12919 (35043)	1555 (1007)	0.012	0.125	-0.353	565	2642 (2211)	28446 (100080)	0.969	0.969	0.005	21371
	4th Vent	2176 (2253)	1096 (678)	0.019	0.128	-0.333	478	2471 (2552)	1144 (439)	0.013	0.306	-0.347	518
	R Cb	1940 (1361)	4666 (11891)	0.144	0.438	-0.193	5752	5019 (4788)	7242 (12130)	0.202	0.517	-0.171	16670
	Vermis	1396 (1470)	554 (198)	0.013	0.125	-0.353	314	25392 (77136)	2362 (1377)	0.084	0.393	-0.245	584
	Midbrain	15440 (34599)	9423 (17630)	0.181	0.461	-0.173	6962	21034 (43148)	13730 (23142)	0.405	0.606	-0.111	9081
	Pons	17300 (45964)	12427 (31338)	0.348	0.513	-0.121	9925	11236 (29952)	6455 (13254)	0.307	0.538	-0.135	6031
	Medulla	3377 (7646)	1370 (2587)	0.243	0.513	-0.158	1537	6264 (14337)	1386 (899)	0.062	0.393	-0.262	410

**The colours in the node column correspond to the colours of the communities that are present in the modularity graph for the group. The communities in the graph are comprised of the left and right basal ganglia (in green and purple respectively), the forebrain (in blue) and the hindbrain (in pink).*

Table 14: Summary of linear regression outputs for various global graph measures in HUU vs. HEU_{pre} infants after FDR correction

Global measure	mean HUU (SD)	mean HEU_{pre} (SD)	q value	std beta	std error
Global efficiency	16424 (36476)	10329 (16636)	0.238	-0.160	7516
Modularity	0.152 (0.047)	0.140 (0.038)	0.195	-0.171	0.011

Table 15: Summary of linear regression outputs for various global graph measures in HUU vs. HEU_{pre} infants after FDR correction

Global measure	mean HUU (SD)	mean HEU_{post} (SD)	q value	std beta	std error
Global efficiency	16424 (36476)	11891 (18290)	0.360	-0.121	7481
Modularity	0.152 (0.047)	0.146 (0.041)	0.526	0.080	0.011

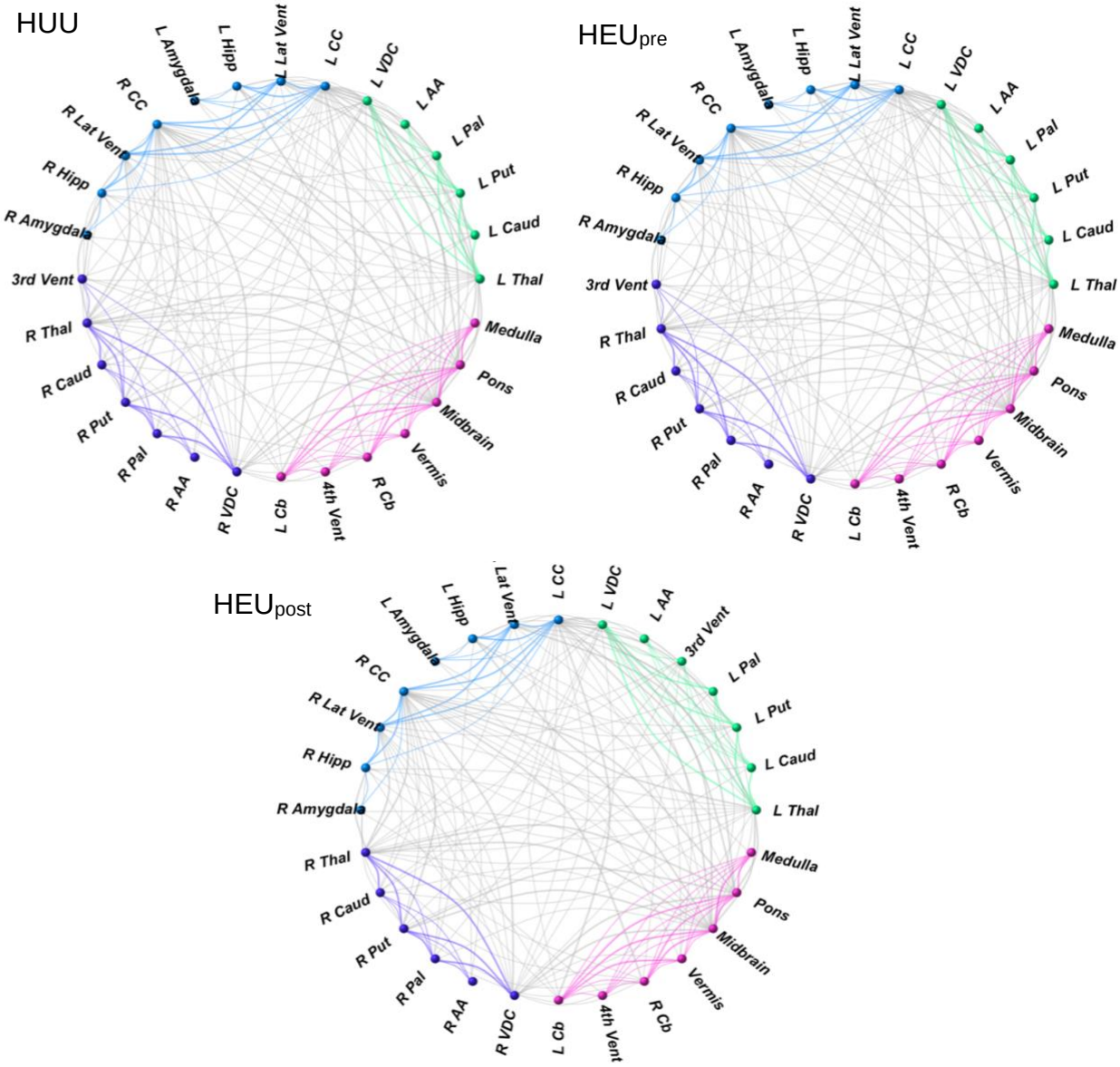

Figure 14: Structural modules for HUU, In HEU_{pre}, and HEU_{post} groups. The modules include: 1. Blue: L & R subcortical nodes from the forebrain; 2. Green: Left subcortical nodes from the basal ganglia; 3. Pink: Brain stem, cortical and subcortical nodes from the hindbrain and 4. Purple: R subcortical nodes from the basal ganglia. In HEU_{post}, the 3rd ventricle changes communities from the left basal ganglia group to the right basal ganglia group, but this has no significant impact on the graph's overall modularity. Structure abbreviations may be referred to in Table 3 above.

Strength

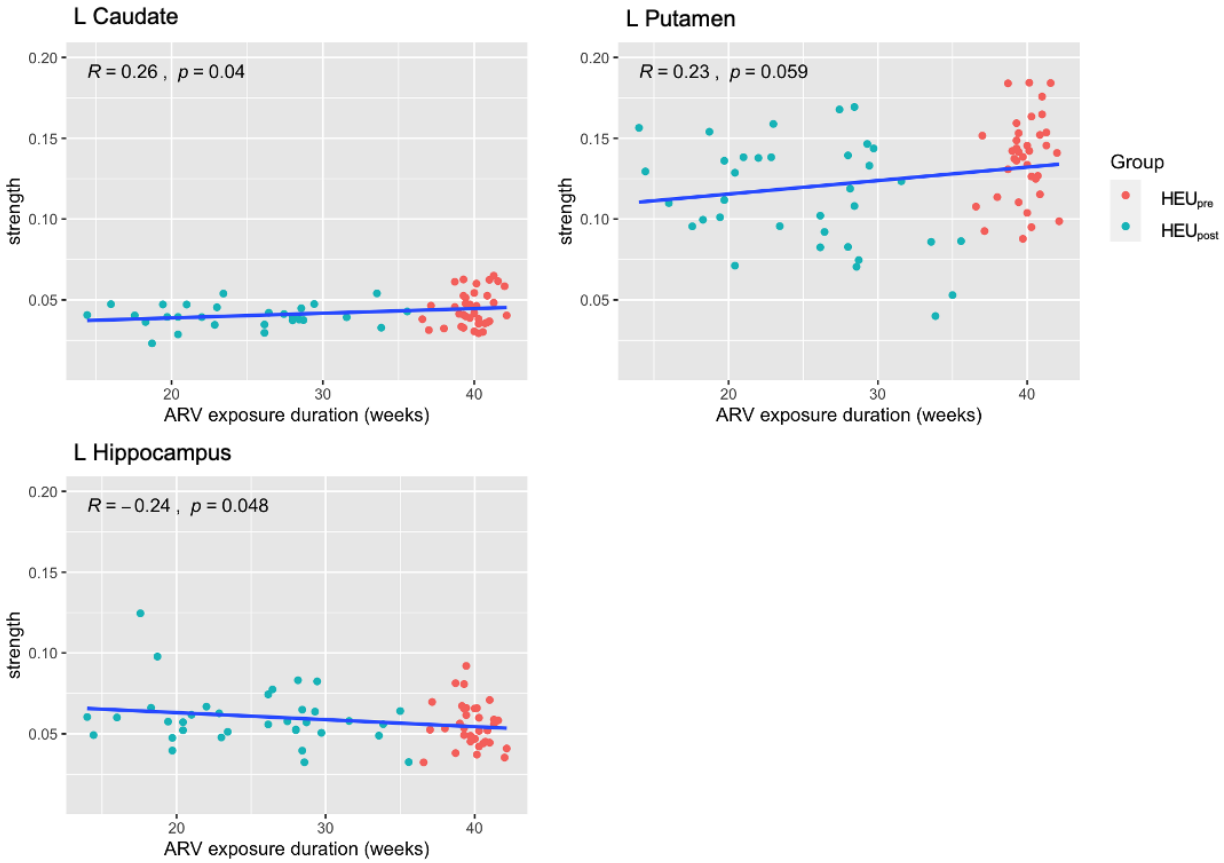

Figure 15: Plots showing associations of strength values in significant regions (p<0.05) among HEU infants with maternal ARV exposure duration. L/R – Left/right hemisphere.

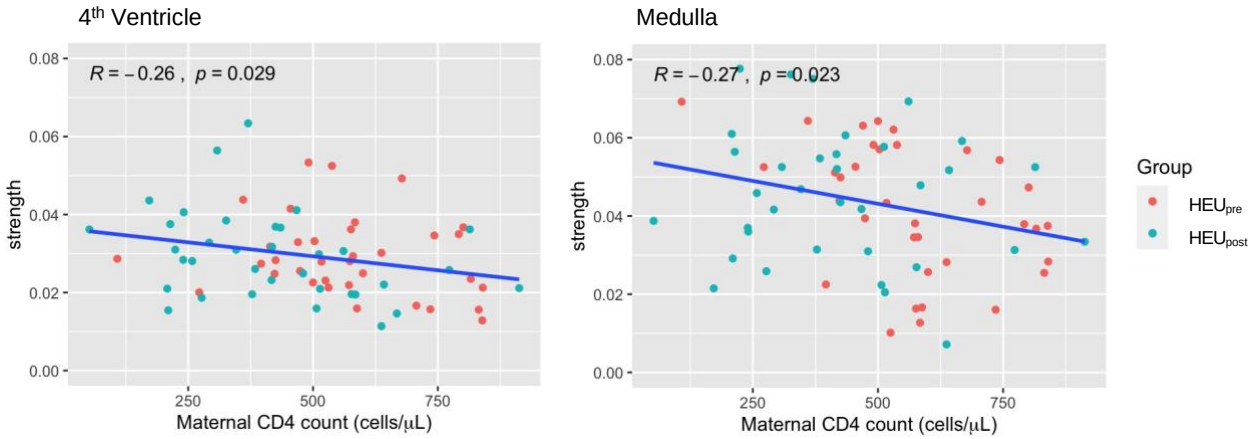

Figure 16: Plots showing associations of strength values in significant regions (p<0.05) among HEU infants with maternal CD4 count. L/R – Left/right hemisphere.

Local efficiency

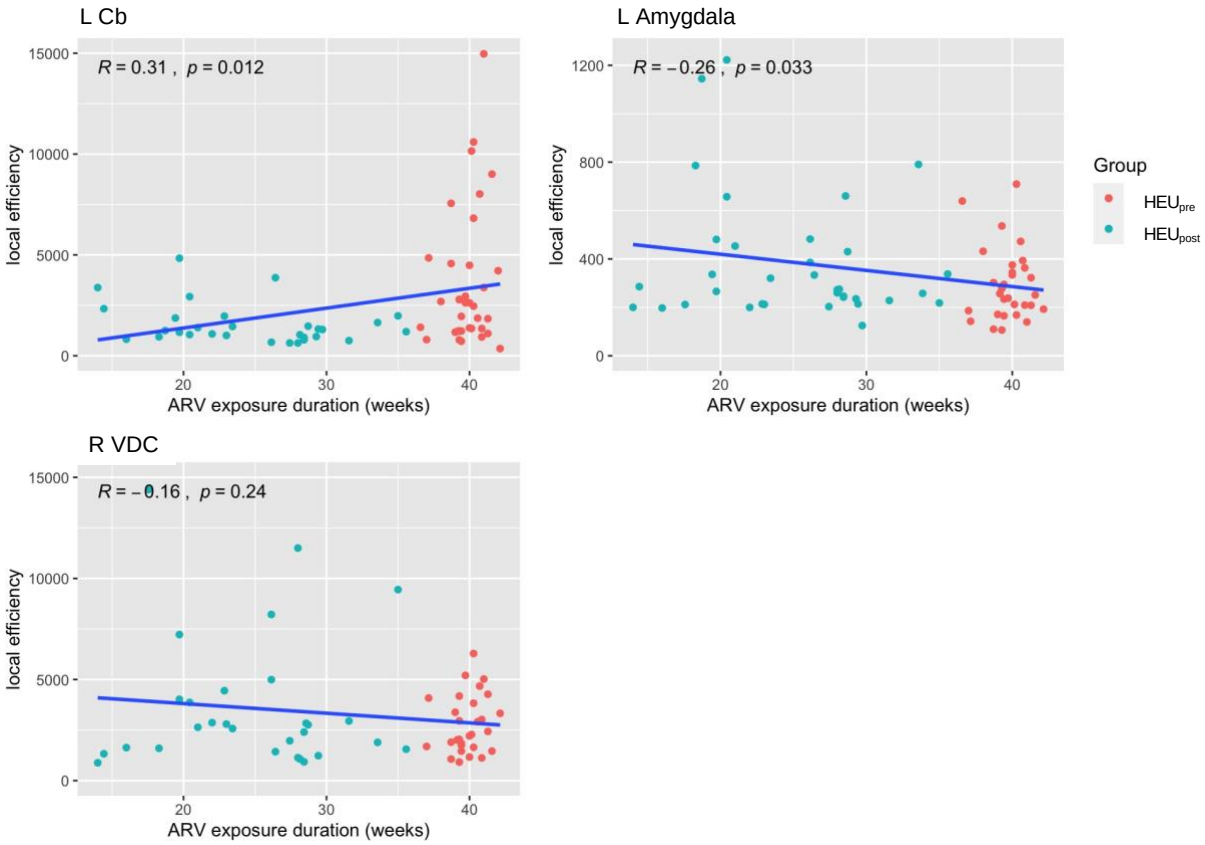

Figure 17: Plots showing associations of local efficiency values in significant regions (p<0.05) among HEU infants with maternal ARV exposure duration. L/R – Left/right hemisphere.

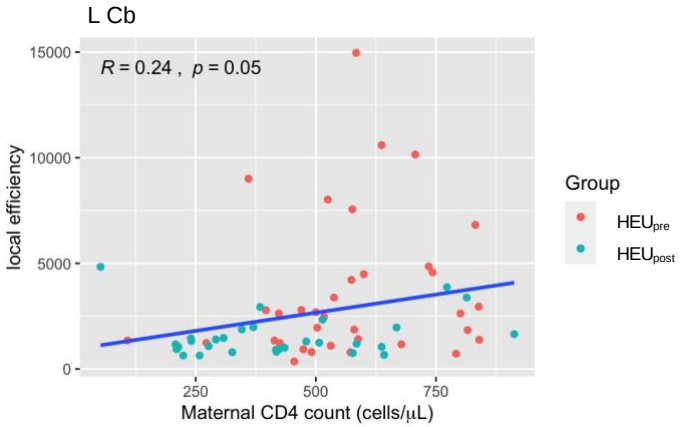

Figure 18: Plots showing associations of local efficiency values in significant regions (p<0.05) among HEU infants with maternal CD4 count. L/R – Left/right hemisphere.

Nodal efficiency

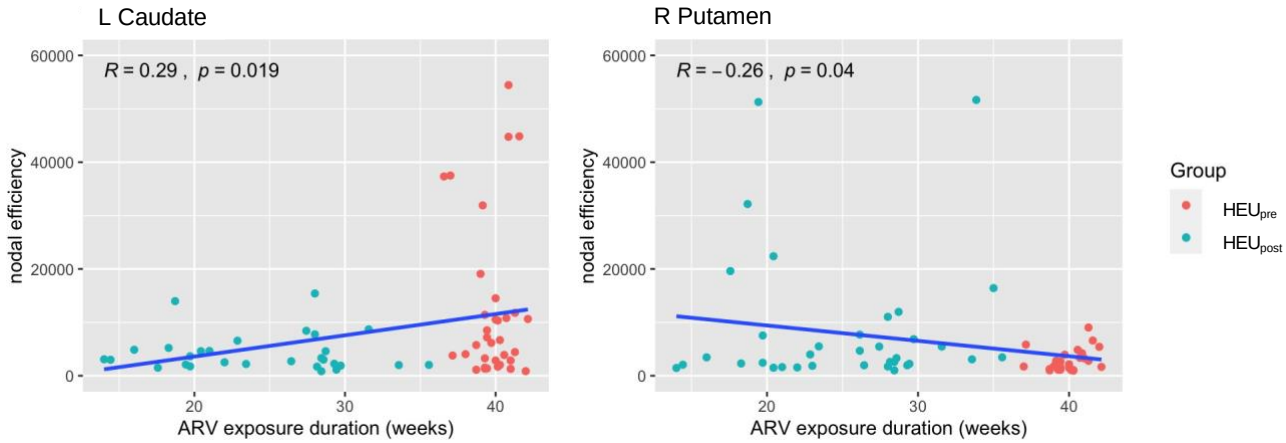

Figure 19: Plots showing associations of nodal efficiency values in significant regions (p<0.05) among HEU infants with maternal ARV exposure duration. L/R – Left/right hemisphere.

5. DISCUSSION

The study investigated the possible influence of HIV and ART exposure in utero at birth on WM integrity and organisation. Using DTI and graph theory, we found that that HIV exposure and duration of ART exposure regionally alters tracts in neonate brains. Interestingly, our results suggest ART and HIV exposure influence different components and regions of developing white matter. Despite many regional HIV/ART alterations, we report very few significant WM organisational differences. Overall, these results indicate developing WM is vulnerable to maternal HIV in utero despite treatment throughout pregnancy. In addition, even in the presence of localised HIV/ART alterations, white matter organisation is preserved.

5.1. WM analysis

5.1.1. FA related differences

We found four tracts with significantly decreased mean FA values across HEU compared to HUU infants. These tracts are from the left cerebral cortex to the left caudate, putamen, ventral diencephalon and midbrain. These WM tracts may reflect regions highly sensitive to HIV exposure in utero since they are independent of ART commencement.

In children and adults, decreased FA is typically related to lower WM connectivity due to less densely packed axons, lower axon diameters and lower myelination or myelination damage (Assaf & Pasternak, 2008; Soares et al., 2013; Curran, Emsell & Leemans, 2016; Jankiewicz et al., 2017). Myelination changes are generally attributed to increased diffusion perpendicular to the axon bundles, which is represented through the perpendicular diffusion tensor RD. A combination of lower FA values and higher RD values has been interpreted in literature as an indication of axonal or myelination complications (Aung, Mar & Benzinger, 2013). Hence, changes in FA are most often driven by changes in RD (Lebel et al., 2012; Tian & Ma, 2017). This can be seen in our data by the uncorrected p values in RD in the tables above.

With neonates, a direct interpretation of the differences in DTI measures may not yet be possible as the brain is still in the early stages of development. White matter – more specifically myelin formation – develops from birth into early adulthood, and has a slightly different composition at birth versus at later stages of life. Thus, interpreting WM changes at birth needs to be done with caution. Instead, the group differences may be used as an initial flag to monitor any further differences that appear over time, and to make cautious judgements about their implications on brain development.

The basal ganglia is a group of subcortical structures including the caudate, putamen, accumbens area and pallidum (Kenhub, 2021). The basal region is highly susceptible to HIV damage with abnormalities frequently reported in adults and children living with HIV, even with ART (Robertson et al., 2018; Wedderburn et al., 2022).

The basal ganglia functions to fine tune voluntary movements of the body, motor control and motor learning (Grohs et al., 2021). The differences in tracts associated

with the basal ganglia may cause future disturbances to general body function. Studies in older HEU children have shown correlations with higher FA scores/lower MD values and higher IQ scores (Jahanshad et al., 2015), suggesting that reduced FA values may have a potential impact on future cognitive abilities.

Preliminary manual segmentation analysis in this cohort reported reduced caudate and putamen volumes (Ibrahim et al., 2020), which may contribute to altered white matter integrity. Previous studies of HEU children and adolescents have also found reduced caudate volumes and reduced total grey matter volumes (Wedderburn et al., 2022).

The majority of tracts with reduced FA were observed in neonates whose mother's initiated ART after conception, suggesting ART may have protected specific regions of the brain in the HEU_{pre} group. Bilaterally we find reduced FA in the cerebral cortex and the thalamus, putamen, cerebellar cortex and ventral diencephalon. The regions most represented include connections to/from the basal ganglia, cerebellum and cerebral cortex. Interestingly, connections with reduced FA tend to be lateralised in the left hemisphere.

While our group analysis indicates a difference based on maternal ART start dates, we also examined associations with ART duration. All of the significant associations occurred with FA values, and only involved subcortical connections. Many of the associated connections involved the cerebellar cortex, which suggests it may be sensitive to ART.

The cerebellum is responsible for motor control, as it organises the brain's directions for skilled repetitive movements and for maintaining posture and balance (Ackerman, 1992). Children with increased exposure to ART may thus potentially perform slightly better in motor cognition tests and may have improved body function.

Both the cerebellum and the basal ganglia have long been established as having roles in motor control (Bostan & Strick, 2018). Initially, both regions were thought to be independent and only communicate on the cortical level, but studies have since found that the cerebellum and basal ganglia, as well as other subcortical regions, are interconnected at the subcortical level (Bostan & Strick, 2018; Pierce & Péron, 2020). As stated above, the basal ganglia has been long established as being susceptible to HIV damage. The link between the basal ganglia and cerebellum may suggest that the cerebellum may also be susceptible to HIV exposure, but through ART the impacts of this exposure are minimised.

We also explored associations with maternal CD4 during pregnancy, and several connections had significant positive associations with FA. However, they did not overlap with tracts related to ART duration with the exception of the midbrain-pons. They also did not overlap with tracts that had significant group differences in FA.

Other studies using DTI to track differences in HEU and HUU children have yielded various results, with one not finding any differences (Jahanshad et al., 2015) and others finding differences in areas/tracts that have not been specified in this study

(Jankiewicz et al., 2017; Yadav et al., 2020). The specified studies find differences in several gyri in the cerebral cortex, but our seeds are broader in scope and only include the cerebral cortex as a whole. One study, by Tran et al. (2016), found a significant difference in FA in the middle cerebellar peduncles of HEU infants compared to HUU, which corresponds to our findings as several tracts coming to/from the cerebellum have been shown to have significantly decreased FA values compared to HUU. While the study finds an increase in FA in this area in HEU infants (Tran et al., 2016), and we find a decrease, both these changes imply that there are structural alterations occurring as a result of HIV and ART exposure.

Our work shows that measures of FA, which represent WM integrity and are susceptible to axon and myelination damage, are sensitive to the duration of maternal ART in utero as well as maternal immune health during pregnancy in newborns.

5.1.2. MD related differences

We report regions with higher MD in HEU infants exposed to ART since conception. MD is associated with axon development and packing as well as structural organisation. Lower MD values typically indicate well organised structure and maturation (Jankiewicz et al., 2017; Yadav et al., 2020).

The tracts with higher MD did not overlap with those with reduced FA. We again find tracts involving the basal ganglia, which further highlights the vulnerability of the basal ganglia to HIV exposure. In contrast to FA differences, here we found connections between several more subcortical structures such as the thalamus, hippocampus, amygdala and ventral diencephalon with increased MD compared to HUU infants.

The tracts within the basal ganglia module, within the forebrain and between the forebrain module and the left and right basal ganglia were most often found to have significantly higher MD values. In MD, tracts between the forebrain and hindbrain (L Hipp – Midbrain, R CC – Midbrain and R Lat Vent – Midbrain) were shown to have significantly higher MD values than their HUU counterparts as well.

In addition to higher MD, these tracts in HEU_{pre} infants also had higher AD and RD values compared to HUU infants. AD and RD are typically associated with axonal density, diameter and myelin integrity(Lebel & Beaulieu, 2011; Curran, Emsell & Leemans, 2016). But in infant brains, the majority of axons are still unmyelinated. As a result, MD, AD and RD values are typically high and decrease with age as increased myelination and dense axon packing occurs (Curran, Emsell & Leemans, 2016).

Higher MD, AD and RD in the HEU newborns whose mothers started ART before conception is an unexpected trend. It suggests that the underlying mechanisms are independent of maternal treatment. We also reported that ARV exposure duration was found to have no associations with the overall HEU group in MD, further supporting this conclusion.

5.1.3. Associations with maternal immune health in pregnancy

We reported associations between DTI measures and maternal CD4 count. For 8 tracts, increased CD4 count was associated with increased FA, while for MD, increased CD4 count was associated with decreased MD values for 3 tracts. The trends associated with CD4 count and increased FA and decreased MD suggest that maternal immune health plays a factor in WM development. However, many of the tracts associated did not demonstrate group differences. Tracts originating from the brainstem in the hindbrain module were most commonly found to be significantly associated with both ARV exposure duration and CD4 count.

CD4 cells are a type of white blood cell that find and destroy bacteria, viruses, and other invading germs in the body. In HIV studies, CD4 counts have long been used as an indicator of immune health in people living with HIV as HIV invades and destroys these cells. Higher CD4 counts are associated with better overall health as CD4 cells mitigate symptoms and complications from HIV (Bell et al., 2018).

Inflammation is part of the body's immune system response to foreign or harmful infections, but often results in painful side effects and, in severe cases, may lead to long term damage to tissues. Maternal inflammation has been hypothesised to be a significant component of neuronal injury and loss in HIV exposed infants and children, since it is associated with the release of proinflammatory neurotoxins in response to HIV-infected immune cells (Baker et al., 2017; Dreier, 2017). The increased secretion of these neurotoxins then leads to neuronal, axonal and myelin damage (Ellis, Langford & Masliah, 2007). Maternal CD4 count could thus be an indicator of the inflammatory response that is occurring within the mothers and impacting neonatal brain development.

5.2. Graph theory analysis

For the graph theory analysis, four modules of GM structures were formed across all newborns regardless of HIV/ART exposure. These were comprised of the left subcortical structures from the basal ganglia, the right subcortical structures from the basal ganglia, the brain stem and cerebellum structures from the hindbrain, and a remainder group containing a mixture of cortical and subcortical structures (the cerebral cortex, left and right hippocampi, amygdala and lateral ventricles) from the forebrain.

The tracts with significant differences in both FA and MD are generally grouped according to their module. In HUU vs HEU_{pre} for FA, the tracts are grouped between the forebrain and the left basal ganglia structures, while in HUU vs HEU_{post}, the tracts are grouped between the left and right forebrain and basal ganglia structures, as well as within the forebrain itself, the hindbrain, and the right forebrain and right basal ganglia structures. In MD, the tracts were grouped within the basal ganglia module, within the forebrain and between the forebrain module and the left and right basal ganglia.

5.2.1. Linear model analysis

Linear models of various graph theory measures (strength, local efficiency, global efficiency, transitivity, and modularity) yielded no significant results after multiple comparison correction. However, in HEU_{pre} infants we reported two regions (left putamen and accumbens area) with reduced nodal efficiency, which measures the ability of information propagation between a node and the remaining nodes in the network (Ma et al., 2018).

Nodal efficiency is a measure of structural segregation in the brain. It represents the capacity for specialised processing within densely interconnected parts of the brain (Griffa et al., 2013). Decreased nodal efficiency in these regions suggests that the regions have decreased processing power and the basal ganglia cluster's ability to communicate within itself may be diminished. This finding is further emphasised by uncorrected results, where we observe significant reductions in strength, transitivity, local and nodal efficiency in the basal ganglia and hindbrain as compared to HUU.

Strength is a network measure, while transitivity and local efficiency are measures of segregation. Strength and transitivity both relate to the density of connections around a node. Transitivity, in particular, gives the overall probability of adjacent nodes being interconnected (Rodrigue, 2020). The extent to which nodes are interconnected directly affects the ability for different nodes within a module to communicate with one another, as given by nodal and local efficiency. Transitivity is an alternative to the clustering coefficient, which has been shown to be related to local and nodal efficiency (Brain Connectivity Toolbox, 2021). Because all the graph measures are related to each other, the differences in these measures before multiple comparison correction may be driving in the differences in nodal efficiency that are seen in the putamen and accumbens area after correction. Although these outcomes do not survive multiple comparison correction, they present a picture of the distribution of the data.

The absence of significant results in graph measures after correction despite significant deviations in DTI measure results highlights how brain organisation may remain unaffected despite localised damage. The brain's dense connective network may bridge gaps from damage in specific tracts throughout the connectome. This is further emphasised by the lack of significant differences in global efficiency, a measure of structural integration.

5.2.2. Associations with maternal clinical and treatment variables

A few nodes in strength, local and nodal efficiency were found to have significant associations with ARV exposure duration and CD4 count. ARV exposure duration was positively associated with strength in the left caudate and left putamen. The positive correlations may be related back to the basal ganglia and highlight how these structures, which are typically implicated by HIV exposure, may be protected by increased ART duration. We find both positive and negative associations between treatment duration and local/nodal efficiency, which is difficult to interpret. However,

we note that the structures involved in these associations – basal ganglia and cerebellum – fit into the DTI results.

For maternal CD4 count, we also find positive and negative associations that do not allow for a straightforward interpretation with the DTI results. However, we again emphasise the presence of the same structures – basal ganglia and cerebellum – being involved. The associations presented, as well as the group differences in nodal efficiency, point to specific structures being more vulnerable to the effects of HIV/ART exposure in utero.

However, we observed a relative lack of HIV/ART exposure group differences, as well as associations with ART duration and maternal CD4 count in pregnancy. We suggest these results represent the robustness of white matter architecture maturation when exposed to HIV/ART in utero.

6. CONCLUSIONS

This study is one of very few that considers the imaging of HEU neonate brains. The study found that, regardless of when ART is started by the mothers, certain regions and tracts in the brain are seemingly influenced by HIV exposure. Infants whose mothers have been on ART pre-conception have higher MD values than their unexposed and uninfected peers, while those who have been exposed to ART post-conception were shown to have lower FA values than their unexposed and uninfected counterparts. These results imply that ART duration influences WM integrity and may be neuroprotective for FA, which is more related to WM integrity, but not for MD, which relates to WM organisation. The differences in MD in infants whose mothers have been on ART pre-conception suggests that underlying mechanisms are independent of maternal treatment.

ARV exposure duration and CD4 count are shown to be positively associated with FA tracts, while CD4 count is negatively associated with MD. This relationship highlights the impact of maternal immune health on fetal brain development.

While there are structural differences in certain WM tracts, the overall structural organisation remains unchanged, as no graph theory measures yielded significant results besides nodal efficiency. The brain's dense connective network may bridge gaps from damage in specific tracts throughout the connectome.

While the study has presented a snapshot of the neonate brains of infants exposed to HIV pre and post conception, interpretations on the consequences of these findings cannot be made. Future studies could investigate the links between these structural differences and cognitive abilities. Associations between other maternal clinical and treatment variables such as trauma and depression scores may also be investigated.

Follow ups of structural measures with age may also be completed to gain further insight on HEU populations as they mature. Studies that look at different imaging modalities may also be done to complement the white matter changes presented.

Future infant studies could be done with larger cohorts to further verify the findings. Studies may also be expanded to other provinces and regions to capture a more varied range of subjects.

REFERENCES

Abu-Raya, B., Michalski, C., Sadarangani, M. & Lavoie, P.M. 2020. Maternal Immunological Adaptation During Normal Pregnancy. *Frontiers in Immunology*. 11:2627. DOI: 10.3389/FIMMU.2020.575197/BIBTEX.

Ackerman, S. 1992. Major Structures and Functions of the Brain. Available: https://www.ncbi.nlm.nih.gov/books/NBK234157/ [2022, January 31].

Assaf, Y. & Pasternak, O. 2008. Diffusion tensor imaging (DTI)-based white matter mapping in brain research: a review. *Journal of molecular neuroscience : MN*. 34(1):51–61. DOI: 10.1007/S12031-007-0029-0.

Aung, W.Y., Mar, S. & Benzinger, T.L. 2013. Diffusion tensor MRI as a biomarker in axonal and myelin damage. *Imaging in medicine*. 5(5):427. DOI: 10.2217/IIM.13.49.

Baker, L.M., Cooley, S.A., Cabeen, R.P., Laidlaw, D.H., Joska, J.A., Hoare, J., Stein, D.J., Heaps-Woodruff, J.M., et al. 2017. Topological Organization of Whole-Brain White Matter in HIV Infection. *Brain Connectivity*. 7(2):115–122. DOI: 10.1089/BRAIN.2016.0457.

Ball, G., Aljabar, P., Zebari, S., Tusor, N., Arichi, T., Merchant, N., Robinson, E.C., Ogundipe, E., et al. 2014. Rich-club organization of the newborn human brain. *Proceedings of the National Academy of Sciences of the United States of America*. 111(20):7456–7461. DOI: 10.1073/PNAS.1324118111/-/DCSUPPLEMENTAL.

Bell, R.P., Barnes, L.L., Towe, S.L., Chen, N., Song, A.W. & Meade, C.S. 2018. Structural connectome differences in HIV infection: brain network segregation associated with nadir CD4 cell count. *Journal of NeuroVirology 2018 24:4*. 24(4):454–463. DOI: 10.1007/S13365-018-0634-4.

Berger, A. 2002. How does it work?: Magnetic resonance imaging. *BMJ : British Medical Journal*. 324(7328):35. DOI: 10.1136/BMJ.324.7328.35.

Berger, J.R. & Arendt, G. 2000. HIV dementia: the role of the basal ganglia and dopaminergic systems. *Journal of psychopharmacology (Oxford, England)*. 14(3):214–221. DOI: 10.1177/026988110001400304.

Berger, J.R. & Nath, A. 1997. HIV Dementia and the Basal Ganglia. *Intervirology*. 40(2–3):122–131. DOI: 10.1159/000150539.

le Bihan, D. 2020. How MRI Makes the Brain Visible. In *Make Life Visible*. Springer, Singapore. 201–212. DOI: 10.1007/978-981-13-7908-6_20.

le Bihan, D. & Johansen-Berg, H. 2012. Diffusion MRI at 25: Exploring brain tissue structure and function. *NeuroImage*. 61(2):324–341. DOI: 10.1016/J.NEUROIMAGE.2011.11.006.

Bostan, A.C. & Strick, P.L. 2018. The basal ganglia and the cerebellum: nodes in an integrated network. *Nature reviews. Neuroscience*. 19(6):338. DOI: 10.1038/S41583-018-0002-7.

Caeyenberghs, K., Leemans, A., de Decker, C., Heitger, M., Drijkoningen, D., vander Linden, C., Sunaert, S. & Swinnen, S.P. 2012. Brain connectivity and postural control in young traumatic brain injury patients: A diffusion MRI based network analysis. *NeuroImage: Clinical*. 1(1):106–115. DOI: 10.1016/J.NICL.2012.09.011.

Caiazzo, G., Fratello, M., Nardo, F. di, Trojsi, F., Tedeschi, G. & Esposito, F. 2003. Structural connectome with high angular resolution diffusion imaging MRI: assessing the impact of diffusion weighting and sampling on graph-theoretic measures. DOI: 10.1007/s00234-018-2003-7.

Campbell, J.S.W. & Pike, G.B. 2014. Potential and limitations of diffusion MRI tractography for the study of language. *Brain and Language*. 131:65–73. DOI: 10.1016/J.BANDL.2013.06.007.

Cohen, R.A., Harezlak, J., Schifitto, G., Hana, G., Clark, U., Gongvatana, A., Paul, R., Taylor, M., et al. 2010. Effects of nadir CD4 count and duration of human immunodeficiency virus infection on brain volumes in the highly active antiretroviral therapy era. *Journal of NeuroVirology*. 16(1):25–32. DOI: 10.3109/13550280903552420.

Cox, R.W. 1996. AFNI: Software for analysis and visualization of functional magnetic resonance neuroimages. *Computers and Biomedical Research*. 29(3):162–173. DOI: 10.1006/cbmr.1996.0014.

Craddock, R.C., Jbabdi, S., Yan, C.G., Vogelstein, J.T., Castellanos, F.X., di Martino, A., Kelly, C., Heberlein, K., et al. 2013. Imaging human connectomes at the macroscale. *Nature methods*. 10(6):524. DOI: 10.1038/NMETH.2482.

Curran, K.M., Emsell, L. & Leemans, A. 2016. Quantitative DTI measures. *Diffusion Tensor Imaging: A Practical Handbook*. (January, 1):65–87. DOI: 10.1007/978-1-4939-3118-7_5.

le Doaré, K., Bland, R. & Newell, M.L. 2012. Neurodevelopment in children born to HIV-infected mothers by infection and treatment status. *Pediatrics*. 130(5). DOI: 10.1542/PEDS.2012-0405.

Dreier, J.W. 2017. *Fever and infections in pregnancy and neurodevelopmental impairment in the child*.

Dubois, J., Dehaene-Lambertz, G., Kulikova, S., Poupon, C., Hüppi, P.S. & Hertz-Pannier, L. 2014. The early development of brain white matter: a review of imaging studies in fetuses, newborns and infants. *Neuroscience*. 276:48–71. DOI: 10.1016/J.NEUROSCIENCE.2013.12.044.

Dubowitz, L., Ricci, D. & Mercuri, E. 2005. The Dubowitz neurological examination of the full-term newborn. *Mental Retardation and Developmental Disabilities Research Reviews*. 11(1):52–60. DOI: 10.1002/mrdd.20048.

Eid, D. 2021. *Forebrain, Midbrain and Hindbrain*. Available: https://www.simplypsychology.org/forebrain-midbrain-hindbrain.html [2022, January 31].

Ellis, R., Langford, D. & Masliah, E. 2007. HIV and antiretroviral therapy in the brain: neuronal injury and repair. *Nature reviews. Neuroscience*. 8(1):33–44. DOI: 10.1038/NRN2040.

Ene, L. 2018. Human Immunodeficiency Virus in the Brain—Culprit or Facilitator? *Infectious Diseases*. 11:117863371775268. DOI: 10.1177/1178633717752687.

Everall, I.P., Heaton, R.K., Marcotte, T.D., Ellis, R.J., McCutchan, J.A., Atkinson, J.H., Grant, I., Mallory, M., et al. 1999. Cortical synaptic density is reduced in mild to moderate human immunodeficiency virus neurocognitive disorder. HNRC Group. HIV Neurobehavioral Research Center. *Brain pathology (Zurich, Switzerland)*. 9(2):209–217. DOI: 10.1111/J.1750-3639.1999.TB00219.X.

Fornito, A., Zalesky, A. & Breakspear, M. 2013. Graph analysis of the human connectome: promise, progress, and pitfalls. *NeuroImage*. 80:426–444. DOI: 10.1016/J.NEUROIMAGE.2013.04.087.

Ginsberg, Y., Khatib, N., Weiner, Z. & Beloosesky, R. 2017. Maternal Inflammation, Fetal Brain Implications and Suggested Neuroprotection: A Summary of 10 Years of Research in Animal Models. *Rambam Maimonides Medical Journal*. 8(2):e0028. DOI: 10.5041/rmmj.10305.

Girault, J.B., Munsell, B.C., Puechmaille, D., Goldman, B.D., Prieto, J.C., Styner, M. & Gilmore, J.H. 2019. White matter connectomes at birth accurately predict cognitive abilities at age 2. *NeuroImage*. DOI: 10.1016/j.neuroimage.2019.02.060.

González, R., Rupérez, M., Sevene, E., Vala, A., Maculuve, S., Bulo, H., Nhacolo, A., Mayor, A., et al. 2017. Effects of HIV infection on maternal and neonatal health in southern Mozambique: A prospective cohort study after a decade of antiretroviral drugs roll out. *PLoS ONE*. 12(6):1–17. DOI: 10.1371/journal.pone.0178134.

Gray, G.E. & McIntyre, J.A. 2007. HIV and pregnancy. *British Medical Journal*. 334(7600):950–953. DOI: 10.1136/bmj.39176.674977.AD.

Griffa, A., Baumann, P.S., Thiran, J.P. & Hagmann, P. 2013. Structural connectomics in brain diseases. *NeuroImage*. 80:515–526. DOI: 10.1016/J.NEUROIMAGE.2013.04.056.

Grohs, M.N., Lebel, C., Carlson, H.L., Craig, B.T. & Dewey, D. 2021. Subcortical brain structure in children with developmental coordination disorder: A T1-weighted volumetric study. *Brain Imaging and Behavior*. 15:2756–2765. DOI: 10.1007/s11682-021-00502-y.

Grover, V.P.B., Tognarelli, J.M., Crossey, M.M.E., Cox, I.J., Taylor-Robinson, S.D. & McPhail, M.J.W. 2015. Magnetic Resonance Imaging: Principles and Techniques:

Lessons for Clinicians. *Journal of Clinical and Experimental Hepatology*. 5(3):246. DOI: 10.1016/J.JCEH.2015.08.001.

He, L., Li, H., Holland, S.K., Yuan, W., Altaye, M. & Parikh, N.A. 2018. Early prediction of cognitive deficits in very preterm infants using functional connectome data in an artificial neural network framework. *NeuroImage: Clinical*. 18:290–297. DOI: 10.1016/J.NICL.2018.01.032.

Heidari, S., Mofenson, L., Cotton, M.F., Marlink, R., Cahn, P. & Katabira, E. 2011. Antiretroviral drugs for preventing mother-to-child transmission of HIV: A review of potential effects on HIV-exposed but uninfected children. *Journal of Acquired Immune Deficiency Syndromes*. 57(4):290–296. DOI: 10.1097/QAI.0B013E318221C56A.

Ibrahim, A., Warton, F., Fry, S., Cotton, M.F., Jacobson, S., Jacobson, J., Molteno, C., Little, F., et al. 2020. Maternal ART throughout pregnancy prevents caudal volume reductions in HIV exposed uninfected neonates. Cape Town.

Jahanshad, N., Couture, M.C., Prasitsuebsai, W., Nir, T.M., Aurpibul, L., Thompson, P.M., Pruksakaew, K., Lerdlum, S., et al. 2015. Brain imaging and neurodevelopment in HIV-uninfected Thai children born to HIV-infected mothers. *The Pediatric infectious disease journal*. 34(9):e211. DOI: 10.1097/INF.0000000000000774.

Jankiewicz, M., Holmes, M.J., Taylor, P.A., Cotton, M.F., Laughton, B., van der Kouwe, A.J.W. & Meintjes, E.M. 2017. White matter abnormalities in children with HIV infection and exposure. *Frontiers in Neuroanatomy*. 11(September):1–9. DOI: 10.3389/fnana.2017.00088.

Jbabdi, S. & Johansen-Berg, H. 2011. Tractography: Where Do We Go from Here? *Brain Connectivity*. 1(3):169. DOI: 10.1089/BRAIN.2011.0033.

Jones, D.K. & Cercignani, M. 2010. Twenty-five pitfalls in the analysis of diffusion MRI data. *NMR in Biomedicine*. 23(7):803–820. DOI: 10.1002/NBM.1543.

Jones, D.K., Knösche, T.R. & Turner, R. 2013. White matter integrity, fiber count, and other fallacies: The do's and don'ts of diffusion MRI. *NeuroImage*. 73:239–254. DOI: 10.1016/J.NEUROIMAGE.2012.06.081.

Kenhub. 2021. *Subcortical structures: Anatomy and function | Kenhub*. Available: https://www.kenhub.com/en/library/anatomy/subcortical-structures-anatomy [2022, January 25].

Konkel, L. 2018. The brain before birth: Using fMRI to explore the secrets of fetal neurodevelopment. *Environmental Health Perspectives*. 126(11):1–5. DOI: 10.1289/EHP2268.

Lebel, C. & Beaulieu, C. 2011. Longitudinal Development of Human Brain Wiring Continues from Childhood into Adulthood. *Journal of Neuroscience*. 31(30):10937–10947. DOI: 10.1523/JNEUROSCI.5302-10.2011.

Lebel, C., Gee, M., Camicioli, R., Wieler, M., Martin, W. & Beaulieu, C. 2012. Diffusion tensor imaging of white matter tract evolution over the lifespan. *NeuroImage*. 60(1):340–352. DOI: 10.1016/J.NEUROIMAGE.2011.11.094.

List of measures - Brain Connectivity Toolbox. n.d. Available: https://sites.google.com/site/bctnet/measures/list#TOC-Efficiency-and-Diffusion [2021, November 02].

Ma, X., Jiang, G., Fu, S., Fang, J., Wu, Y., Liu, M., Xu, G. & Wang, T. 2018. Enhanced Network Efficiency of Functional Brain Networks in Primary Insomnia Patients. *Frontiers in Psychiatry*. 9(FEB). DOI: 10.3389/FPSYT.2018.00046.

de Macedo Rodrigues, K., Ben-Avi, E., Sliva, D.D., Choe, M., Drottar, M., Wang, R., Fischl, B., Grant, P.E., et al. 2015. A FreeSurfer-compliant consistent manual segmentation of infant brains spanning the 0–2 year age range. *Frontiers in Human Neuroscience*. 9(FEB):21. DOI: 10.3389/FNHUM.2015.00021.

Madzime, J., Holmes, M., Cotton, M.F., Laughton, B., van der Kouwe, A.J.W., Meintjes, E.M. & Jankiewicz, M. 2021. Altered White Matter Tracts in the Somatosensory, Salience, Motor, and Default Mode Networks in 7-Year-Old Children Living with Human Immunodeficiency Virus: A Tractographic Analysis. *Brain connectivity*. (August, 23). DOI: 10.1089/BRAIN.2020.0948.

Maier-Hein, K.H., Neher, P.F., Houde, J.C., Côté, M.A., Garyfallidis, E., Zhong, J., Chamberland, M., Yeh, F.C., et al. 2017. The challenge of mapping the human connectome based on diffusion tractography. *Nature Communications 2017 8:1*. 8(1):1–13. DOI: 10.1038/s41467-017-01285-x.

Mathis, S., Khanlari, B., Pulido, F., Schechter, M., Negredo, E., Nelson, M., Vernazza, P., Cahn, P., et al. 2011. Effectiveness of protease inhibitor monotherapy versus combination antiretroviral maintenance therapy: a meta-analysis. *PloS one*. 6(7). DOI: 10.1371/JOURNAL.PONE.0022003.

McHenry, M.S., McAteer, C.I., Oyungu, E., McDonald, B.C., Bosma, C.B., Mpofu, P.B., Deathe, A.R. & Vreeman, R.C. 2018. Neurodevelopment in Young Children Born to HIV-Infected Mothers: A Meta-analysis. *Pediatrics*. 141(2). DOI: 10.1542/PEDS.2017-2888.

Mori, S. & Zhang, J. 2006. Principles of diffusion tensor imaging and its applications to basic neuroscience research. *Neuron*. 51(5):527–539. DOI: 10.1016/J.NEURON.2006.08.012.

Moser, E., Stadlbauer, A., Windischberger, C., Quick, H.H. & Ladd, M.E. 2009. Magnetic resonance imaging methodology. *European Journal of Nuclear Medicine and Molecular Imaging*. 36(SUPPL. 1):30–41. DOI: 10.1007/S00259-008-0938-3/FIGURES/7.

Mudaly, V. & Voget, J. 2020. The Western Cape Consolidated Guidelines for HIV Treatment: Prevention of Mother-to-Child Transmission of HIV (PMTCT), Children, Adolescents and Adults.

Muller, P., Parmigiani, G. & Rice, K. 2006. FDR and Bayesian multiple comparisons rules. *Bayesian Statistics 8*. 0(1995):349–370. Available: http://biostats.bepress.com/jhubiostat/paper115/.

National Department of Health. 2019. *health-annual-report*. Pretoria.

Newell, M.-L., Coovadia, H., Cortina-Borja, M., Rollins, N., Gaillard, P. & Dabis, F. 2004. Mortality of infected and uninfected infants born to HIV-infected mothers in Africa: a pooled analysis. *The Lancet*. 364(9441):1236–1243. DOI: 10.1016/S0140-6736(04)17140-7.

NIH & NIBIB. 2021. *Magnetic Resonance Imaging (MRI)*. Available: https://www.nibib.nih.gov/science-education/science-topics/magnetic-resonance-imaging-mri [2022, February 07].

Ohene, Y. 2020. Development of non-invasive MRI to measure water permeability across the blood-brain interface. Available: https://www.researchgate.net/publication/340225510_Development_of_non-invasive_MRI_to_measure_water_permeability_across_the_blood-brain_interface [2022, February 08].

Pannek, K., Hatzigeorgiou, X., Colditz, P.B. & Rose, S. 2013. Assessment of structural connectivity in the preterm brain at term equivalent age using diffusion MRI and T2 relaxometry: a network-based analysis. *PloS one*. 8(8). DOI: 10.1371/JOURNAL.PONE.0068593.

Pierce, J.E. & Péron, J. 2020. The basal ganglia and the cerebellum in human emotion. *Social Cognitive and Affective Neuroscience*. 15(5):599–613. DOI: 10.1093/SCAN/NSAA076.

Pierpaoli, C., Walker, L., Irfanoglu, M.O., Barnett, A., Basser, P., Chang, L.-C., Koay, C., Pajevic, S., et al. 2010. TORTOISE: an integrated software package for processing of diffusion MRI data. *ISMRM 18th annual meeting*. Available: www.tortoisedti.org. [2022, January 28].

Pooley, R.A. 2005. Fundamental physics of MR imaging. *Radiographics*. 25(4):1087–1099. DOI: 10.1148/RG.254055027/ASSET/IMAGES/LARGE/G05JL24G26X.JPEG.

R Core Team. 2020. R: A Language and Environment for Statistical Computing. Available: http://www.gnu.org/copyleft/gpl.html. [2022, January 28].

Racicot, K. & Mor, G. 2017. Risks associated with viral infections during pregnancy. *Journal of Clinical Investigation*. 127(5):1591–1599. DOI: 10.1172/JCI87490.

Ramesh, G., Maclean, A.G. & Philipp, M.T. 2013. Cytokines and Chemokines at the Crossroads of Neuroinflammation, Neurodegeneration, and Neuropathic Pain. *Mediators of Inflammation*. 2013:20. DOI: 10.1155/2013/480739.

Rita Carter. 2019. *The Brain Book: An Illustrated Guide to its Structure, Functions, and Disorders*. Third ed. Penguin Random House. Available: https://books.google.co.za/books/about/The_Brain_Book.html?id=rxGnDwAAQBAJ&printsec=frontcover&source=kp_read_button&hl=en&redir_esc=y#v=onepage&q&f=false [2022, January 31].

Robertson, F.C., Holmes, M.J., Cotton, M.F., Dobbels, E., Little, F., Laughton, B., van der Kouwe, A.J.W. & Meintjes, E.M. 2018. Perinatal HIV infection or exposure is associated with low n-acetylaspartate and glutamate in basal ganglia at age 9 but not 7 years. *Frontiers in Human Neuroscience*. 12:145. DOI: 10.3389/FNHUM.2018.00145/BIBTEX.

Robinson-Papp, J. & Saylor, D. 2021. HIV in the Brain. *Neurology*. 96(14):645–646. DOI: 10.1212/WNL.0000000000011735.

Rodrigue, J.-P. 2020. The Geography of Transport Systems. *The Geography of Transport Systems*. (May, 7). DOI: 10.4324/9780429346323.

Rubinov, M. & Sporns, O. 2010. Complex network measures of brain connectivity: Uses and interpretations. *NeuroImage*. 52(3):1059–1069. DOI: 10.1016/J.NEUROIMAGE.2009.10.003.

Setsompop, K., Cohen-Adad, J., Gagoski, B.A., Raij, T., Yendiki, A., Keil, B., Wedeen, V.J. & Wald, L.L. 2012. Improving diffusion MRI using simultaneous multi-slice echo planar imaging. *NeuroImage*. 63(1):569. DOI: 10.1016/J.NEUROIMAGE.2012.06.033.

Sirois, P.A., Huo, Y., Williams, P.L., Malee, K., Garvie, P.A., Kammerer, B., Rich, K., van Dyke, R.B., et al. 2013. Safety of Perinatal Exposure to Antiretroviral Medications: Developmental Outcomes in Infants. *The Pediatric infectious disease journal*. 32(6):648. DOI: 10.1097/INF.0B013E318284129A.

Slogrove, A.L., Cotton, M.F. & Esser, M.M. 2010. Severe infections in HIV-exposed uninfected infants: clinical evidence of immunodeficiency. *Journal of tropical pediatrics*. 56(2):75–81. DOI: 10.1093/TROPEJ/FMP057.

Slogrove, A.L., Powis, K.M., Johnson, L.F., Stover, J. & Mahy, M. 2020. Estimates of the global population of children who are HIV-exposed and uninfected, 2000–18: a modelling study. *The Lancet Global Health*. 8(1):e67–e75. DOI: 10.1016/S2214-109X(19)30448-6/ATTACHMENT/EB243DC6-BA5E-4D7B-B120-2EA5DC24B5BE/MMC1.PDF.

Soares, J.M., Marques, P., Alves, V. & Sousa, N. 2013. A hitchhiker's guide to diffusion tensor imaging. *Frontiers in Neuroscience*. 0(7 MAR):31. DOI: 10.3389/FNINS.2013.00031/BIBTEX.

Song, L., Mishra, V., Ouyang, M., Peng, Q., Slinger, M., Liu, S. & Huang, H. 2017. Human Fetal Brain Connectome: Structural Network Development from Middle Fetal Stage to Birth. *Frontiers in neuroscience*. 11(OCT). DOI: 10.3389/FNINS.2017.00561.

Taylor, P.A. & Saad, Z.S. 2013. FATCAT: (An Efficient) Functional And Tractographic Connectivity Analysis Toolbox. *Brain Connectivity*. 3(5):523. DOI: 10.1089/BRAIN.2013.0154.

Tian, L. & Ma, L. 2017. Microstructural changes of the human brain from early to mid-adulthood. *Frontiers in Human Neuroscience*. 11:393. DOI: 10.3389/FNHUM.2017.00393/BIBTEX.

Tran, L.T., Roos, A., Fouche, J.P., Koen, N., Woods, R.P., Zar, H.J., Narr, K.L., Stein, D.J., et al. 2016. White Matter Microstructural Integrity and Neurobehavioral Outcome of HIV-Exposed Uninfected Neonates. *Medicine*. 95(4). DOI: 10.1097/MD.0000000000002577.

UNAIDS. 2021. *Global HIV & AIDS statistics — Fact sheet | UNAIDS*. Available: https://www.unaids.org/en/resources/fact-sheet [2022, January 26].

Unicef. 2012. *Options B and B+: key considerations for countries to implement an equity-focused approach | SAFAIDS*. New York. Available: http://catalogue.safaids.net/publications/options-b-and-b-key-considerations-countries-implement-equity-focused-approach [2022, January 28].

Vassar, R.L., Barnea-Goraly, N. & Rose, J. 2014. Identification of Neonatal White Matter on DTI: Influence of More Inclusive Thresholds for Atlas Segmentation. *PLOS ONE*. 9(12):e115426. DOI: 10.1371/JOURNAL.PONE.0115426.

Vassiliou, V.S., Cameron, D., Prasad, S.K. & Gatehouse, P.D. 2018. Magnetic resonance imaging: Physics basics for the cardiologist. *JRSM cardiovascular disease*. 7:2048004018772237. DOI: 10.1177/2048004018772237.

Vecchio, F., Miraglia, F. & Maria Rossini, P. 2017. Connectome: Graph theory application in functional brain network architecture. *Clinical Neurophysiology Practice*. 2:206–213. DOI: 10.1016/J.CNP.2017.09.003.

Vera, J.H., Guo, Q., Cole, J.H., Boasso, A., Greathead, L., Kelleher, P., Rabiner, E.A., Kalk, N., et al. 2016. Neuroinflammation in treated HIV-positive individuals: A TSPO PET study. *Neurology*. 86(15):1425–1432. DOI: 10.1212/WNL.0000000000002485.

Wachsler-Felder, J.L. & Golden, C.J. 2002. Neuropsychological Consequences of HIV in Children: A Review of Current Literature. *Clinical Psychology Review*. 22(3):443. DOI: 10.1016/S0272-7358(01)00108-8.

Watson, C.G., DeMaster, D. & Ewing-Cobbs, L. 2019. Graph theory analysis of DTI tractography in children with traumatic injury. *NeuroImage: Clinical*. 21:101673. DOI: 10.1016/J.NICL.2019.101673.

Wedderburn, C.J., Evans, C., Yeung, S., Gibb, D.M., Donald, K.A. & Prendergast, A.J. 2019. Growth and Neurodevelopment of HIV-Exposed Uninfected Children: a Conceptual Framework. *Current HIV/AIDS reports*. 16(6):501–513. DOI: 10.1007/S11904-019-00459-0.

Wedderburn, C.J., Groenewold, N.A., Roos, A., Yeung, S., Fouche, J., Rehman, A.M., Gibb, D.M., Narr, K.L., et al. 2022. Early structural brain development in infants exposed to HIV and antiretroviral therapy *in utero* in a South African birth cohort. *Journal of the International AIDS Society*. 25(1). DOI: 10.1002/JIA2.25863.

WHO, UNAIDS & Unicef. 2010. *Towards universal access: Scaling up priority HIV/AIDS interventions in the health sector | WHO*. Available: https://www.afro.who.int/publications/towards-universal-access-scaling-priority-hivaids-interventions-health-sector [2022, January 28].

Williams, P.L., Crain, M.J., Yildirim, C., Hazra, R., van Dyke, R.B., Rich, K., Read, J.S., Stuard, E., et al. 2015. Congenital anomalies and in utero antiretroviral exposure in human immunodeficiency virus-exposed uninfected infants. *JAMA pediatrics*. 169(1):48–55. DOI: 10.1001/JAMAPEDIATRICS.2014.1889.

World Health Organisation. 2013. Consolidated Guidelines on the Use of Antiretroviral Drugs for Treating and Preventing HIV Infection. *Geneva: World Health Organization*. 14(7):269. Available: https://www.ncbi.nlm.nih.gov/books/NBK195400/ [2022, January 26].

World Health Organisation. 2016. Available: https://www.who.int/publications/i/item/9789241549684 [2022, January 26].

World Health Organisation & UNAIDS. 1998. HIV in Pregnancy : A Review.

Yadav, S.K., Gupta, R.K., Hashem, S., Nisar, S., Azeem, T., Bhat, A.A., Syed, N., Garg, R.K., et al. 2020. Brain microstructural changes support cognitive deficits in HIV uninfected children born to HIV infected mothers. *Brain, Behavior, & Immunity - Health*. 2:100039. DOI: 10.1016/J.BBIH.2020.100039.

Yuan, J.P., Henje Blom, E., Flynn, T., Chen, Y., Ho, T.C., Connolly, C.G., Dumont Walter, R.A., Yang, T.T., et al. 2019. Test-Retest Reliability of Graph Theoretic Metrics in Adolescent Brains. *Brain connectivity*. 9(2):144–154. DOI: 10.1089/BRAIN.2018.0580.

Zaba, B., Calvert, C., Marston, M., Isingo, R., Nakiyingi-Miiro, J., Lutalo, T., Crampin, A., Robertson, L., et al. 2013. Effect of HIV infection on pregnancy-related mortality in sub-Saharan Africa: Secondary analyses of pooled community based data from the network for Analysing Longitudinal Population-based HIV/AIDS data on Africa (ALPHA). *The Lancet*. 381(9879):1763–1771. DOI: 10.1016/S0140-6736(13)60803-X.

Zenko, J. 2020. *When (and Why) to use Heat Maps*. Available: https://www.dundas.com/resources/blogs/best-practices/when-and-why-to-use-heat-maps [2022, February 04].

Zöllei, L., Iglesias, J.E., Ou, Y., Grant, P.E. & Fischl, B. 2020. Infant FreeSurfer: An automated segmentation and surface extraction pipeline for T1-weighted

neuroimaging data of infants 0–2 years. *NeuroImage*. 218:116946. DOI: 10.1016/J.NEUROIMAGE.2020.116946.